Contribution to the modeling of rolling element bearing – rotor system for railway application

Shaocheng Zhu

N°d'ordre NNT : 2017LYSEI136

THESE de DOCTORAT DE L'UNIVERSITE DE LYON
opérée au sein de
l'INSA LYON
et délivré en partenariat international avec
SOUTHWEST JIAOTONG UNIVERSITY

Ecole Doctorale N° EDA162
Mécanique, Energétique, Génie civil, Acoustique (MEGA)

Spécialité / discipline de doctorat :
Mécanique -Génie Mécanique

Soutenue publiquement le 22/12/2017, par :
Shaocheng ZHU

Contribution to the modeling of rolling element bearing – rotor system for railway application

Devant le jury composé de :

DUFRENOY, Philippe	Professeur	Université de Lille	Rapporteur
YIN, Honoré	DR	ENPC	Rapporteur
ROUHAUD, Emmanuelle	Professeur	Université Techno. de Troyes	Examinatrice
NELIAS, Daniel	Professeur	INSA Lyon	Directeur de thèse
ZHANG, Weihua	Professeur	Southwest Jiaotong University	Co-Directeur de thèse

Département FEDORA – INSA Lyon - Ecoles Doctorales – Quinquennal 2016-2020

SIGLE	ECOLE DOCTORALE	NOM ET COORDONNEES DU RESPONSABLE
CHIMIE	**CHIMIE DE LYON** **http://www.edchimie-lyon.fr** Sec : Renée EL MELHEM Bat Blaise Pascal 3e etage secretariat@edchimie-lyon.fr Insa : R. GOURDON	M. Stéphane DANIELE Institut de Recherches sur la Catalyse et l'Environnement de Lyon IRCELYON-UMR 5256 Équipe CDFA 2 avenue Albert Einstein 69626 Villeurbanne cedex directeur@edchimie-lyon.fr
E.E.A.	**ELECTRONIQUE, ELECTROTECHNIQUE, AUTOMATIQUE** **http://edeea.ec-lyon.fr** Sec : M.C. HAVGOUDOUKIAN Ecole-Doctorale.eea@ec-lyon.fr	M. Gérard SCORLETTI Ecole Centrale de Lyon 36 avenue Guy de Collongue 69134 ECULLY Tél : 04.72.18 60.97 Fax : 04 78 43 37 17 Gerard.scorletti@ec-lyon.fr
E2M2	**EVOLUTION, ECOSYSTEME, MICROBIOLOGIE, MODELISATION** **http://e2m2.universite-lyon.fr** Sec : Safia AIT CHALAL Bat Darwin - UCB Lyon 1 04.72.43.28.91 Insa : H. CHARLES Safia.ait-chalal@univ-lyon1.fr	Mme Gudrun BORNETTE CNRS UMR 5023 LEHNA Université Claude Bernard Lyon 1 Bât Forel 43 bd du 11 novembre 1918 69622 VILLEURBANNE Cédex Tél : 06.07.53.89.13 e2m2@ univ-lyon1.fr
EDISS	**INTERDISCIPLINAIRE SCIENCES -SANTE** **http://www.ediss-lyon.fr** Sec : Safia AIT CHALAL Hôpital Louis Pradel - Bron 04 72 68 49 09 Insa : M. LAGARDE Safia.ait-chalal@univ-lyon1.fr	Mme Emmanuelle CANET-SOULAS INSERM U1060, CarMeN lab, Univ. Lyon 1 Bâtiment IMBL 11 avenue Jean Capelle INSA de Lyon 696621 Villeurbanne Tél : 04.72.68.49.09 Fax :04 72 68 49 16 Emmanuelle.canet@univ-lyon1.fr
INFOMATHS	**INFORMATIQUE ET MATHEMATIQUES** **http://infomaths.univ-lyon1.fr** Sec :Renée EL MELHEM Bat Blaise Pascal, 3e etage infomaths@univ-lyon1.fr	Mme Sylvie CALABRETTO LIRIS – INSA de Lyon Bat Blaise Pascal 7 avenue Jean Capelle 69622 VILLEURBANNE Cedex Tél : 04.72. 43. 80. 46 Fax 04 72 43 16 87 Sylvie.calabretto@insa-lyon.fr
Matériaux	**MATERIAUX DE LYON** **http://ed34.universite-lyon.fr** Sec : M. LABOUNE PM : 71.70 –Fax : 87.12 Bat. Saint Exupéry Ed.materiaux@insa-lyon.fr	M. Jean-Yves BUFFIERE INSA de Lyon MATEIS Bâtiment Saint Exupéry 7 avenue Jean Capelle 69621 VILLEURBANNE Cedex Tél : 04.72.43 71.70 Fax 04 72 43 85 28 Ed.materiaux@insa-lyon.fr
MEGA	**MECANIQUE, ENERGETIQUE, GENIE CIVIL, ACOUSTIQUE** **http://mega.universite-lyon.fr** Sec : M. LABOUNE PM : 71.70 –Fax : 87.12 Bat. Saint Exupéry mega@insa-lyon.fr	M. Philippe BOISSE INSA de Lyon Laboratoire LAMCOS Bâtiment Jacquard 25 bis avenue Jean Capelle 69621 VILLEURBANNE Cedex Tél : 04.72.43.71.70 Fax : 04 72 43 72 37 Philippe.boisse@insa-lyon.fr
ScSo	**ScSo*** **http://recherche.univ-lyon2.fr/scso/** Sec : Viviane POLSINELLI Brigitte DUBOIS Insa : J.Y. TOUSSAINT viviane.polsinelli@univ-lyon2.fr	Mme Isabelle VON BUELTZINGLOEWEN Université Lyon 2 86 rue Pasteur 69365 LYON Cedex 07 Tél : 04.78.77.23.86 Fax : 04.37.28.04.48

*ScSo : Histoire, Géographie, Aménagement, Urbanisme, Archéologie, Science politique, Sociologie, Anthropologie

Acknowledgment/Remerciements

This Ph.D. work is conducted in both **TPL** (Traction Power National Laboratory**)** of **Southwest Jiaotong University** and **LaMCoS** (Laboratoire de Mécanique des Contacts et des Structures) of **INSA-Lyon**, CNRS UMR5259, F69621, directed by Professor Weihua ZHANG and Professor Daniel NELIAS.

I would like to express to Mr. Zhang my very deep gratitude to have provided me with advanced projects of National level, financial supports and technical advice, especially of brilliant ideas in train techniques, and for the most exciting encouragement he gave and for the constant interest that he showed during these five years.

I am extremely sensitive to the honor that Mr. Nelias has allowed me to follow him for over two years to study bearing techniques, completely grateful for technical documents he gave, very pleased by the nice discussions we had and always thankful to his constant kindness. I could never forget what I experienced these years in Lyon, thanks to him.

I always feel indebted to my parents and other members in my family. I spent less time with them, until my grandfather (maternal) passed away 2 months ago, I suddenly find something in my life lost and some space in my heart empty. Now, I really miss him.

I would like to thank particularly Professor Shuying Gao and her husband-Professor Luming Wu, who passed away on the same day when I returned from Lyon back to China one year ago. I cannot forget him forever; he firstly gave me the hope in bearing research and gave me great help in my road abroad administratively.

The work for a Ph.D. candidate is to find a road in the maze. Even although a lot of exits can be in fine found, a lot of blind alleys can also be possibly in the front. It sometimes needs immediate retreats and timely helps from colleagues and friends.

I would like to thank Professor Dongli Song, Professor Guiming Mei, and my colleagues Q. Xiong, L. Wei, H.L. Wu for their helps in China, and a lot of other colleagues, Y.C. Zhang, S. Chen, W.J. Gao, Eric, Damien, etc. for their support in France.

I would also like to thank my Chinese friend, W. Gong, headman of hardware test department in Huawei Company, Chengdu, who gave me a lot of suggestions in programming

and my French friend A. Domissy, who helped me a lot in French learning, and gave his precious help in correcting my written French of abstract.

At last, I must acknowledge the financial support provided by China Scholarship Council (CSC), and the conferences funding from National natural fund Committee of China and State key laboratory of Traction power, SWJTU, China， as well as relevant courses funding given by LaMCoS, INSA Lyon. Many thanks.

Preface

Bearing technology is a kind of old knowledge, the traditional questions about dynamic interfacial parameters are always welcome in both bearing and relevant transmission applications, since accurate and efficient coupling analysis on different dynamic relations and subsequent design of structural composition and parameters are always required according to diverse demands. Bearing interference characterized by coefficient matrices and its coupling approaches with rotor system are of prime interest in this thesis.

More accurate knowledge about contact inside a bearing and much simpler approach of interpreting bearing contact loads are very important to correspondingly understand and depict the errors that simplified contact parameters used to bring into bearing stiffness and damping matrices. Inversely, how to interpret distributed roller contact parameters with lumped parameters is also a long-term question of interest and importance, since lumped contact parameters are more easily involved into bearing transmission matrices.

This thesis explains in Chapter 1 and 2:

How the distributed damping and stiffness coefficients of oil film correspond to the distributed oil film thickness under steady and transient states? (Chapter 1)

Whether edge effect of roller/race contact affects load and motion transmissions? How to numerically interpret this effect in a simpler manner? (Chapter 2)

Complex calculations performed in Chapter 1 and 2 attempt to describe distributed roller contact parameters at rolling and roller length directions, and to explain some resultant vibration characteristics of rotor, and so on. However, due to calculation cost, this complexity is more preferred in calculation of steady states, than in calculation of transient states. Under steady states rather than under transient states, dominating vibration characteristics of system should be more necessarily distinguished and be more accurately understood.

This thesis also explains in Chapter 3:

How to develop more practical bearing matrices and more reliable methods of solving nonlinear bearing-rotor model in a uniform and economic way? Whether frequency-domain method performs a better computer-aided identification capacity than time-domain method?

Time/frequency domain analysis on Rotor dynamics system performed in Chapter 3 either qualitatively or quantitatively gives useful information hidden between bearing and rotor. Some corresponding test verifications are required to recognize bearing parameters or rotor behaviors, as well as to assess bearing fatigue conditions. A first generation bearing test bench proposed reproduces rotor dynamic behaviors with different bearing characteristics appearing under different excitations. However, intense vibration with large contact load fluctuatingly imposed inside a bearing cannot be easily reproduced, since most vibrators are not capable of vibrating giant bearing test bench intensively.

This thesis at last introduces in Chapter 4:

How to build up an alternative bearing test bench to reproduce contact behaviors inside a bearing under large loading and high-frequency vibration?

Abstract

Some developments on bearing applications are emphasized in this thesis, from contact model to bearing model, and from bearing-rotor model to bench reproduction technique.

First, perturbation method is extended to prove that steady-state EHL distributed damping and stiffness do not satisfy the transient conditions, and steady-state EHL lumped coefficients are not suitable for dynamic analysis.

Distribution law of EHL oil film damping and stiffness is attemptly proposed. Combining initial state of steady-state solution with transient EHL distributed stiffness and damping, dynamic behaviors of oil film are predicted.

Second, edge effect of roller/race contact is considered in bearing transmissions. First and second approximation methods are proposed to numerically interpret this effect. First approximation method concentrates on adopting influence coefficient method to replay edge effect as well as using normalization process to respect empirical results, while second approximation method focuses on a fast-analytical manner of describing Hertz pressure inside roller slice.

Third, practical bearing matrices are used to develop 3D bearing-rotor dynamics code, based on classical Hertz and EHL formulas. In time domain, four-order Adams method is improved to solve incremental nonlinear dynamics equations; In frequency domain, analytical method of HB-AFT is particularly employed to bridge 3D bearing matrices and 3D steady-state solutions, besides, arc-length continuation method increases calculation speed. Using both methods, some factors can be considered qualitatively and quantitatively, including initial states, damping, eccentricity, internal and external excitations.

Last, an alternative technique is proposed to reproduce contact behaviors inside bearings under heavy loading and high-frequency vibrations, when working parameters are beyond bench capacity.

This thesis gives new but simple insights into what happens to rolling and longitudinal contacts of bearing roller, how to model and solve nonlinear bearing-rotor system in both time and frequency domains, and where a way is to reproduce extreme contact conditions inside bearings using bench.

Keywords: Elasto-hydrodynamic Lubrication (EHL), contact model in bearing matrices, bearing-rotor model, alternative bearing bench

Introduction

From contact model to bearing model, and from bearing-rotor model to bench reproduction technique, the four chapters deliver the author's understandings in bearing engineering application.

Chapter 1:

A new method is proposed to solve transient elasto-hydrodynamic lubrication (EHL) problem. First, original dynamic EHL behavior is estimated by steady-state EHL solution, where elastic deformation theory is specifically combined with oil film stiffness distribution equation instead of steady-state Reynolds equation. Second, subsequent dynamic EHL procedure develops from recursively using transient distributed oil film stiffness and damping, where each time-marching solution is iteratively searched by ensuring both oil film force growth and elastic deformation's update to follow external contact load increment. This method, in fine, not only increases calculation speed, but also evidences availability of distributed EHL stiffness and damping by acquiring ideal transient EHL curves. The fast method analyzing dynamic film contact in bearing, gear, etc. could be technically convenient.

Keywords: Elasto-hydrodynamic Lubrication (EHL), transient EHL, oil film stiffness and damping distributions

Chapter 2:

This chapter enhances classic slicing technique to calculate forces and moments acting on bearing rollers in direct bearing model. First, calculations of both deformation and classic empirical load are reviewed; second, first and second approximation models of roller contact are versatilely developed to consider pressure concentration in roller edge; third, considering capacity in application, an engineering-adequate model is proposed, using normalization process. Roller forces and moments can be obtained in a faster and more accurate manner, which in fine permits to obtain the bearing load distribution as well as to predict bearing stiffness matrix in complex transmissions and gearboxes in a faster way.

Keywords: Direct bearing model, roller bearing, slicing technique, interaction among slices, force and moment distributions, bearing stiffness

Chapter 3:

A uniform derivation for overall stiffness and damping matrices of both tapered and ball bearings is conducted, using the pioneer work of Luc-Houpert (1997), with slice technique considered in distributed roller load calculation and varying contact angle considered in fluctuating ball transmission load calculation. Simplified EHL and Hertz relations are linearly included in contact force and in fine analytically facilitate formulated matrices. Nonlinear bearing-rotor system is modeled with a better linear mathematical equation and solved in simpler enhanced numerical manner of Adams. Meanwhile, nonlinear bearing-rotor system is also remodeled and resolved with analytical method of HB-AFT. It performs a faster efficiency and an easier system behavior-identifying capacity, especially when considering 3D condition. Besides modeling and solving nonlinear bearing-rotor system, some factors participated can also be qualitatively and quantitatively considered, including initial states, damping, and eccentricity, internal and external excitations.

Keywords: Bearing damping and stiffness matrices, ball and roller bearings, slice technique, varying contact angle, bearing-rotor system, enhanced Adams method, HB-AFT.

Chapter 4:

This chapter shows a new design of bearing test bench. Two ideas are presented herein: 1 functionally, it reproduces dynamic loads acting on rotor by considering internal and external excitations. Internal excitations are applied, as most bearing manufacturers manipulate, in the manner of motor drive, while external excitations are specifically loaded herein by generating housing motions and corresponding rotor inertial loads, which requires programming an electromagnetic vibrator which supports entire system. It appeals to the idea the authors have ever delivered in work about nonlinear bearing-rotor system dynamics. Meanwhile, an alternative idea of uniquely reproducing bearing contact load is also performed for bearing study. 2 financially, to reduce costs for the electricity used in bearing tests (e.g. for train products) conducted in our first-generation bench, a second-generation bench is also proposed to increase usage of vibrator, where a sliding mode control idea is also used in optimized design. With the construction of bearing test platform, a series of research ideas on high-speed, over-loading and vibration conditions can be explored.

Keywords: Bearing test bench; inertial loading; topological optimization; electromagnetic vibrator; sliding mode control

Préface

La technologie des roulements est un savoir connu, les questions traditionnelles sur les paramètres interfaciaux dynamiques sont toujours populaires à la fois dans les roulements et également dans les applications adéquates de transmission, puisque les analyses de couplage précises et efficientes sur les relations dynamiques différentes et les conceptions subséquentes de la composition structurelle et des paramètres sont toujours requis en fonction des exigences diverses. L'interférence des roulements caractérisée par les matrices de coefficients et son association avec le système des rotors sont de primeure intérêt à cette thèse.

Davantage de connaissance adéquate sur le contact à l'intérieur d'un roulement et son approche beaucoup plus simple d'interpréter les charges de contact du roulement sont très importants pour comprendre et décrire de manière correspondante les erreurs que les paramètres simplifiés de contact ont autrefois introduit dans les matrices de rigidité et d'amortissement des roulements. Inversement, comment interpréter les paramètres distribués de contact de roulement avec les paramètres assemblés est également une question à long terme d'intérêt et d'importance, puisque les paramètres assemblés de contact sont plus facilement impliqués dans les matrices de transmission des roulements.

Cette thèse explique dans le chapitre 1 et 2:

Comment les coefficients d'amortissement et de rigidité distribués de film d'huile correspondent à l'épaisseur distribuée du film d'huile sous des états stables et transitoires? (Chapitre 1)

Si l'effet du contact en bordure entre le cylindre et le courant affecte les transmissions de charge et de motion? Comment interpréter numériquement cet effet de manière plus simple ? (Chapitre 2)

Les calculs complexes réalisés dans les chapitres 1 et 2 essaient de décrire les paramètres distribués de contact des cylindres en axes rotatif et longitudinal, et d'expliquer les caractéristiques résultantes des vibrations du rotor, etc. Cependant, dû aux coûts des calculs, cette complexité est davantage préférée dans le calcul des états stables que dans celui des états transitoires. Sous des états stables plutôt que dans les états transitoires, les caractéristiques

dominantes de vibration du système devraient être plus nécessairement distinguées et être plus précisément compréhensibles.

Cette thèse explique également dans le chapitre 3:

Comment développer des matrices de roulement plus pratiques et des méthodes plus fiables de résoudre des modèles de roulements-rotor non linéaires de manière uniforme et économique?

Si les méthodes de fréquence-domaine représentent une meilleure capacité d'identification par assistance informatique plutôt que les méthodes de temps-domaine ?

L'analyse des domaines temps/fréquence sur le système dynamique du rotor présenté au chapitre 3 donne soit qualitativement soit quantitativement des informations utiles cachées entre le roulement et le rotor. Quelques vérifications par des tests correspondants sont requis pour reconnaître les paramètres des roulements ou les motions du rotor, de même que pour estimer les conditions de fatigue du roulement. Une première génération de banc d'essai de roulement proposé reproduit les comportements dynamiques du rotor avec différentes caractéristiques de roulements émergeant sous différentes tensions. Cependant, une vibration intense couplée à une charge importante de contact imposée de manière fluctuante à l'intérieur d'un roulement ne peut pas être reproduit facilement, puisque la plupart des vibreurs ne sont pas capables de faire vibrer intensément les bancs d'essais géants des roulements.

Cette thèse présente enfin dans le chapitre 4:

Comment construire un banc d'essai alternatif des roulements pour reproduire les comportements de contact à l'intérieur d'un roulement sous une charge importante et une vibration à haute fréquence.

Résumé

Quelques développements sont démontrés dans cette thèse, du modèle de contact au modèle de roulement et du modèle de roulement-rotor à la technique de reproduction par bancs.

Tout d'abord, la méthode de perturbation est étendue afin de prouver que la rigidité et l'amortissement distribués en état stable EHL ne remplissent pas les conditions transitoires et que les coefficients intégrés ne sont pas appropriés pour les analyses dynamiques。

La loi de distribution de la rigidité et l'amortissement du film d'huile de l'EHL est proposée. En combinant l'état initial d'une solution stable avec l'amortissement et la rigidité distribués de l'EHL transitoire, les comportements du film d'huile peuvent être prédits.

Par la suite, l'effet du contact en bordure entre le cylindre et le courant est pris en compte dans les transmissions de roulement. Les méthodes d'approximation première et seconde sont proposées pour interpréter numériquement cet effet. La méthode d'approximation première se concentre sur l'adoption de la méthode du coefficient d'influence pour reproduire l'effet de contact de même que l'utilisation du procédé de normalisation pour respecter les résultats empiriques ; alors que la méthode d'approximation seconde se concentre sur une manière analytique rapide de décrire la pression Hertz au contact entre le cylindre et le courant.

Ensuite, les matrices de roulements pratiques sont utilisées pour développer un code de dynamiques 3D du roulement-rotor, basé sur des formules Hertz et EHL classiques. En temps-domaine, la méthode Adams quatre-ordres est améliorée pour résoudre les équations incrémentées des dynamiques non-linéaires. En fréquence-domaine, la méthode analytique de HB-AFT est particulièrement employée pour combler des matrices de roulement en 3D et des solutions d'état stable 3D. De plus, la méthode de continuation arc-longueur augmente la vitesse de calcul. En utilisant les deux méthodes, certains facteurs peuvent être considérés qualitativement et quantitativement, en incluant les états initiaux, l'amortissement, l'excentricité et les tensions internes et externes.

Enfin, une technique alternative est proposée pour reproduire les comportements de contact à l'intérieur des roulements sous une forte charge et des vibrations à haute fréquence, lorsque les paramètres actifs sont en sous capacité du banc.

Cette thèse apporte des visions nouvelles mais simples sur ce qui se produit sur les contacts roulants et longitudinaux d'un roulement circulaire ; sur comment modéliser et résoudre le système non-linéaire de roulement-rotor en domaines à la fois temps et fréquence ; et sur le moyen de reproduire des conditions de contact extrême à l'intérieur des roulements

Mots clés : Lubrification Elasto-Hydrodynamique (EHL); Modèle de contact des matrices de roulement; Modèle de rotor-roulement; Banc alternatif d'essais de roulements

Introduction

A partir du modèle de contact au modèle de roulement, et à partir du modèle de roulement-rotor à la technique de reproduction par bancs, les quatre chapitres délivrent notre compréhension dans l'application de l'ingénierie des roulements.

Chapitre 1:

Une nouvelle méthode est proposée pour résoudre le problème de lubrification transitoire élasto-hydrodynamique (EHL). Tout d'abord, le comportement de dynamique EHL commence par une solution de EHL à l'état stable, où la théorie de la déformation élastique est spécifiquement combinée à l'équation de la rigidité distribuée du film d'huile au lieu de l'équation de Reynolds à l'état stable. Ensuite, le comportement subséquent de dynamique EHL se développe en utilisant récursivement la rigidité et l'amortissement distribués du film d'huile transitoire, où chaque solution transitoire est itérativement recherchée par l'assurance que le chargement externe par échelon s'associe à la fois avec la croissance de la force du film d'huile ainsi que la révision de la déformation élastique. In fine, cette méthode, non seulement augmente la vitesse de calcul, mais aussi démontre la disponibilité de la rigidité et de l'amortissement distribués de l'EHL en acquérant des courbes idéales de EHL transitoire. La méthode rapide d'analyse du contact de film dynamique sur les roulements, les engrenages, etc. pourrait convenir techniquement.

Mots clés: Lubrification Elasto-Hydrodynamique (EHL), EHL transitoire, distribution de la rigidité et de l'amortissement du film d'huile.

Chapitre 2:

Ce chapitre renforce la technique partielle classique pour calculer les forces et les moments agissant sur les roulements ronds avec un modèle direct de roulement. Tout d'abord, les calculs de déformation et de charge empirique classique sont revus.

Ensuite, les modèles d'approximation premier et second du contact du roulement sont développés de façon polyvalente pour prendre en compte la concentration de la pression dans le bord du roulement. Enfin, en considérant la capacité lors de l'application, un modèle adéquat d'ingénierie est proposé, en utilisant le process de normalisation. Les forces et moments du roulement peuvent être obtenus d'une manière plus rapide et plus précise, ce qui

au final permet d'obtenir la charge distribuée du roulement rond comme d'envisager la matrice de rigidité du roulement dans des transmissions complexes et des boîtes d'engrenages d'une manière plus rapide.

Mots clés: modèle direct de roulement, roulement rond, technique des portions, interactions parmi les portions, distributions des forces et moments, rigidité du roulement.

Chapitre 3:

Une dérivation uniforme sur les matrices de rigidité et d'amortissement des roulements à la fois coniques et ronds est menée, utilisant le travail initial de Luc Houpert (1997), avec une technique des portions considérant le calcul distribué de la charge du cylindre et l'angle variable de contact considéré dans le calcul de la charge en transmission fluctuante. Les relations simplifiées des EHL et Hertz sont incluses linéairement dans la force de contact et in fine facilitent les matrices formulées analytiquement. Le système des roulements-rotor non linéaires est modelé avec une meilleure équation mathématique linéaire et résolu d'une manière numérique de Adams plus simplifiée. Cependant, le système de roulements-rotor est également démontré et résolu avec la méthode analytique de HB-AFT. Celui-ci exécute un fonctionnement plus rapide et une capacité d'identification simplifiée de comportement du système, spécialement en condition 3D. En plus de modeler et de résoudre le système des roulements-rotor non linéaires, certains facteurs peuvent être également qualitativement et quantitativement pris en compte, incluant les statuts initiaux, l'amortissement et l'excentricité, les tensions internes et externes.

Mots clés : Matrices de rigidité et d'amortissement des roulements ; roulements ronds et cylindriques ; technique des portions, angle variable de contact ; système de roulements-rotor, méthode améliorée de Adams, HB-AFT

Chapitre 4:

Ce chapitre démontre une nouvelle conception de banc d'essais de roulement. Deux idées sont présentées ci-dessous. 1- fonctionnellement: il reproduit les charges dynamiques agissant sur le rotor en considérant des tensions internes et externes. Les tensions internes sont exercées, comme le font la plupart des fabricants de roulement, avec un moteur d'entraînement, pendant que les tensions externes sont exercées spécifiquement en générant à la fois des mouvements du logement et des charges inertielles correspondantes du rotor, ce qui

requiert la programmation d'un vibrateur électromagnétique qui soutient le système entier. Cela appuie l'idée des auteurs qui ont remis le rapport sur la dynamique du système des roulements-rotor non linéaires. Cependant, une idée alternative en reproduisant uniquement la charge du contact du roulement est également présentée pour l'étude des roulements. 2- financièrement. Afin de réduire les coûts d'électricité utilisés dans les tests de roulements (par exemple les produits ferroviaires) menés dans le banc de première génération, un banc de seconde génération est proposé pour augmenter l'usage du vibrateur, où une idée de contrôle en mode glissant est également utilisée en conception optimisée. Avec la construction d'une plateforme de banc d'essais, une série d'idées de recherches sur des conditions à grande vitesse, surcharge et vibrations peuvent être explorées.

Mots clés : banc d'essais de roulements ; charge inertielle ; optimisation topologique ; vibrateur électromagnétique ; contrôle en mode glissant.

Content

Chapter 1
Calculation on Elasto-hydrodynamic Lubrication

1.1 Introduction

EHL contact qualities in transmitting components (bearing, gear, etc.) and in special dynamic systems with open connections (wheel-rail contact, etc.), can be measured by stiffness and damping parameters. In dynamic design, integrated (or lumped) parameters are often preferred instead of distributed values due to their feasibility in multi-body dynamic system, and it must be also recognized that steady-state parameters are used exclusively since transient values are technically hard to seize.

In the past decades, strenuous efforts have gone into improving the accuracy and efficiency of steady state EHL calculation, direct iterative method for light load in point contact was introduced by Hamrock and Dowson**[1]**, inverse method was also developed for heavy load, first employed in line contact by Dowson and Higginson **[2]**, and later in point contact by Evans and Snidle **[3]**. Since Newton Raphson method was used, relevant researches in EHL problem have become more popular **[4], [5], [6]**. When multigrid method was introduced by Lubrecht **[7]**, incredibly high efficiency in calculation was obtained. Interest in numerical technique also led to relevant developments of derived methods, such as multilevel multi-integration method **[8]**, FFT method **[9]**, etc.

No matter for what method, it is still difficult to apply it to dynamic systems, from transient EHL problem to subsequent application in vibration system.

Apart from full numerical methods, a simplified method neglecting the Poiseuille term used by L.Chang **[10]**, S. Messé and Lubrecht,A.A. **[11]**, and others has brought some efficiency in analysis on transient EHL problems.

As for integrated EHL behaviors, other efforts were made. A rough and direct integration of Reynolds equation was proposed and often used in parallel to Hertz relation in bearing dynamic calculation **[12]~[16]**. Recently, another rough and direct integration method was also used, oil film parameters are integrated within different spaces in **[17], [18]**, but in series with Hertz stiffness. Both numerical method and curve fitting method were used to extract lumped parameters from distributed EHL parameters by Shriniwas P. Chippa and Mihir

Sarangi**[19], [20], [21]**, and until now, this could be the most complex way to get EHL damping and stiffness coefficients. Before getting transient lumped parameters, transient distributed parameters should be studied.

This chapter is oriented towards the study of transient distributed EHL behaviors. Besides the mentioned manners, we focus on improving Reynolds equation. With distributed damping and stiffness, distributed transient EHL behaviors will be fast described.

1.2 Decomposition of Transient EHL force

This paragraph discusses in depth interacting mechanism on EHL surface and introduces new principle of simplification.

Generally, oil film stiffness and damping co-exist on EHL surface. Distributed behaviors are reduced to three concentrated interactions. It has been well understood that zero effect at exit zone on total load is due to cavitation caused by generation of negative pressure, and oil film also performs indifferently at Hertz's contact zone since central approach is dominated by Hertz deformation, so that, by neglecting these two weak interactions, oil film's effect on contact load is described at entry zone by a rough and direct integration of Reynolds equation, in the form of parallel normal supporting load **[12]**,

$$Q=\frac{4\eta_0 R_y u_y L}{h_{\min,iso}}+\frac{6.66\eta_0 u_z R_y^{1.5} L}{h_{\min,iso}^{1.5}} \quad (1.1)$$

Inlet equivalent relation and central hertz relation turn one EHL pair to damping and stiffness coefficients, having been widely used to perform bearing dynamic calculation or to formulate bearing stiffness or damping matrices in the past.

However, this simplification fails to consider the deformation outside Hertz area. Materials compress at hertz area (primary stiffness), but stretch at entry zone (extra damping produced by "inciting wings"). Grubin **[22]** predicted inlet oil film thickness according to this assumption.

Meanwhile, preceding analytical expression well matches highly-loaded contacts, but fails to serve weakly-loaded contacts, thought by Benedikt Wiegert, etc. **[17]**. He proposed a new force model to apply in oscillatory system with multiple EHL contacts by interpreting each contact as hydrodynamic force in series with Hertz force. In his study, hydrodynamic

force was reduced to a complex function with regard to the cavitation position and its height, so that he reported another study **[18]** to get an approximate relation for the normal force of hydrodynamic line contacts under transient conditions by means of numerical results; Meanwhile, structural force equal to hydrodynamic force was organized by kinematic constraint, so that their new force model was expressed as a function of approach value, approach velocity and steady-state central oil film thickness. However, both film and static structural contact coefficients were derived separately according to Reynolds equation or Hertz theory, more daring an assumption of introducing a linear damping constant into the elastic structure was also specially used in his paper.

Although two preceding methods are well performed, surface loading is distributed around entire deformed area, interaction between elastic structure and lubricant should be considered, that is why Grubin's prediction was incomplete. Until full numerical method is introduced into the coupling calculation, accurate distributed solution can be obtained in a time-consuming way. Chippa, S.P. and Sarangi, M. worked on this method to extract lumped parameters, but their perturbation method was still based on steady-state results. Wherein, a same oil film perturbation was used along entire contact surface, still leading to rough estimations of integrated contact coefficients by directly accumulating each parameter.

In this chapter, elastic deformation keeps original calculating strategy; but lubricant film stiffness and damping forces decompose from Reynolds equation. The mutual effect between oil film and elastic deformation under transient EHL can be maintained by transient damping and stiffness distributions. Theoretically, this simplification is more accurate than two preceding methods.

Reynolds equation:

$$\frac{\partial}{\partial x}\left(\frac{h^3}{\eta}\frac{dp}{dx}\right)=12u\frac{\partial h}{\partial x}+12\frac{\partial h}{\partial t} \qquad (1.2)$$

Based on boundary assumption $\frac{\partial P}{\partial x}|x_e=0$, transient stiffness and damping distributions are derived.

$$\begin{cases} \dfrac{dF_{k\ film}}{dx}=\dfrac{12\eta u_x h(x)}{(h_e+h(x))^3} \\ \dfrac{dF_{c\ film}}{dx}=\dfrac{12\eta\int\dfrac{d(h(x)+h_e)}{dt}dx}{(h_e+h(x))^3} \end{cases} \tag{1. 3}$$

$$\begin{cases} \dfrac{dk_{\ film}}{dx}=\dfrac{12\eta u_x(h_e+h(x))^3-3(h_e+h(x))^2 12\eta u_x h(x)}{(h_e+h(x))^6}=-\dfrac{36\eta u_x h(x)}{(h_e+h(x))^4}+\dfrac{12\eta u_x}{(h_e+h(x))^3} \\ \dfrac{dc_{\ film}}{dx}=\dfrac{12\eta x}{(h_e+h(x))^3} \end{cases} \tag{1. 4}$$

Under steady states, formulation **(1. 4)** can be transformed into

$$\begin{cases} \dfrac{h_0^3}{\eta}\dfrac{dP_h}{dx}+\dfrac{3h_0^2}{\eta}\dfrac{dP_0}{dx}=12u_x \\ \dfrac{h_0^3}{\eta}\dfrac{dP_{\dot{h}}}{dx}=12x \end{cases} \tag{1. 5}$$

Where, $P_h=k_{\ film}, P_{\dot{h}}=c_{\ film}$

It agrees perfectly with Chippa, S.P.'s results based on perturbation method **[16]** (see **Appendix A**).

Perturbation method performs well for one parameter in dynamic equations, but not for multiple (or distributed) parameters simultaneously perturbed, using a same condition. No comparability exists among different variables.

More hidden information of perturbed Reynolds equation is discovered based on two following equations, where $o(\Delta h^2)$ and $o(\Delta \dot{h}^2)$ are neglected.

$$\frac{\partial}{\partial x}\left(\frac{(h_0+\Delta h)^3}{\eta}\left(\frac{dP_0}{dx}+\frac{dP_h}{dx}\Delta h+\frac{dP_{\dot{h}}}{dx}\Delta\dot{h}+P_h\frac{d\Delta h}{dx}+P_{\dot{h}}\frac{d\Delta\dot{h}}{dx}\right)\right)=12u\frac{\partial(h_0+\Delta h)}{\partial x}+12\frac{\partial(h_0+\Delta h)}{\partial t} \tag{1. 6}$$

$$\frac{\partial}{\partial x}\left(\frac{h_0^3}{\eta}\left(\frac{dP_0}{dx}+\frac{dP_h}{dx}\Delta h+\frac{dP_{\dot{h}}}{dx}\Delta\dot{h}\right)+\frac{3h_0^2\Delta h}{\eta}\left(\frac{dP_0}{dx}\right)\right)+\frac{\partial}{\partial x}\left(\frac{h_0^3}{\eta}\left(P_h\frac{d\Delta h}{dx}+P_{\dot{h}}\frac{d\Delta\dot{h}}{dx}\right)\right)=12u\frac{\partial(h_0+\Delta h)}{\partial x}+12\frac{\partial(h_0+\Delta h)}{\partial t} \tag{1. 7}$$

Chippa, S.P. assumes that $\frac{d\Delta h}{dx}=\frac{d\Delta\dot{h}}{dx}=0$ exists under transient condition, so that total stiffness and damping coefficients can be derived by $\begin{cases} K=\int P_h dx \\ C=\int P_{\dot{h}} dx \end{cases}$.

$$\frac{\partial}{\partial x}\left(\frac{{h_0}^3}{\eta}\left(\frac{dP_0}{dx}+\frac{dP_h}{dx}\Delta h+\frac{dP_{\dot{h}}}{dx}\dot{h}\right)+\frac{3{h_0}^2\Delta h}{\eta}\left(\frac{dP_0}{dx}\right)\right)=12u\left(\frac{\partial h_0}{\partial x}+\frac{\partial \Delta h}{\partial x}\right)+12\dot{h} \tag{1. 8}$$

To boil down to formula **(1.8)** and to respect differences between original and simplified equations, some comparisons among internal terms in original equation **(1.6)** tell the approximating conditions.

$$\frac{\frac{dP_h}{dx}\Delta h}{P_h\frac{d\Delta h}{dx}}=\frac{\frac{d\ln P_h}{dx}}{\frac{d\ln \Delta h}{dx}}>1 \Leftrightarrow \frac{d\ln P_h}{dx}-\frac{d\ln \Delta h}{dx}=\frac{\ln\frac{P_{h_{i+1}}}{P_{h_i}}-\ln\frac{\Delta h_{i+1}}{\Delta h_i}}{\Delta x}=\frac{\ln\frac{P_{h_{i+1}}\Delta h_i}{P_{h_i}\Delta h_{i+1}}}{\Delta x}>0 \Leftrightarrow \frac{P_{h_{i+1}}\Delta h_i}{P_{h_i}\Delta h_{i+1}}>1$$

It is found that only $P_{h_{i+1}}>P_{h_i}$ from inlet to exit of EHL contact can get $\frac{d\Delta h}{dx}=\frac{d\Delta\dot{h}}{dx}=0$ ($\Delta h_i=\Delta h_{i+1}$).

Further to this, dynamic distribution of oil film calculated by steady-state distributed stiffness and damping can clarify its non-robustness.

Steady-state equation and fluctuation equation of transient Δh can be collected based on equation **(1. 7)**.

$$\begin{cases}\dfrac{\partial}{\partial x}\left(\dfrac{{h_0}^3}{\eta}\dfrac{dP_0}{dx}\right)=12u\dfrac{\partial h_0}{\partial x}\\ \dfrac{\partial}{\partial x}\left(\left(\dfrac{{h_0}^3}{\eta}\dfrac{dP_h}{dx}+\dfrac{3{h_0}^2}{\eta}\left(\dfrac{dP_0}{dx}\right)\right)\Delta h\right)+\dfrac{\partial}{\partial x}\left(\dfrac{{h_0}^3}{\eta}\dfrac{dP_{\dot{h}}}{dx}\dot{h}\right)+\dfrac{\partial}{\partial x}\left(\dfrac{{h_0}^3}{\eta}\left(P_h\dfrac{d\Delta h}{dx}+P_{\dot{h}}\dfrac{d\dot{h}}{dx}\right)\right)=12u\dfrac{\partial \Delta h}{\partial x}+12\dot{h}\end{cases} \tag{1. 9}$$

P_h^k and $P_{\dot{h}}^k$ come from steady-state EHL solution, and serve fluctuation equation. To test the usability of P_h^k and $P_{\dot{h}}^k$, fluctuation between continuous steady-state EHL solutions should satisfy load conservation **(1. 11)**.

Transient EHL curves will be generated by calculating Δh. If transient EHL curves show reasonable transitions, P_h^k and $P_{\dot{h}}^k$ from each steady-state EHL solution may be useful.

Oil film force evolves,

$$P^k=P_0^k+P_h^k\Delta h+P_{\dot{h}}^k\dot{h} \tag{1. 10}$$

Where, $\dot{h}=\frac{h_{0t}^{k}+\Delta h_{t}^{k}-h_{t-1}^{k}}{\Delta t}$.

Keep surface loading unchanged,

$$\sum(P_{h}^{k}\Delta h+P_{\dot{h}}^{k}\dot{h})=0 \tag{1. 11}$$

With equations **(1.5),** the fluctuation equation in **(1.9)** is reduced and architectured by perturbed Δh, variable $\dot{h}$ and some items incorporating steady-state solution (marked with A,B,C,D).

$$\begin{aligned}&12x\frac{d\dot{h}}{dx}+\frac{\partial}{\partial x}\left(\frac{{h_0}^3}{\eta}(P_h\frac{d\Delta h}{dx}+P_{\dot{h}}\frac{d\dot{h}}{dx})\right)\\&=12x\frac{d\dot{h}}{dx}+\frac{d\Delta h}{dx}\frac{\partial}{\partial x}(\frac{{h_0}^3}{\eta}P_h)+\frac{{h_0}^3}{\eta}P_h\frac{d^2\Delta h}{dx^2}+\frac{d\dot{h}}{dx}\frac{\partial}{\partial x}(\frac{{h_0}^3}{\eta}P_{\dot{h}})+\frac{{h_0}^3}{\eta}P_{\dot{h}}\frac{d^2\dot{h}}{dx^2}\\&=\underbrace{(\frac{\partial}{\partial x}(\frac{{h_0}^3}{\eta}P_{\dot{h}})+12x)}_{A}\frac{d\dot{h}}{dx}+\underbrace{\frac{{h_0}^3}{\eta}P_{\dot{h}}}_{B}\frac{d^2\dot{h}}{dx^2}+\underbrace{\frac{\partial}{\partial x}(\frac{{h_0}^3}{\eta}P_h)}_{C}\frac{d\Delta h}{dx}+\underbrace{\frac{{h_0}^3}{\eta}P_h}_{D}\frac{d^2\Delta h}{dx^2}=0\end{aligned} \tag{1. 12}$$

Distributed perturbed Δh and variable $\dot{h}$ are substituted by discrete forms.

$$\begin{cases}\frac{d\Delta h}{dx}=\frac{(\Delta h_t^k-\Delta h_t^{k-1})}{\Delta x^k}\\\frac{d^2\Delta h}{dx^2}=\frac{(\Delta h_t^k-\Delta h_t^{k-1})-(\Delta h_t^{k-1}-\Delta h_t^{k-2})}{(\Delta x^k)^2}\\\frac{d\dot{h}}{dx}=\frac{d\frac{h_{0t}^k+\Delta h_t^k-h_{t-1}^k}{\Delta t}}{dx}=\frac{(h_{0t}^k-h_{0t}^{k-1})+(\Delta h_t^k-\Delta h_t^{k-1})-(h_{t-1}^k-h_{t-1}^{k-1})}{\Delta x^k\Delta t}\\\frac{d^2\dot{h}}{dx^2}=\frac{(h_{0t}^k-2h_{0t}^{k-1}+h_{0t}^{k-2})+(\Delta h_t^k-2\Delta h_t^{k-1}+\Delta h_t^{k-2})-(h_{t-1}^k-2h_{t-1}^{k-1}+h_{t-1}^{k-2})}{(\Delta x^k)^2\Delta t}\end{cases} \tag{1. 13}$$

Where, the superscript k denotes the film thickness at location x_k and the subscript t the film thickness at time t.

Substituting **(1. 13)** into **(1. 12)**,

$$A\frac{(h_{0t}^{k}-h_{0t}^{k-1})-\Delta h_t^{k-1}-(h_{t-1}^{k}-h_{t-1}^{k-1})}{\Delta t}+B\frac{(h_{0t}^{k}-2h_{0t}^{k-1}+h_{0t}^{k-2})+(-2\Delta h_t^{k-1}+\Delta h_t^{k-2})-(h_{t-1}^{k}-2h_{t-1}^{k-1}+h_{t-1}^{k-2})}{\Delta x^{k}\Delta t}$$

$$-C\Delta h_t^{k-1}+D\frac{-2\Delta h_t^{k-1}+\Delta h_t^{k-2}}{\Delta x^{k}}=-A\frac{\Delta h_t^{k}}{\Delta t}-B\frac{\Delta h_t^{k}}{\Delta x^{k}\Delta t}-C\Delta h_t^{k}-D\frac{\Delta h_t^{k}}{\Delta x^{k}}$$

$$\Rightarrow$$

$$\underbrace{(A\frac{(h_{0t}^{k}-h_{0t}^{k-1})}{\Delta t}+B\frac{(h_{0t}^{k}-2h_{0t}^{k-1}+h_{0t}^{k-2})}{\Delta x^{k}\Delta t})}_{E}-\underbrace{(A\frac{(h_{t-1}^{k}-h_{t-1}^{k-1})}{\Delta t}+B\frac{(h_{t-1}^{k}-2h_{t-1}^{k-1}+h_{t-1}^{k-2})}{\Delta x^{k}\Delta t})}_{F}+\underbrace{(\frac{-A}{\Delta t}+\frac{-2B}{\Delta x^{k}\Delta t}-C+\frac{-2D}{\Delta x^{k}})}_{G}\Delta h_t^{k-1} \quad (1.\ 14)$$

$$+\underbrace{(\frac{B}{\Delta x^{k}\Delta t}+\frac{D}{\Delta x^{k}})}_{H}\Delta h_t^{k-2}=-\Delta h_t^{k}\underbrace{(\frac{A}{\Delta t}+\frac{B}{\Delta x^{k}\Delta t}+C+\frac{D}{\Delta x^{k}})}_{I}$$

$$\Rightarrow \Delta h_t^{k}=-\frac{E-F+G\Delta h_t^{k-1}+H\Delta h_t^{k-2}}{I}$$

Assume that two first increments of film thickness are zero at each state. **Dimensional** results under both steady and transient states:

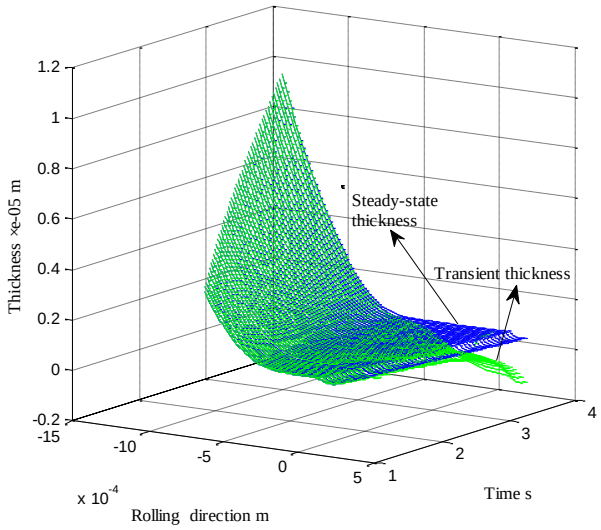

(Simulation step=0.00025s)

Figure1. 1: Transient oil film thickness distributions generated by steady-state solution

The figures briefly give the perturbed values, to find that steady-state P_h^k and $P_{\dot{h}}^k$ distributions cannot be used under transient EHL conditions, so that real transient values can't be perturbed with respect to steady-state solutions.

Under transient states, oil film changes Δh , $\Delta \dot{h}$ lead to new P_h , $P_{\dot{h}}$ and in turn affect integrated stiffness and damping coefficients. To upgrade the robustness, an extended usage of distributed parameters is performed below.

2.3 Solution of Transient EHL contact

Transient EHL procedure starts from steady-state solution. Newton-Raphson method has been explored explored by Houpert to solve steady-state EHL, as seen in **Appendix B**. To take advantage of proposed contact stiffness distribution, a new steady-state EHL algorithm is performed instead.

Film thickness equation is,

$$\begin{cases} h(x)=h^{*}+\dfrac{x^2}{2R}+\delta_k \\ \delta_k=-\dfrac{4}{\pi E}\int_{-b}^{b} p(s)\ln\left|\dfrac{s-x}{s-x_0}\right|ds \end{cases}$$

Based on deformation-matrix method,

$$\begin{cases} \delta_k=-\dfrac{2}{\pi E}\int_{x1}^{x2} p(s)\ln(x_k-s)^2 ds=-\dfrac{2}{\pi E}\sum_{i=1}^{n} p_i \int_{x1}^{x2}\varphi_i(s)\ln(x_k-s)^2 ds=\sum_{i=1}^{n} p_i D_{ik} \\ D_{ik}=\dfrac{1}{2\pi}(X_k-X_{k-1})\ln(X_k-X_i)^2 \qquad (i\neq k) \end{cases}$$

Film thickness equation turns into,

$$h(x)=h^{*}+\frac{x^2}{2R}+\sum_{i=1}^{n} p_i D_{ik} \tag{1.15}$$

Newton iterative method and the following frame constitute the solver.

$$A \qquad h_0=h^{*}+\frac{x^2}{2R}+\sum_{i=1}^{n} p_i D_{ik}$$

$$B \qquad \frac{h_0^3}{\eta}\frac{dP_h}{dx}+\frac{3h_0^2}{\eta}\frac{dP_0}{dx}=12u_x$$

$$C \qquad P^k=P_0^k+P_h^k\Delta h$$

$$D \qquad \frac{2b_{Hertz}}{N}\sum(P_h^k\Delta h)=0$$

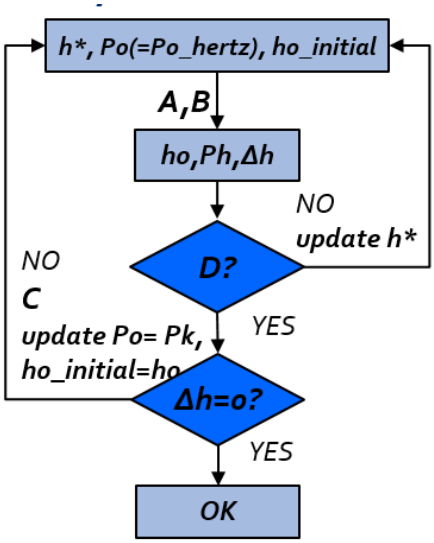

Figure1. 2: Reduced algorithm for steady-state EHL solution

The same advantage of proposed contact stiffness and damping distributions in solving transient EHL problem is also discovered.

Contact stiffness and damping distributions **(1. 4)** will fluctuate under transient states, changing film thicknesses along contact line. The successive states will be obtained by continuation method.

Assume that pressure increment along contact line relative to previous moment is Δp distribution. Thus, the updated film thickness and its increment are,

$$\begin{cases} h_t(x)=h^*+\dfrac{x^2}{2R}+\sum_{i=1}^{n}(p_i+\Delta p_i)D_{ik} \\ \Delta h(x)=h_t(x)-h_{t-1}(x) \end{cases} \tag{1. 16}$$

Real-time stiffness and damping distributions are $k(x), c(x)$ (equations **(1. 4)**) establish,

$$\Delta h(x)k(x)+\Delta\dot{h}(x)c(x)=\Delta p(x) \tag{1. 17}$$

Combining **(1. 16)** with **(1. 17)**,

$$[h^*+\frac{x^2}{2R}+\sum_{i=1}^{n}(p_i+\Delta p_i)D_{ik}-h_{t-1}(x)](k_{t-1}(x)+\frac{1}{\Delta t}c_{t-1}(x))=\Delta p_i \tag{1. 18}$$

Besides **(1. 18)**, conservation of load increment should be also satisfied.

$$\frac{2b_{Hertz}}{N}\sum\Delta p_i=Q(t+\Delta t)-Q(t) \tag{1. 19}$$

Combining **(1. 18)** with **(1. 19)**, the increments of film thickness and contact pressure under transient conditions can be obtained within a few steps by Newton iterative method.

Please note, in the dynamic process,

- Real-time update of contact grids
- Zero distributed stiffness under pure squeezing condition, but non-zero under both rolling and squeezing conditions

Newton iterative method and the following frame constitute the solver.

$$E \qquad h_t(x) = h^* + \frac{x^2}{2R} + \sum_{i=1}^{n}(p_i + \Delta p_i)D_{ik}$$

$$F \qquad \Delta h(x) = h_t(x) - h_{t-1}(x)$$

$$G \qquad \Delta p_i = P_h^k \Delta h + P_{\dot{h}} \Delta \dot{h}$$

$$H \qquad \frac{2b_{Hertz}}{N}\sum \Delta p_i = Q(t+\Delta t) - Q(t)$$

Using equation **(1. 18)**, equations *E*, *H*, *G* can turn to *I*, where $D = [D_{ik}]$.

$$\underbrace{h^* + \frac{x^2}{2R} + D\{p_i\} - \{h_{t-1}\}}_{\{h_c^*\}} + D\{\Delta p_i\} = \left\{ \frac{\Delta p_i}{\underbrace{k_{film} + \frac{c_{film}}{\Delta t}}_{CK(i,i)}} \right\}$$

$$I \qquad \{\Delta p_i\} = inv[I(N) - \frac{2\delta_{Hertz}}{P_{Hertz}} \times \underbrace{CIJ}_{=CK\times D}] \times (\underbrace{CK}_{=diag(CK(i,i))} \times \{h_c^*\})$$

$$CIJ(i,:) = D(i,:) \times CK(i,i)$$

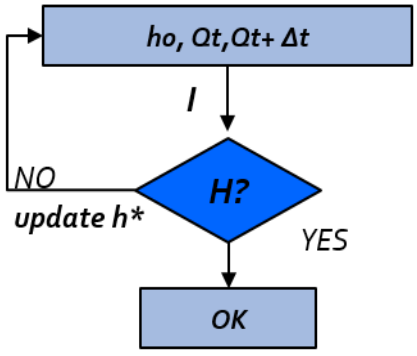

Figure1. 3: Reduced algorithm for transient EHL solution

Using proposed semi-analytical method, pure squeezing effect is calculated below, and its behaviours are studied after a sudden halting at rotating speed of U.

Case 1: U= 14.205 *m/s*, R=0.5*m*, E_0=2.273e+11, W= (1.0e-5+1.0e-5 t) E_0 R *N/m*, η_0=0.08

Dimensional results are given,

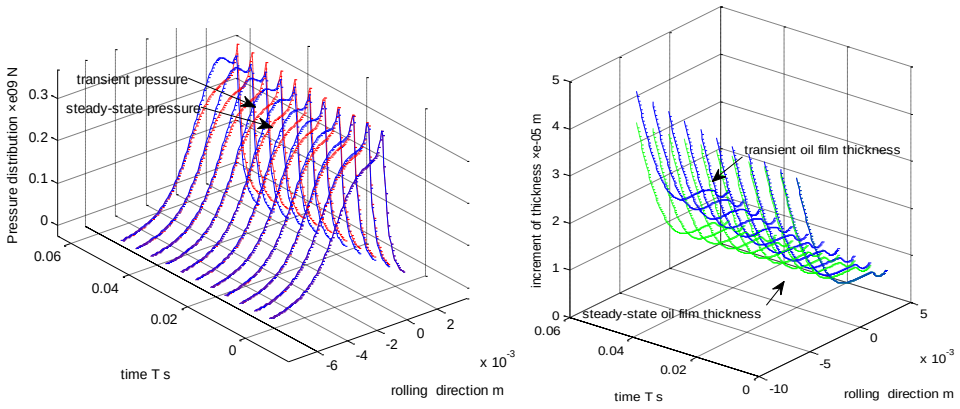

(Simulation step=0.005s)

Figure1. 4: Comparison of steady-state and transient EHL contact pressures and oil film thicknesses

During rapid acceleration and deceleration, the film behaviors are governed by two different mechanisms-fluid entrainment and film squeeze.

When load, speed and others fluctuate or experience essential changes in operation, transient squeeze effect occurs inevitably. **Figure1. 5** captures what happens when squeeze effect takes place during loading, and immediate disappearance of rolling speeds involved enables pure squeeze effect to be specifically considered. Zero time is assumed to halt rolling motions.

Case 2: R=0.5*m*, E_0=2.273e+11, W= (1.0e-5+1.0e-5 t) E_0 R *N/m*, η_0=0.08.

Dimensional results are given,

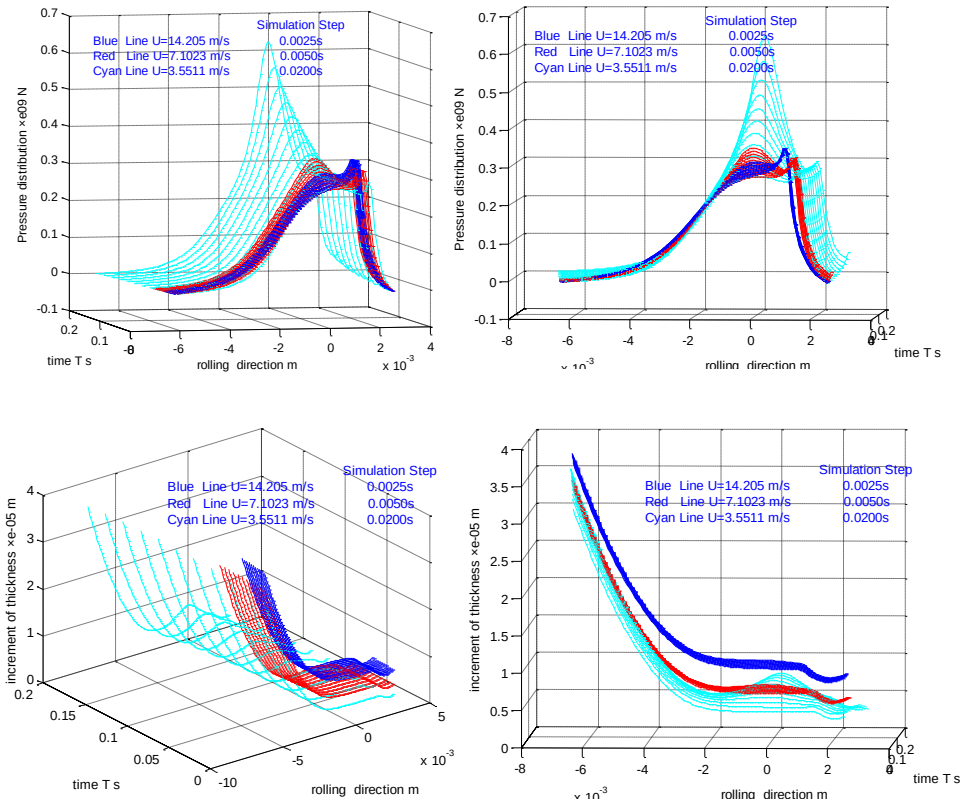

Figure1. 5: Transient EHL solutions under different entrainment velocities

Figure1. 5 advocates how the curves change under pure squeeze action when initial oil film state is differently selected. These initial states are generated under different entrainment speeds.

The findings are

- Two pressure peaks occur near Hertzian contact centre and outlet. With load increasing, the second pressure peak tends to approach Hertz pressure curve, the mutual influence (lubricant and elastic bodies) is fading away at a longer loading time.
- The transient oil film distributes more thickly compared to the steady-state solutions. With load increasing, both film peak and the second pressure peak slowly move towards contact centre.
- The overall effect of entrainment speed (exits only at zero moment) on transient EHL resembles that on steady-state EHL. Distributed damping and stiffness of oil film are excited differently under distinct rolling speeds.

Considering engineering facts, only squeezing action remains when the contact media stop rolling. The method proposed herein cannot work for a long simulation time since squeezing effect is fading away with time going by. Fortunately, some traces have been found at the early stage of this simulation that Hertz pressure distribution will replace it eventually.

As for oil film growth at contact center, lubricants are explained to fail to escape immediately due to the sudden stop of rolling motion. Practically, motion change needs time. The pure squeezing action rarely exists if it evolves from normal lubricating operation. However, according to transient phenomena of oil film tested under ball longitudinal oscillation (**Figure1. 6**), Romeo P. Glovnea and Hugh A. Spikes **[23]** gave the same reason that during rapid deceleration, the formation of fluid entrapment dominated the film thickness over the contact; meanwhile, the depth and shape of this entrapment is dependent of the rate of speed variation. Zero halting time assumed in this chapter is an extreme situation, but also tells a same significant truth of existence of fluid entrapment.

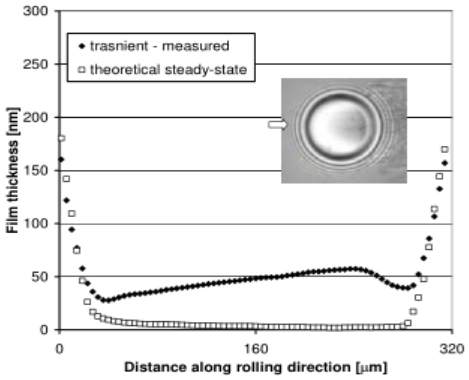

Figure1. 6: Film thickness profile during rapid deceleration in longitudinal oscillatory motion (Romeo P. Glovnea and Hugh A. Spikes, 2005)

In most cases, both entrainment and squeezing effects participate, even in the machine halting. The corresponding case is calculated below.

R=0.5*m*, E_0=2.273e+11, W= (1.0e-5+1.0e-5 t) E_0 R *N/m*, η_0=0.08

Dimensional results are given,

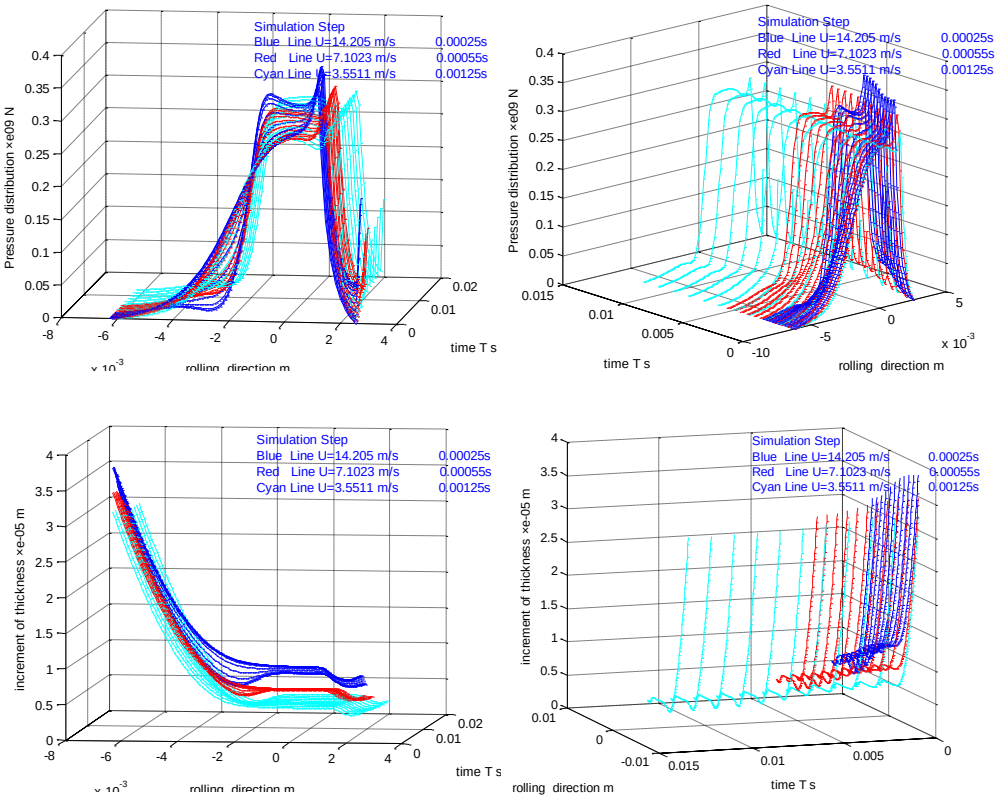

Figure1. 7: Transient EHL solutions under different entrainment velocities

The figures show:

- Two pressure peaks occur near inlet and outlet. The pressure near inlet point distributes more steeply than steady-state solution. Besides, the more load increases, the more steeply inlet pressure climbs..
- The transient oil film distributes less thickly with load increasing. The oil films also shrink at inlet point compared to steady-state solution.
- With entrainment velocity increasing, pressure tends to distribute close to contact center. Oil film thickness increases and takes more effect.

Oil film transition between successive states is simulated with oil film stiffness and damping fluctuating at the same contact area. But pressure and thickness distributions involved should be updated in time to reproduce each new transient state.

Please remember, it is still a dummy transition. Different from the simulation on pure squeeze effect, in this case, the growth in oil inlet can be well predicted, but the recovery in oil exit cannot. Due to rolling, the oil film stiffness and damping distributed near the oil outlet

should be partly abandoned. If cavitation can be well located during rolling, the force jump at the oil outlet will naturally disappear in simulation.

2.4 Conclusion

An extended use of perturbation method is made to prove that steady-state EHL contact damping and stiffness distributions should not be used to analyze the transient conditions, let alone acquire equivalent total contact damping and stiffness coefficients for dynamic analysis.

By regarding the steady-state solution of EHL as initial state, and continuously acquiring EHL stiffness and damping distributions, dynamic mechanical behaviors of oil film are predicted. The method proposed herein in fine provides a possible insight to understand the distributions of EHL oil film damping and stiffness, which can be extended for transient point EHL problem as a fast calculating technique. The idea proposed can be easily delivered to any engineer.

2.5 References

[1] Hamrock, B. J., and Dowson, D., 1976, Isothermal EHD Lubrication of Points Contacts: Part I—Theoretical Formulation, ASME J. Lubr. Technol., 98, No. 2, pp. 223–229.

[2] Dowson, D., Higginson, G. R., 1966, Elasto-Hydrodynamic Lubrication, SI, Oxford, Pergamon Press Ltd, p. 236.

[3] Evans H P, Snidle R W. Inverse solution of Reynolds equation of lubrication under point-contact elasto-hydrodynamic conditions. Journal of Lubrication Technology, 1981, 103(4): 539–546.

[4] Rohde SM, Oh KP. A unified treatment of thick and thin film elasto-hydrodynamic problems by using higher order element methods. Proceedings of the Royal Society A: Mathematical, Physical and Engineering Sciences, 1975; 343(1634): 315–331.

[5] Oh K P, Rohde S M. Numerical solution of the point contact problem using the finite element method. International Journal for Numerical Methods in Engineering, 1977, 11(10): 1507–1518

[6] Houpert, L.G., Hamrock, B.J., Fast Approach for calculating Film Thicknesses and Pressures in Elasto-hydrodynamically Lubricated Contacts at High Loads, J. of Tribology, Vol.108, No.3, 411~420,1986.

[7] Lubrecht A A, Ten Napel W E, Bosma R. Multigrid, An alternative method for calculating film thickness and pressure profiles in elasto-hydrodynamically lubricated line contacts. ASME Journal of Tribology, 1986, 108(4): 551–556.

[8] Venner C H. Multilevel solution of the EHL line and point contact problems. PhD Thesis, University of Twente, Endschende, the Netherlands, 1991.

[9] Wang Z J, Wang W Z, Wang H, and Hu Y Z. Stress Analysis on Layered Materials in Point Elastohydrodynamic-Lubricated Contacts. Tribology Letters, 2009, 35(3):229-244.

[10] Chang, L., "A Simple Accurate Method to Calculate Transient EHL Film Thickness in Machine Components Undergoing Operation Cycles," Trib. Trans., 43, 1, 116~222, 2000.

[11] Messe, S., and Lubrecht, A. A., "Approximating EHL Film Thickness Profiles Under Transient Conditions", ASME J. Tribol., 124, 443~447, 2002.

[12] Walford T.L.H., Stone B., J. "The sources of damping in rolling element bearings under oscillating conditions", Proc. Instn Mech. Engrs, Part C: J. Mechanical Engineering Science, 197, 225~232, 1983.

[13] G.D.Hagiu, M.D.Gafitanu. "Dynamic characteristics of high speed angular contact ball bearings", Wear, 211, 22~29, 1997.

[14] Dietl P. Damping and stiffness characteristics of rolling element bearings. PhD thesis. Technischen Universität Wien; 1997.

[15] Wensing J. On the dynamics of ball bearings. PhD thesis. University of Twente, Enschede; 1998.

[16] Nonato F, Cavalca K. "On the non-linear dynamic behaviour of elasto-hydrodynamic lubricated point contact". Journal of Sound and Vibration 2010;329: 4656–71.

[17] Benedikt Wiegert, Hartmut Hetzler, etc., "A simplified elasto-hydrodynamic contact model capturing the nonlinear vibration behaviour", Tribology International, 59 (2013) 79–89.

[18] Wiegert B, Hetzler H, Seemann W. "An analytical expression of the normal force of hydrodynamic line contacts under transient conditions". Tribology International, 61 (2013) 32–39.

[19] Sarangi, M., Majumdar, B.C., and Sekhar, A.S. “Stiffness and damping characteristics of lubricated ball bearings. Part 1: theoretical formulation” Proc. Instn Mech. Engrs, Part J: J. Engineering Tribology, 218(6), 529~538, 2004.

[20] Chippa, S.P. and Sarangi, M., “On the Dynamics of Lubricated Cylindrical Roller Bearings, Part I: Evaluation of Stiffness and Damping Characteristics”, Tribology Transactions, 56, 1087~1096, 2013.

[21] Chippa, S. P. and Sarangi, M., “On the Dynamics of Lubricated Cylindrical Roller Bearings, Part ii: linear and nonlinear vibration analysis”, Tribology Transactions 56 (6), 1097~1108, 2013.

[22] Grubin, A. N., "Fundamentals of the Hydrodynamic Theory of Lubrication of Heavily Loaded Cylindrical Surfaces." Central Scientific Research Institute for Technology and Mechanical Engineering, 30. Moscow, Kh. F. Ketova (ed.), D.S.I.R. London Translations No. 337, 115~166, 1949.

[23] Romeo P. Glovnea and Hugh A. Spikes, "EHD contacts in low-amplitude oscillatory motion". Proceedings of World Tribology Congress 2005, Washington, D.C., USA, September 12-16, 2005.

Appendix A Perturbation Formulation for stiffness and damping distribution

In Reynolds equation, main variables are perturbed with respect to its steady-state values, so the perturbed film thickness terms and corresponding pressure changes are given by,

$$\begin{cases} h=h_0+\Delta h \\ P=P_0+P_h\Delta h+P_{\dot{h}}\Delta\dot{h} \end{cases} \tag{A.1}$$

Where,

$$P_h=\frac{\partial P}{\partial h}, P_{\dot{h}}=\frac{\partial P}{\partial \dot{h}} \tag{A.2}$$

After substituting the perturbed terms **(A.1)** into Reynolds equation:

$$\frac{\partial}{\partial x}\left(\frac{(h_0+\Delta h)^3}{\eta}\frac{d(P_0+P_h\Delta h+P_{\dot{h}}\Delta\dot{h})}{dx}\right)=12u\frac{\partial(h_0+\Delta h)}{\partial x}+12\frac{\partial(h_0+\Delta h)}{\partial t} \tag{A.3}$$

Where, terms containing $\Delta\dot{h}^n\Delta h^m,(n+m>1)$ are neglected.

According to what is referred in **[19]**, three equations are acquired,

$$\begin{cases} \frac{\partial}{\partial x}\left(\frac{h_0^3}{\eta}\frac{dP_0}{dx}\right)=12u\frac{\partial h_0}{\partial x}\ \text{for}(\Delta h,\Delta\dot{h})^0 \\ \frac{\partial}{\partial x}\left(\frac{h_0^3}{\eta}\frac{dP_h}{dx}+\frac{3h_0^2}{\eta}\frac{dP_0}{dx}\right)=0\ \text{for}(\Delta h)^1 \\ \frac{\partial}{\partial x}\left(\frac{h_0^3}{\eta}\frac{dP_{\dot{h}}}{dx}\right)-12=0\ \text{for}(\Delta\dot{h})^1 \end{cases} \tag{A.4}$$

Appendix B Solution of steady-state EHL problem

Newton-Raphson method (Houpert etc.) is used to calculate it.

Reynolds equation, $f(p)=\frac{d}{dx}\left(\frac{\rho h^3}{\eta}\frac{dp}{dx}\right)-12u\frac{d(\rho h)}{dx}=0$

For compressible fluids, $f(p)=\frac{dp}{dx}-12\eta u\frac{(1-\frac{\rho_e h_e}{\rho h})}{h^2}=0$

By Newton-Raphson method, it is changed to $f(p_k)+(p_{k+1}-p_k)\frac{df(p_k)}{dp}=0$

Dimensionless variables are made below,

$$X=\frac{x}{b},\quad P=\frac{p}{p_H},\quad \delta_H=\frac{b^2}{2R},\quad H_0=\frac{h_0}{2\delta_H},\quad \bar{\rho}=\frac{\rho}{\rho_0},\quad \bar{\eta}=\frac{\eta}{\eta_0},$$
$$\bar{W}=\frac{w}{ER},\quad G=\alpha E,\quad \bar{\delta}=\frac{\delta}{\delta_H},\quad H=\frac{h}{2\delta_H},\quad K=\frac{3}{4}\pi^2\frac{\bar{U}}{\bar{W}^2}$$

Dimensionless form of Reynolds equation is given by,

$$f_i=H_i^3\left(\frac{dP}{dX}\right)_i-K\bar{\eta}_i\left(H_i-\frac{\bar{\rho}_e H_e}{\bar{\rho}_i}\right)=0 \tag{B.1}$$

Thickness is given by

$$H_i=H_0+\frac{X_i^2}{2}+\sum_{j=1}^{N}D_{ij}P_j \tag{B.2}$$

$\bar{\rho}_i$ is given by,

$$\bar{\rho}_i=1+\frac{0.6\times10^{-9}P_H P_i}{1+1.7\times10^{-9}P_H P_i} \tag{B.3}$$

The viscosity-pressure is given by Roeland,

$$\bar{\eta}_i=\frac{\eta_i(\text{unit,Pa·s})}{\eta_0}=\exp\{\frac{\alpha P_L}{z}[(1+\frac{P}{P_L})^z-1]\} \tag{B.4}$$

Where, $\alpha(\text{unit, GPa}^{-1})=\frac{z}{P_L}(\ln\eta_0+9.67)$, $P_L=0.196GPa$, z = 0.5 □ 0.98

It will be solved with load balance condition and boundary conditions.

$$w=\int_{x_1}^{x_e} p dx \text{ or } \int_{x_1}^{x_e} P dx=\frac{\pi}{2} \text{ and } P_{x_1}=0\,,\ \frac{\partial P}{\partial x}|x_e=0$$

By setting iterative increments $(\Delta\bar{\rho}_e H_e)^n,(\Delta P_j)^n,(\Delta H_0)^n$,

$$\begin{cases}(\bar{\rho}_e H_e)^n=(\bar{\rho}_e H_e)^o+(\Delta\bar{\rho}_e H_e)^n\\ P_j^n=P_j^o+(\Delta P_j)^n\\ H_0^n=H_0^o+(\Delta H_0)^n\end{cases}$$

Iterative style is

$$(\frac{\partial f_i}{\partial(\bar{\rho}_e H_e)})^o(\Delta(\bar{\rho}_e H_e))^n+\sum_{j=2}^{N}(\frac{\partial f_i}{\partial P_i})^o(\Delta P_j)^n+(\frac{\partial f_i}{\partial H_0})^o(\Delta H_0)^n=-f_i^o,i=1,..,N \tag{B.5}$$

Load balance condition is $\int_{X_1}^{X_e}(\Delta P)^n dX=\frac{\pi}{2}-\int_{X_1}^{X_e}P^o dX=(\Delta W)^o$

And the corresponding matrices style is

$$\begin{bmatrix}\frac{\partial f_1}{\partial(\bar{\rho}_e H_e)} & \frac{\partial f_1}{\partial P_2} & \cdots\cdots & \frac{\partial f_1}{\partial P_N} & \frac{\partial f_1}{\partial H_0}\\ \frac{\partial f_2}{\partial(\bar{\rho}_e H_e)} & \frac{\partial f_2}{\partial P_2} & \cdots\cdots & \frac{\partial f_2}{\partial P_N} & \frac{\partial f_2}{\partial H_0}\\ \cdots\cdots & \cdots\cdots & \cdots\cdots & \cdots\cdots & \cdots\cdots\\ \frac{\partial f_N}{\partial(\bar{\rho}_e H_e)} & \frac{\partial f_N}{\partial P_2} & \cdots\cdots & \frac{\partial f_N}{\partial P_N} & \frac{\partial f_N}{\partial H_0}\\ 0 & c_2 & \cdots\cdots & c_N & 0\end{bmatrix}^o\begin{Bmatrix}\Delta(\bar{\rho}_e H_e)\\ \Delta P_2\\ \vdots\\ \Delta P_N\\ \Delta H_0\end{Bmatrix}^n=\begin{Bmatrix}-f_1\\ -f_2\\ \vdots\\ -f_N\\ \Delta W\end{Bmatrix}^o \tag{B.6}$$

The numerical method of Gaussian elimination is used to get the solution.

Chapter 2
Calculation on distributed forces and moments of bearing

2.1 Introduction

Poor roller end design as well as misalignment in bearing-shaft motion gives rise to pressure concentration and potential damage. In practice, SRBs (Spherical roller bearing) or TRBs (Taper roller bearing) frequently accept multidirectional motions or loads, so that misalignment turns into one of the main failure factors. Some researches **[24]** point out that the logarithmic roller profile produces uniform pressure distribution along roller length under uniform loading, but regular tilting motions (uneven loading) still cause frequent pressure concentration. So it requires an accurate calculation on force and moment distributions in a bearing for predicting bearing stiffness matrix, which is essential to demonstrate how well bearing accepts misalignments in transmission system.

How lamina load relates to local deflection determines roller position and load distribution in bearing equilibrium. Slicing technique is a popular way to describe complex load distribution in a bearing, but it is also understood that it fails to consider interaction among laminas. The question that arouses our interest is the choice between classical slicing technique **[25]** and essential contact algorithm **[26]~[29]**, when it refers to bearing transmission analysis under heavy-loaded conditions, under frequent tilting motions, and others.

Bruno Mevel **[30]~[31]** recently(2013,2016) addresses how the roller equilibrium is influenced by the calculation method. His work happens to meet with our interest in improving bearing stiffness. Since tilting motion takes responsibility for load concentration in roller end, this effect will be on significant components of bearing stiffness matrix, affecting prediction on stability of system when applied to dynamic system. More concerns about how to find a better solution in bearing transmission should be taken, both in calculation efficiency and in accuracy.

Linear classical lamina load is applied along roller length, as Harris formula explained by Taylor expansion. This failure of missing edge effect requires better codes development in simulation.

Although CG-mlms **[32]** or CG-FFT **[33]** methods greatly extend our insight into knowledge about contact problem including roughness, indents etc., most engineering problems still need time-saving solution. This spectacular performance is not necessary for bearing transmitting calculation. Interest is to find time-saving solution of existing theories.

Based on Bousinesq work, second approximation method was typically performed by Reusner H.(1960) **[27]**, Hartnett(1980)**[28]**and Jan M. de Mul, Joost J. Kalker (1998) **[29]** and others. They solved it in a similar way. However, pressure distribution in each slice was differently assumed to be semi-elliptical, uniform and parabolic. Technically, the first needs a time-consuming numerical calculation; the second presented by an analytical formulation causes a gross error; the third is also formulated analytically, but needs more discussion on potential error of contact width. Following their steps, the author of this thesis also develops an improved calculation by using some transverse rectangular strips to symmetrically replace elliptically-distributed pressure shape.

Compared to second approximation method, first approximation method is less popular in accuracy, but more in efficiency. In this chapter, first approximation method of R.Teutsch **[26]** will be developed from a new perspective.

Involved in this alternative technique, the fundamental load-deflection relation is particularly important. Hertz gave a width relation in line contact, but did not publish its deflection relation. The unknown issue was later discussed over a century. The relevant results are listed in **Appendix C**. N.Ahmadi and M.R. Hoeprich used numerical method, Palmgren and Kunert empirical method, others analytical method; Palmgren**[34]**, Kunert**[35]**, Houpert**[36]** and Teutsch R.**[26]**obtained explicit solutions, while Lundberg**[36]**, Tripp**[38]**, Dinnik**[39]**, Kowalsky**[39]** and others acquired implicit solutions.

Incorporated in this alternative technique, roller discretization (slice number) is also crucial to solution accuracy as found by Singh and Paul**[26].** An average technique (ever called as Method of redundant field points) was then adopted**[26]**. A similar strategy of normalization by mean values of all weighting functions was used by R.Teutsch[**26]** as well.

The accuracy of AST is skillfully discussed in this chapter. The corresponding strategies and another reduced roller contact algorithm are proposed to maintain its technical robustness and convenience to engineering problems.

With bearing questions differently argued, plenty of works are also differently performed to consider from normal contact to tangential contact and from contact model to bearing model. However, effective lubrication functionally ensures little tangential force. Bearing force is transmitted by normal contact rather than by tangential contact considering order of magnitude of force. Although insufficient and uneven oil film forces could result in roller slip and roller skewing respectively, tangential oil film damping, roller/rib resistance and cage constraint would ensure assumption on the normal contact in direct bearing model.

In order to reduce repeated calculations for each roller balance, as well as to easily solve bearing stiffness matrix, direct bearing model (Stribeck, Harris, Luc-Houpert 1997**[40]**) is technically convenient to use, compared to equilibrium loop model (Liu, J. 1989**[41]**, D.N Gias 2003**[42]**, etc.) and dynamic model (Gupta**[43]**, etc.). And, it is wise to choose relative motions between races as model inputs, in which case, by being part of dynamic system, races are balanced dynamically instead of statically.

In this chapter, the works to better predict bearing stiffness matrix include,

1. First and second approximation methods are versatilely used to develop alternative slicing technique (AST) and reduced roller contact algorithm (RRCA), with the error caused by AST explained.

2. Improvements of second approximation method;

- Semi-analytical method of flexible rectangular pressure strips inside slice is versatilely used to bridge an analytical and fast way to calculation;

- Semi-empirical method of enhanced load-deflection relation along slice thickness is used to stably obtain roller moment distributions;

3. Direct bearing model is used to calculate loads (three forces F_x,F_y,F_z and two moments M_y,M_z) with five relative displacements acknowledged (three linear displacements d_x,d_y,d_z and two angular displacements $d\theta_y$,$d\theta_z$);

4. Bearing-rotor vibrating characteristics are predicted by bearing stiffness matrix calculated by finite differential method **[44]**.

2.2 Deformation distribution in direct bearing model

With five known displacements applied on the bearing as showed in **Figure2. 1**, initial and general relative positions of cone and cup are shown, and the rollers occupied in loading area undergo elastic deformation which will be calculated in this part.

To develop general codes, initial geometric relations in a bearing are prescribed.

- When *dy* and *dz* are nil, central lines of cone and cup coincide with each other.
- *dx* equal to zero corresponds to both raceways just touching rolling elements.

Please note, the same "zero" convention still works when describing a double-row rolling element bearing.

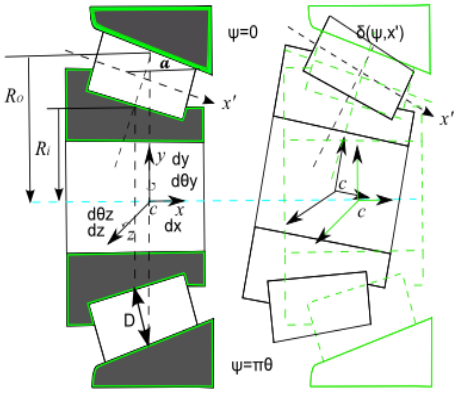

Figure2. 1 Geometric relation in taper roller bearing (Houpert)

Using Euler angles, relative rotations between raceways are described. Under the provision that rotation is successively around *z* axis and updated *y* axis, additional displacement of roller/cup contact position $\begin{bmatrix} x \\ y \\ z \end{bmatrix} = \begin{bmatrix} D\sin\alpha + x'/\cos\gamma \times \cos\alpha \\ (R_O - x'/\cos\gamma \times \sin\alpha)\cos\psi \\ (R_O - x'/\cos\gamma \times \sin\alpha)\sin\psi \end{bmatrix}$ caused by tilting motions between races is given.

$$\begin{bmatrix} \Delta d_x \\ \Delta d_y \\ \Delta d_z \end{bmatrix} = \begin{bmatrix} x \\ y \\ z \end{bmatrix} - \begin{bmatrix} \cos(d\theta_y)\cos(d\theta_z) & \cos(d\theta_y)\sin(d\theta_z) & -\sin(d\theta_y) \\ -\sin(d\theta_z) & \cos(d\theta_z) & 0 \\ \sin(d\theta_y)\cos(d\theta_z) & \sin(d\theta_y)\sin(d\theta_z) & \cos(d\theta_y) \end{bmatrix} \begin{bmatrix} x \\ y \\ z \end{bmatrix} \tag{2.1}$$

Deflection calculation follows the assumption made in the model, so that different manners in which deformation distributes in the roller should be distinguished between different models to clarify the possibly induced error.

In both equilibrium loop model and dynamic model, deflection is measured between geometric centers of mating bodies, while, in direct bearing model, displacement of contact point at mating surface is directly used without considering the shape of contact bodies.

Herein, the effect of contact body shapes on deflection distribution in direct bearing model is considered. Roller/cup interference along roller length at azimuth angle ψ is suggested as

$$\delta(\psi, x') = (d_x + \Delta d_x)\sin\alpha + \{(d_y + \Delta d_y)\cos\psi + (d_z + \Delta d_z)\sin\psi + \ldots$$
$$\ldots[(R_O - (x'/\cos\gamma \times \sin\alpha + (d_X + \Delta d_X)\tan\alpha))(1 - \cos\Delta\psi(x'))]\}\cos\alpha \quad (2.2)$$

It is specifically proposed that in case of tilting motions, the roller needs to deform curved part in cup. This part overcome by additional loading will recover with time going by, as shown by $A^2_{initial}$ in **Figure2.2**. Proposed deformation consists of (a) displacement of contact point at azimuth angle ψ (penetrating into a wedge with conical degree α), and (b) curved part before penetrating into a wedge.

As shown in **Figure2.3,** contact curve C_1C_2 in the cup incorporating contact point (ψ, x') will axially move due to $d_X, \Delta d_X$ rather than $d_y, \Delta d_y, d_z, \Delta d_z$.

Where, x' is abscissa along the roller length.

$\Delta\psi(x')$ is increment of azimuth angle due to deformation recovery of cup edge.

$$\Delta\psi(x') = \arcsin\frac{(d_y+\Delta d_y)\sin\psi+(d_z+\Delta d_z)\cos\psi}{R_O-(x'/\cos\gamma\times\sin\alpha+(d_X+\Delta d_X)\tan\alpha)} \quad (2.3)$$

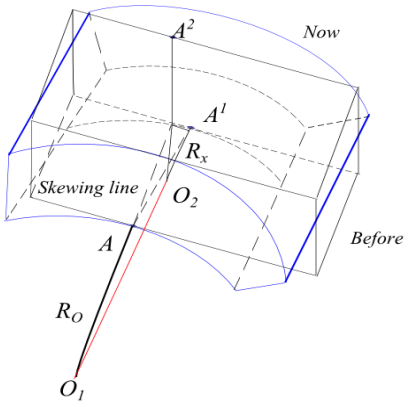

Figure2.2

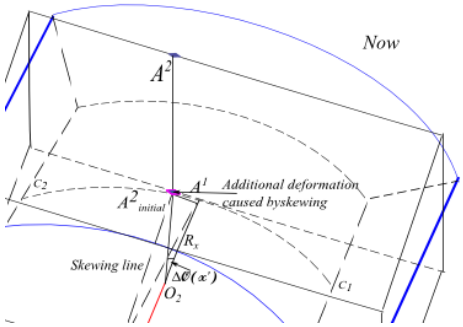

Figure2.3

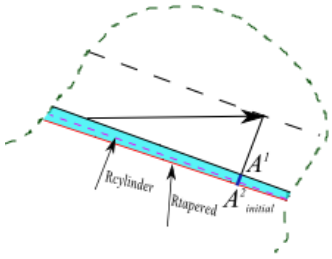

Figure2.4

Figure 2.2~2.4 additional skewing deformation

Please note, point A^2 is attached in the roller, moving from point A and penetrating into the cup, while point A^1 is the original position of roller point A^2 and point $A^2_{initial}$ the recovering position of cup edge point A^2.

2.3 Calculating strategies for Bearing force and moment

In one roller, load applied on contact point *x* will be calculated herein by alternative slicing technique (AST, used by R.Teutsch**)** instead of classical slicing technique (CST) to investigate interaction among *N* slices in roller of length *L*.

$$x=-L/N+0.5L/N: L/N: L/N+0.5L/N \tag{2. 4}$$

2.3.1 Classical Roller Contact Calculations (Classical Slicing Technique)

In general use, deflection-load relation is described analytically and explicitly.

$$\delta=0.39[4(1-\upsilon_1^2)/E_1+4(1-\upsilon_2^2)/E_2]^{0.9}.\frac{Q^{0.9}}{L^{0.8}}(N, m) \tag{2. 5}$$

(Palmgren, empirical formula)

$$\delta_o=\delta_i=3.84\times10^{-5}.\frac{Q^{0.9}}{L^{0.8}}\ (N,\ mm) \tag{2. 6}$$

(Palmgren, $E_1 = E_2 = 206Gpa, \nu_1 = \nu_2 = 0.3$)

In slicing technique, $p=\frac{Q}{N}$ is exercised, and $c=\frac{Q_i}{Q_o}=\frac{\sin(\theta_o+\theta_f)}{\sin(\theta_i+\theta_f)}\approx0.99$ is used to revise the mechanical relation in a tapered roller (**Figure2.5**).

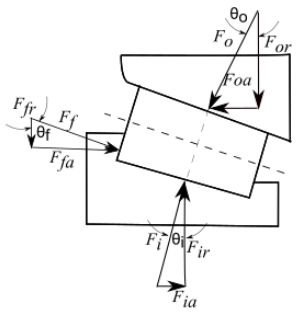

Figure2.5 Loading in a tapered roller

Slice/unit force is given by Harris (1984), using a linearized fraction of total roller stiffness calculated from Palmgren's equation to describe each slice in case of misalignment.

$$p(x)=k_{lc}(\delta_i+\delta_o)^{1.1} \tag{2. 7}$$

$$k_{lc} = 7.85\times10^{4}\cdot[1+c^{0.9}\cos(\theta_o-\theta_i)]^{-1.11}\cdot L^{0.8889}/L\ \text{(Tapered Roller, N, mm)}$$

$$k_{lc} = 3.6735\times10^{10}\cdot L^{0.8889}/L(orN)\ \text{(Cylindrical roller, N, m)}$$

$$(E_1 = E_2 = 206Gpa, \nu_1 = \nu_2 = 0.276)$$

Generalized binomial expansion enables integration method (Houpert **[40]** and others) to calculate it very fast.

$$p(x) = k_{lc}\left(\delta_{centre}+\Delta\delta\right)^{1.1} = k_{lc}\left(\delta_{centre}+x\theta\right)^{1.1} \approx k_{lc}\left[\delta_{centre}^{1.1}+1.1\delta_{centre}^{0.1}x\theta\right] \tag{2. 8}$$

$$M = \left[p(x)-p(0)\right]x \approx 1.1k_{lc}\delta_{centre}^{0.1}\theta x^2 \tag{2. 9}$$

$$p = \int_{-\frac{L}{2}}^{\frac{L}{2}} p(x)dx = k_{lc}L\delta_{centre}^{1.1} \tag{2. 10}$$

$$M = \int_{-\frac{L}{2}}^{\frac{L}{2}} M(x)dx = \frac{1.1}{2} k_{lc} L^2 \delta_{centre}^{0.1} \theta \tag{2. 11}$$

Summation method can also provide the load and moment distributions.

$$\begin{cases} F_{\varphi x} = \sin\alpha \sum_{i=1}^{N} p_i \\ F_{\varphi y} = \cos\varphi\cos\alpha \sum_{i=1}^{N} p_i \\ F_{\varphi z} = \sin\varphi\cos\alpha \sum_{i=1}^{N} p_i \end{cases} \quad \begin{cases} M_{\varphi y} = -\sin\varphi\cos\alpha \sum_{i=1}^{N} p_i \cdot (i - \frac{N-1}{2} - 1) \cdot L/N \\ M_{\varphi z} = \cos\varphi\cos\alpha \sum_{i=1}^{N} p_i \cdot (i - \frac{N-1}{2} - 1) \cdot L/N \end{cases} \tag{2. 12}$$

Equivalent forces and moments at all roller centers are transmitted to $R_i \tan\alpha$ point in cone central line. Within scope of theoretical mechanics, bearing loads are calculated.

$$\begin{cases} Q_x = \sum_{\varphi=\varphi_0}^{\varphi_N} F_{\varphi x} \\ Q_y = \sum_{\varphi=\varphi_0}^{\varphi_N} F_{\varphi y} \\ Q_z = \sum_{\varphi=\varphi_0}^{\varphi_N} F_{\varphi z} \end{cases} \quad \begin{cases} M_y = +R_i \cdot \tan\alpha \cdot Q_z + \sum_{\varphi=\varphi_0}^{\varphi_N} M_{\varphi y} \\ M_z = -R_i \cdot \tan\alpha \cdot Q_y + \sum_{\varphi=\varphi_0}^{\varphi_N} M_{\varphi z} \end{cases} \tag{2. 13}$$

General codes are also developed for double-row tapered roller bearing. Due to symmetry of the rollers at double rows, integrated model can be decomposed into uniform sub-models which accept inputs and transmit loads in different manners. Both coordinates transformation and load reconfiguration used improve general calculation in input and output stages.

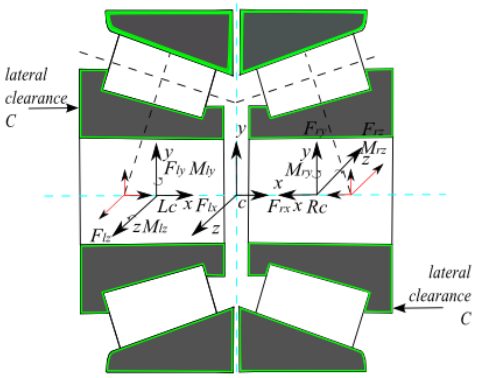

Figure2. 6 Load transmissions in double row tapered roller bearing

According to equation **(2.1)**, line displacements of each row center caused by five displacements of entire bearing are given by,

$$\begin{bmatrix} d_x\_i^{th}row \\ d_y\_i^{th}row \\ d_z\_i^{th}row \end{bmatrix} = \begin{bmatrix} x \\ y \\ z \end{bmatrix} - \begin{bmatrix} \cos(d\theta_y)\cos(d\theta_z) & \cos(d\theta_y)\sin(d\theta_z) & -\sin(d\theta_y) \\ -\sin(d\theta_z) & \cos(d\theta_z) & 0 \\ \sin(d\theta_y)\cos(d\theta_z) & \sin(d\theta_y)\sin(d\theta_z) & \cos(d\theta_y) \end{bmatrix} \begin{bmatrix} x \\ y \\ z \end{bmatrix} + \begin{bmatrix} d_x \\ d_y \\ d_z \end{bmatrix} \quad (2.\ 14)$$

$$\begin{bmatrix} d_{realx}\_i^{th}row \\ d_{realy}\_i^{th}row \\ d_{realz}\_i^{th}row \end{bmatrix} = \begin{bmatrix} \pm d_x\_i^{th}row \\ d_y\_i^{th}row \\ \pm d_z\_i^{th}row \end{bmatrix} - \begin{bmatrix} C \\ 0 \\ 0 \end{bmatrix} \quad (2.\ 15)$$

Where, $\begin{bmatrix} x \\ y \\ z \end{bmatrix} = \begin{bmatrix} -e_r \\ 0 \\ 0 \end{bmatrix}$, $^{+}(\text{in}^{\pm})$ for left row, and $\begin{bmatrix} x \\ y \\ z \end{bmatrix} = \begin{bmatrix} e_r \\ 0 \\ 0 \end{bmatrix}$, $^{-}(\text{in}^{\pm})$ for right row.

Angular displacements of each row are also revised according to relative change of right and left coordinate systems.

$$\begin{cases} d\theta_{yreal}\_right^{th}row = d\theta_{yreal}\_left^{th}row = d\theta_y \\ d\theta_{zreal}\_right^{th}row = -d\theta_{zreal}\_left^{th}row = -d\theta_z \end{cases} \quad (2.\ 16)$$

Hence, total load that cup applies on cone is derived according to **Figure2. 6**.

$$\begin{cases} F_x = F_{lx} - F_{rx} \\ F_y = F_{ly} + F_{ry} \\ F_z = F_{lz} - F_{rz} \end{cases} \qquad \begin{cases} M_y = -(F_{lz} + F_{rz})e_r + (M_{ly} + M_{ry}) \\ M_z = -(F_{rz} - F_{ly})e_r + (M_{lz} - M_{rz}) \end{cases} \quad (2.\ 17)$$

It is exposed that load peaks (summation method) will be weakened compared to integrated results when bearing rotates, for higher order items in "generalized binomial expansion" vanish in integration method. Summation method performs more accurately in the case of gross tilting motions (see **Figure2.8**).

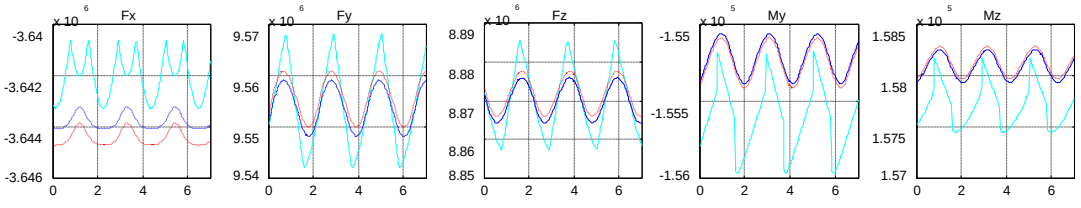

dx=0.8/1000;dy=0.8/1000;dz=0.8/1000; w=5/180×π; $d\Theta z$ =0.1/180×π; $d\Theta y$ =0.1/180×π;

Figure2.7 Load results in rotation

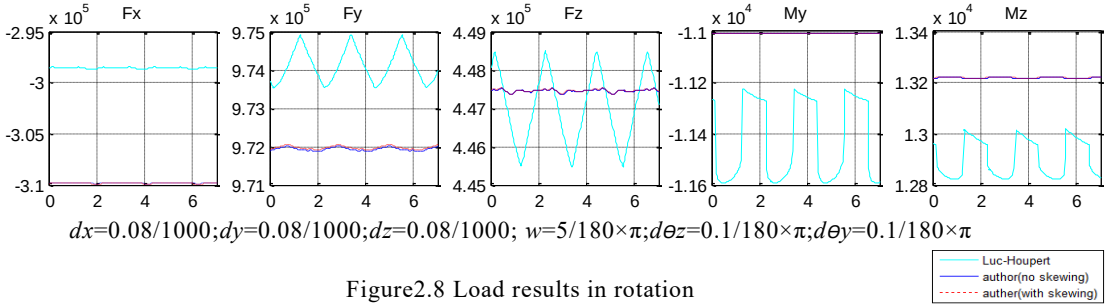

Figure2.8 Load results in rotation

2.3.2 Alternative Roller Contact Calculations (First Approximation Model)

Uniform Harris' relation used to be applied in independent slice calculation. Relevant deflection relations in **Appendix C** are also useful either empirically or analytically.

CST enables each slice to share linearized fraction of single roller stiffness, but not to interact with other slices. Differently, approximation methods focus on analytical and direct interacting relations between distributed load and deformation. Second approximation gives an accurate 2D relation, while first approximation describes an inaccurate 1D relation.

To compensate for this inaccuracy in 1D relation, distributed load and mean load is bridged indirectly. Average slice load is described by both linearized fraction of single roller load and weighted average value of each slice load.

In the former description, linearized fraction of single roller load is,

$$\bar{p}(x) = k_{lc}\delta^{1.1} \tag{2. 18}$$

Using Palmgren's empirical formula for crowned roller,

$$\delta=0.39[4(1-\upsilon_1^2)/E_1+4(1-\upsilon_2^2)/E_2]^{0.9}\cdot\frac{Q^{0.9}}{L^{0.8}}\ (\mathrm{N,\ m})$$

$$k_{lc} = 8.0560\times10^{10}L^{8/9}/L \tag{2. 19}$$

$$(E_1 = E_2 = 206Gpa, \nu_1 = \nu_2 = 0.3)$$

In the latter description, weighted average value of slice load vector is,

$$\{\bar{p}(x)\} = [S_w]_{N_e\times N_e}\{q\}_{N_e\times1} \tag{2. 20}$$

$$\left[S_w\right]=\frac{n}{\sum_{j,k} w_{jk}}\begin{bmatrix} w_{jk} & \cdots & w_{jn} \\ \vdots & \ddots & \vdots \\ w_{nk} & \cdots & w_{nn} \end{bmatrix} \qquad j,k=1...n$$

Where, basic weighting function is generated newly,

$$\frac{\partial \overline{p}_i}{\partial p_j}=\frac{\partial \overline{p}_i}{\partial \delta_i}\frac{\partial \delta_i}{\partial p_j}\propto (\delta_i)^{coef-1}\left(1/r_{ij}\right) \tag{2. 21}$$

With influence coefficient reduced to,

$$w_{jk}=\begin{cases}(\delta_j)^{coef-1}\left(\dfrac{1}{r_{j,k}}\right) & j\neq k \\ (\delta_j)^{coef-1}\left(\dfrac{4}{L/N}\right) & j=k\end{cases} \quad \textbf{(New)} \tag{2. 22}$$

$$w_{jk}=\begin{cases}\left(\dfrac{1}{r_{j,k}}\right)^{coef} & j\neq k \\ \left(\dfrac{4}{L/N}\right)^{coef} & j=k\end{cases} \quad \textbf{(R. Teutsch)} \tag{2. 23}$$

When $j=k$, the influence is considered between slice edge and slice mid-plane for two half slices.

Different from the half-space theory, a force at slice j contributing to the deformation in another slice k was ever interpreted by first approximation suggested by Singh and Paul**[26]**. Contribution of pressure at slice j to the deflection in another slice k decreases by $1/r$, where r is the distance between slice j and k.

Using different deflection-load relation coefficients, influence function between slice load and average slice load can be predicted differently.

E.g. Using Palmgren relation, the governing equation is,

$$\frac{n}{\sum_{j,k} w_{jk}}\begin{bmatrix} w_{jk} & \cdots & w_{jn} \\ \vdots & \ddots & \vdots \\ w_{nk} & \cdots & w_{nn} \end{bmatrix}\{q\}_{N_e\times 1}=\left\{k_{lc}\delta^{1.1}\right\}$$

The alternative strategy of influence coefficients in bearing calculation includes another three aspects: the manner of roller balance, the selection of slice number and contact relation

incorporated. This comprehensive consideration is responsible for a clear bearing prediction on different applications.

This chapter removes rollers from the equilibrium loop, and uses direct model to perform load calculation. Influenced deformation on both roller sides are adjusted by a most stable manner, in which each slice is balanced in a same way.

E.g., in cylindrical roller bearing, a pair of equal loads is applied on both slice sides; in tapered roller bearing, a same ratio ***c*** of load pair takes place on each slice. The manner ensures entire roller balanced in the safest way.

Based on AST, the simplified line-contact system involved in tapered roller bearing is architectured in matrix form.

$$\{q_i\}_{N_e\times 1} = [S_w]^{-1}_{N_e\times N_e} \cdot \{k_{lc}\delta_i^{1.1}\}_{N_e\times 1} = c\{q_o\}_{N_e\times 1} = c[S_w]^{-1}_{N_e\times N_e} \cdot \{k_{lc}\delta_o^{1.1}\}_{N_e\times 1}$$

$$\{q_o\}_{N_e\times 1} = [S_w]^{-1}_{N_e\times N_e} \cdot \left\{k_{lc}\frac{(\delta_i+\delta_o)^{1.1}}{(1+c^{1/1.1})^{1.1}}\right\}_{N_e\times 1} \quad (2.\ 24)$$

Load intensity in one roller is observed below with different slice number considered.

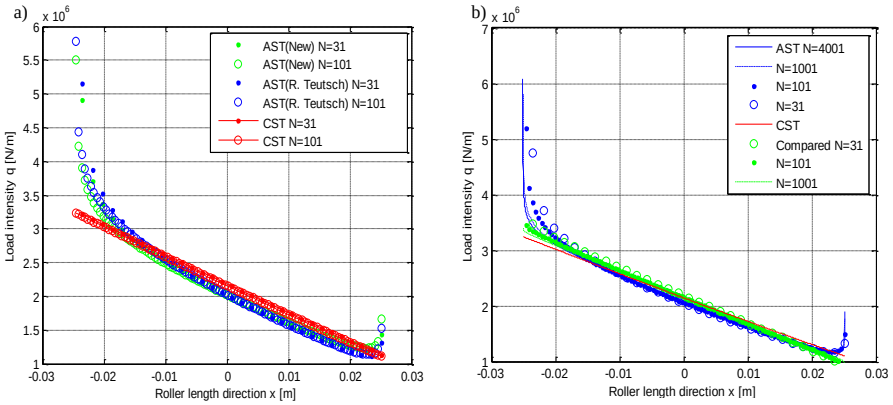

Figure2. 9 Load intensity of one roller with different slice number used

Figure2.9 pictures distributed load intensity. It is found that new results move towards the largely deformed roller end compared to R. Teutsch's results.

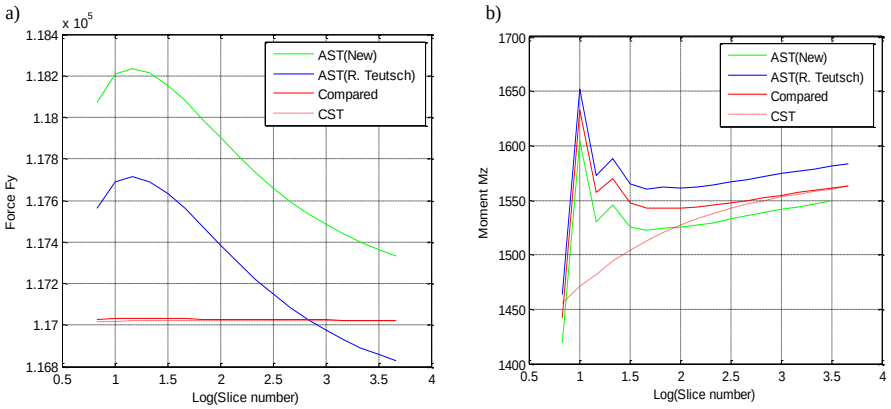

Figure2. 10 Influence of slice number on roller calculation

The influence of slice number on roller load is also investigated.

Figure2.10 gives slice number–roller loads relation curves. It illustrates that each load is nearly linear to the common (decadic) logarithm of slice number. So it could be objected that adequate slices are more accurate in first approximate use than a small number of slices.

To explain the phenomenon, a compared governing equation is supplemented.

$$\begin{bmatrix} \frac{1}{\sum_{1,k} w_{1k}} & \cdots & 0 \\ \vdots & \ddots & \vdots \\ 0 & \cdots & \frac{1}{\sum_{n,k} w_{nk}} \end{bmatrix} \begin{bmatrix} w_{jk} & \cdots & w_{jn} \\ \vdots & \ddots & \vdots \\ w_{nk} & \cdots & w_{nn} \end{bmatrix} \{q\}_{N_e \times 1} = \left\{ k_{lc} \delta^{1.1} \right\} \quad \textbf{(Compared)} \qquad (2.25)$$

This compared governing equation and **Figure2.10** show that the weighted average function in first approximation is the cause to this natural error.

An accurate prediction on integrated roller load is very difficult, but a reasonable depiction of distributed roller contact load tendency can be accessible and compensated in use more or less.

A simplest way in engineering is to apply load normalization method by using experimental value $Q_{\exp}$.

$$q_{correct}(i) = \frac{q_{predict}(i)}{\sum q_{predict}(i)} Q_{\exp}$$

More complicated works can be also performed to confirm slice number. Load concentration is reflected in computed roller force and moment. The experimental manner can

help to find a good agreement with a required tendency of load distribution, by comparing either measured moment or force with numerical result with different slice number used. This work should be numerically feasible, as **Figure2.10** tells that each load is monotonically related to the common logarithm of slice number, and slice number can be searched at its law.

Compared to slice number, the error comes more from fundamental deflection-load relation. When the curvatures and thicknesses of contact bodies are considered, the formula in **Appendix C** can be used. E.g. in railways axle-box bearing, the Palmgren formula performed in this chapter can be adopted, since the corresponding structures are all very thick.

Alternative roller contact calculation is in essence based on first approximation. With Palmgren formula used, it is a semi-empirical method. Besides AST, a semi-analytical method is also proposed in next two paragraphs.

2.3.3 Complex Roller Contact Calculations (Second Approximation Model)

Similarly, a second approximation used in slice technique can also fabricate a group of non-linear equations.

According to Boussinesq-cretu theory **[46]**, the deformation at any point is given by integrating the pressure field $p(x,y)$ and $\mu p(x,y)$ over the effective contact area (Sc),

$$K_1 \iint_{S_C} \frac{p(x,y)dxdy}{\sqrt{(x-x_i)^2+(y-y_i)^2}} + K_2 \iint_{S_C} \mu \frac{(x-x_i)\cos\xi+(y-y_i)\sin\xi}{(x-x_i)^2+(y-y_i)^2} p(x,y)dxdy = \delta - f(x_i, y_i) \tag{2. 26}$$

$$K_1 = \frac{1}{2\pi}\left(\frac{1-\nu_1}{G_1} + \frac{1-\nu_2}{G_2}\right)$$

$$K_2 = \frac{1}{2\pi}\left(\frac{1-2\nu_1}{2G_1} - \frac{1-2\nu_2}{2G_2}\right)$$

It can be solved numerically by deformation matrices and equivalent pressure in each finite and adequately small rectangular contact patch.

$$K_1 \sum_{j=(0,0)}^{(N,N)} P_j D_{ij} + K_2 \sum_{j=(0,0)}^{(N,N)} \mu P_j D_{ij}^{*} = \delta - f(x_i, y_i) \tag{2. 27}$$

$$D_{ij}=\int_{x_j-a_j}^{x_j+a_j}\int_{y_j-\Delta}^{y_j+\Delta}\frac{1}{\sqrt{(x-x_i)^2+(y-y_i)^2}}dxdy$$
$$=F(|x_i-x_j|+a_j,|y_i-y_j|+\Delta)+F(|x_i-x_j|-a_j,|y_i-y_j|-\Delta)$$
$$-F(|x_i-x_j|-a_j,|y_i-y_j|+\Delta)-F(|x_i-x_j|+a_j,|y_i-y_j|-\Delta)$$

$$D_{ij}^{*}=\int_{x_j-a_j}^{x_j+a_j}\int_{y_j-\Delta}^{y_j+\Delta}\frac{(x-x_i)\cos\xi+(y-y_i)\sin\xi}{(x-x_i)^2+(y-y_i)^2}dxdy$$
$$=F^{*}(|x_i-x_j|+a_j,|y_i-y_j|+\Delta)+F^{*}(|x_i-x_j|-a_j,|y_i-y_j|-\Delta)$$
$$-F^{*}(|x_i-x_j|-a_j,|y_i-y_j|+\Delta)-F^{*}(|x_i-x_j|+a_j,|y_i-y_j|-\Delta)$$

Where, $F(X,Y)=\iint\frac{1}{\sqrt{X^2+Y^2}}dXdY=X\ln(Y+\sqrt{X^2+Y^2})+Y\ln(X+\sqrt{X^2+Y^2})$

$$F^{*}(X,Y)=\iint\frac{X\cos\xi+Y\sin\xi}{X^2+Y^2}dXdY=[Y\ln(\sqrt{X^2+Y^2})+X\tan^{-1}(\frac{Y}{X})]\cos\xi+[X\ln(\sqrt{X^2+Y^2})+Y\tan^{-1}(\frac{X}{Y})]\sin\xi$$

P_j , as an equivalent normal load, occurs at the area of $2a_j\times2\Delta$, whose center is (x_j,y_j) .

Assuming that

1. Roller is divided into *N* slices (**Figure2.** 11**)** with *N* indent values discretized. These values are more determined by distributed pressure along roller length than that along roller width.
2. Longitudinal distribution of roller load is more related to tilting than skewing.
3. Both mating bodies of the same material,

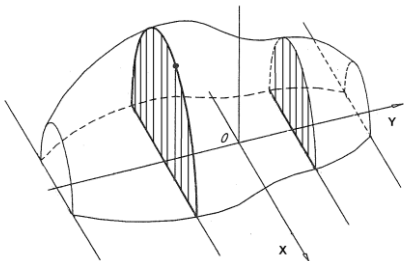

Figure2. 11

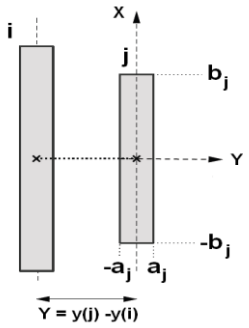

Figure2. 12

Figure 2.11~2.12 Slice division scheme (Bruno Mevel)

A reduction from 2D question to 1D question ($x_j = x_i = 0$) is performed by uniquely calculating contact relation in central indent line. Contribution of j^{th} slice on central deformation of i^{th} slice is interpreted by introducing distributed Hertz pressure inside a slice.

$$\delta_{ij}=\frac{2}{\pi E'}\int_{-a_j}^{+a_j} p_{\max,j}\sqrt{1-\left(\frac{x}{a_j}\right)^2}\ln\left(\frac{\left(\left|y_i-y_j\right|+\Delta\right)+\sqrt{\left(\left|y_i-y_j\right|+\Delta\right)^2+x^2}}{\left(\left|y_i-y_j\right|-\Delta\right)+\sqrt{\left(\left|y_i-y_j\right|-\Delta\right)^2+x^2}}\right)dx \tag{2. 28}$$

Another versatile method simplified by the analytical equations uses a uniform pressure strip (**Figure2.13)** to replace Hertz distribution inside each slice. Herein, an alternative model is developed based on them.

Simplified model

$$\delta_{ij}=\frac{2P_jD_{ij}}{\pi E'}=\frac{2p_{mean,j}}{\pi E'}\int_{-a_j}^{+a_j}\int_{y_j-\Delta}^{y_j+\Delta}\frac{1}{\sqrt{(x)^2+(y-y_i)^2}}dxdy=\frac{2p_{mean,j}D_{ij}}{\pi E'} \tag{2. 29}$$

$$\begin{aligned}D_{ij} &= \int_{-a_j}^{+a_j}\int_{y_j-\Delta}^{y_j+\Delta}\frac{dxdy}{\sqrt{(x)^2+(y-y_i)^2}}\\ &= F(+a_j,\left|y_i-y_j\right|+\Delta)+F(-a_j,\left|y_i-y_j\right|-\Delta)\\ &-F(-a_j,\left|y_i-y_j\right|+\Delta)-F(+a_j,\left|y_i-y_j\right|-\Delta)\end{aligned}$$

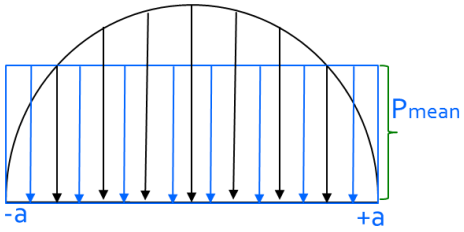

Figure2.13 Uniform method

Analytical Hertz relations $\begin{cases} p_{mean,j} = \frac{\pi}{4} p_{\max,j} \\ a_j = \frac{2R}{E'} p_{\max,j} \end{cases}$ are substituted to finalize a condensed matrix formulation of uniform variables $\{p_{\max,j}\}_{N_e \times 1}$.

$$\{\delta_j\}_{N_e \times 1} = \frac{1}{2E'} [D]_{N_e \times N_e} \{p_{\max,j}\}_{N_e \times 1} \tag{2. 30}$$

Where, N_e donates effective slices constituting contact area.

$y_j = (-(N_e+1)/2+j) \times \frac{L}{N}$ and $\Delta = 0.5\frac{L}{N}$ are required geometric relations in equation.

$\delta_i = \sum_{j=1}^{N_e} \frac{p_{\max,j} D_{ij}}{2E'}, i = 1 \cdots N_e$ is one resultant element in $\{\delta_j\}_{N_e \times 1}$.

Alternative model

Compared to empirical results (**Figure2.17**), enhanced results reveal that mean Hertz pressure performed in calculation led to overestimated results. Besides uniform, semi-elliptical and parabolic pressure distributions involved in the preceding calculations by other researchers, several rectangular pressure strips symmetrically superposed on each slice is also proposed in this chapter to replace semi-elliptically distributed Hertz pressure. An evident advantage is that distributed loads and deformation will be bridged analytically.

In this alternative method, rectangular pressure strips can be organized differently. Below tentatively gives three situations (**Figure2.14~2.16)**. A better use of proposed method can be claimed.

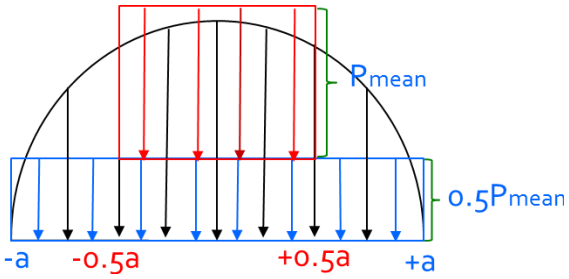

Figure2.14 Two strips, uneven strip height

$$\{\delta_j\}_{N_e\times 1}=\frac{1}{2E'}\begin{Bmatrix}[D|_{=a}]_{N_e\times N_e}\{0.5p_{\max,j}\}_{N_e\times 1}\cdots\\+[D|_{=0.5a}]_{N_e\times N_e}\{p_{\max,j}\}_{N_e\times 1}\end{Bmatrix} \quad (2.\ 31)$$

Where, $[D|_{=a}]_{N_e\times N_e}$ refers to deformation matrix incorporating N_e effective slices (effective contact) and each slice of Hertz contact width. (Similarly hereinafter)

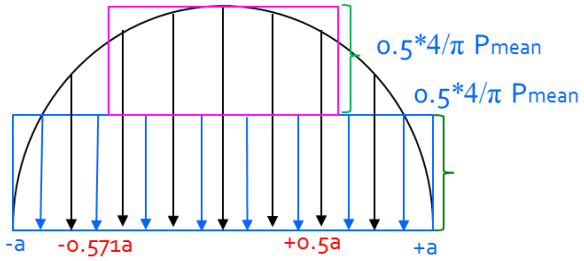

Figure2.15 Two strips, even strip height

$$\{\delta_j\}_{N_e\times 1}=\frac{1}{2E'}\begin{Bmatrix}[D|_{=a}]_{N_e\times N_e}\left\{\frac{2}{\pi}p_{\max,j}\right\}_{N_e\times 1}\cdots\\+[D|_{=0.571a}]_{N_e\times N_e}\left\{\frac{2}{\pi}p_{\max,j}\right\}_{N_e\times 1}\end{Bmatrix} \quad (2.\ 32)$$

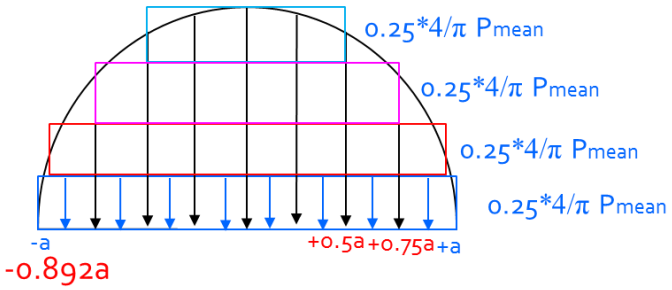

Figure2.16 Four strips, even strip height

$$\{\delta_j\}_{N_e\times 1}=\frac{1}{2E'}\begin{Bmatrix}[D|_{=a}]_{N_e\times N_e}+[D|_{=0.892a}]_{N_e\times N_e}\cdots\\+[D|_{=0.75a}]_{N_e\times N_e}+[D|_{=0.5a}]_{N_e\times N_e}\end{Bmatrix}\left\{\frac{1}{\pi}p_{\max,j}\right\}_{N_e\times 1} \quad (2.\ 33)$$

According to these condensed matrices, the resultant bearing load curves are compared below.

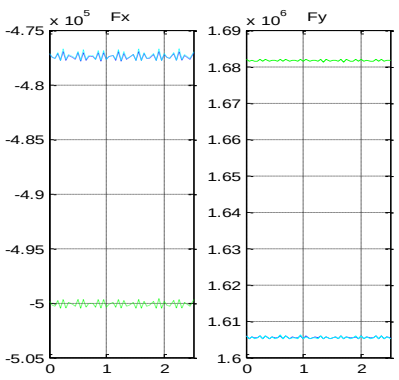

Figure2. 17 one strip

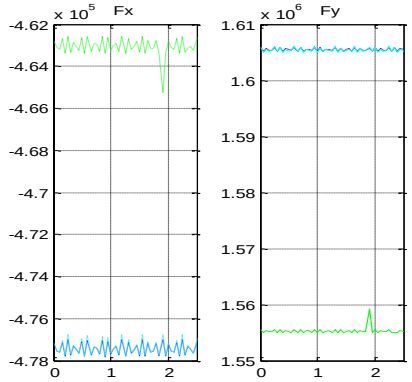

Figure2. 18 Two strips, uneven strip height

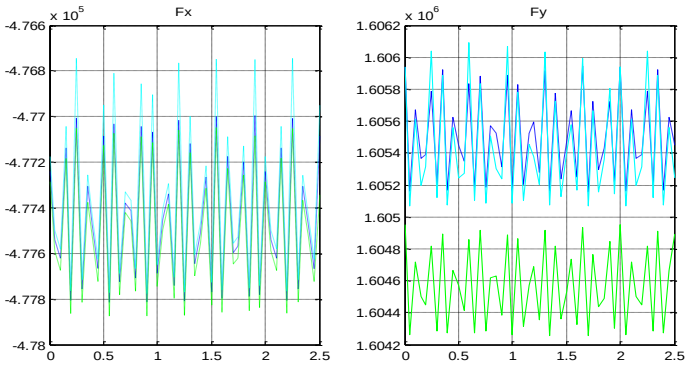

Figure2. 19 Two strips, even strip height

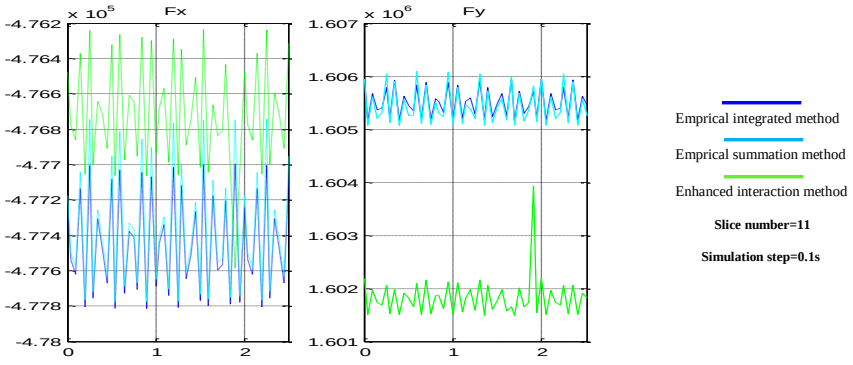

Figure2. 20 Four strips, even strip height

dx=0.08/1000;dy=0.18/1000;dz=0.08/1000; w=5/180×π; $d\Theta z$=0.01/180×π;$d\Theta y$=0.01/180×π;

Figure 2.17~2.20 Comparison between empirical and enhanced bearing loads

The upshots show that the latter two methods of $\{\delta_j\}_{N_e\times 1}^{2strips}$, $\{\delta_j\}_{N_e\times 1}^{4strips}$ perform better in use, but more time will be consumed if more strips are chosen.

A versatile idea can be employed in the following way. It is relevant to think that it is significant to have a more detailed description for the contact points of large deformation, but

it is still acceptable to have a less detailed description for the ones of small deformation, since loaded area is much smaller and error caused by transverse pressure distribution is smaller. So the way of involving different number of strips in each slice is given below.

As such, the condensed matrix will be modified with a product factor c_j. The product factor is used to describe the importance (strong or weak) of load distribution to each slice, in order to reduce the calculating scale of elastic deformation in equilibrium loop.

$$\{\delta\}_{N_e\times 1} = k_s \begin{bmatrix} D_{11} & \cdots & \boxed{D_{1j}} & \cdots & D_{1n} \\ \vdots & \ddots & & & \vdots \\ D_{i1} & & D_{ij} & & D_{in} \\ \vdots & & & \ddots & \vdots \\ D_{n1} & \cdots & D_{nj} & \cdots & D_{nn} \end{bmatrix}_{N_e\times N_e} \begin{bmatrix} p_{\max,1} \\ \vdots \\ \boxed{p_{\max,j}} \\ \vdots \\ p_{\max,n} \end{bmatrix}_{N_e\times 1} = k_s \left[D_{sn}\right]_{N_e\times N_e} \left\{p_{\max,j}\right\}_{N_e\times 1} \tag{2.34}$$

Preceding matrices for two strips, four strips or more have a basic format **(2.34)** with different coefficients k_s used. The information in rectangles refers to how slice *j* interacts with others.

If the load in j^{th} slice contributes less to others' deformations, fewer strips can be used for slice *j*, it means that each column of $\{D_{ij}\}$ can be specially selected.

$$\{\delta\}_{N_e\times 1} = \sum_{j=1}^{n} \left[k_{sj1}\left[D_{sj}\right]_{N_e\times N_e}\cdot c_1 \quad k_{sj2}\left[D_{sj}\right]_{N_e\times N_e}\cdot c_2 \quad \cdots \quad k_{sjn}\left[D_{sj}\right]_{N_e\times N_e}\cdot c_n \right] \cdot \{p_{\max}\}_{N_e\times 1} \tag{2.35}$$

Where, *sj* donates *j* strips used in the deformation matrix, and *j* varies from 1 to n.

k_s, k_{sj} are constant coefficients corresponding to different strips.

$c_j = \begin{bmatrix} 0 & \cdots & \underset{slice\ \ j}{1} & \cdots & 0 \end{bmatrix}^T$ is the product factor of selecting j^{th} column of influence coefficients matrix.

Equilibrium loop method

Besides interaction among slices, unequal loads generally acting on two sides of each slice should be also comprehensively considered in the equilibrium loop model.

Using discretized pressure $\left\{p_{\text{mean},j}\right\}_{N_e\times 1}$ distributed along contact line as variable in Hertz line contact relation, deflections distributed at both inner and outer races are calculated.

$$\begin{cases}\left\{\delta_j^i\right\}_{N_e\times 1}=\dfrac{2}{\pi E'}\sum\limits_{layers} k\left[D^i\right]_{N_e\times N_e}\times\left\{p^i_{\text{mean},j}\right\}_{N_e\times 1}\\ \left\{\delta_j^o\right\}_{N_e\times 1}=\dfrac{2}{\pi E'}\sum\limits_{layers} k\left[D^o\right]_{N_e\times N_e}\times\left\{p^o_{\text{mean},j}\right\}_{N_e\times 1}\end{cases} \tag{2. 36}$$

In tapered roller bearing, different contact geometries at inner and outer races participate in calculation.

$$p_{\max,j}=\sqrt{\frac{p_S E'}{2\pi R_X}}\propto\sqrt{\frac{p_S}{R_X}}$$

$$\frac{p^i_{\max,j}}{p^o_{\max,j}}=\sqrt{\frac{R_X^o\cdot c}{R_X^i}},\ \left(\frac{{p_S}^i}{{p_S}^o}=c\right) \tag{2. 37}$$

$$a_j=\frac{2R_X}{E'}p_{\max,j}\propto R_x p_{\max,j}$$

$$\frac{a_j^i}{a_j^o}=\sqrt{\frac{R_X^i\cdot c}{R_X^o}} \tag{2. 38}$$

$p^i_{\max,j}, p^o_{\max,j}$ and a^i_j, a^o_j in **(2. 36)** are synchronically calculated, using a uniform variable. If the mechanical relation $\frac{F_i}{F_o}=c$ for entire roller replaces $\frac{{p_S}^i}{{p_S}^o}=c$ assumed for each slice, developed deflection relation for line contact (in **Appendix C**) should be employed by setting distributed deformation in **(2. 39)** as variable, where contact width involved in deformation matrix $\left[D^i\right]_{N_e\times N_e}$ is calculated explicitly.

$$\begin{cases}\left\{p_j^i\right\}_{N_e\times 1}=\dfrac{\pi E'}{2}inv\left(\sum\limits_{layers} k\left[D^i\right]_{N_e\times N_e}\right)\times\left\{\delta_j^i\right\}_{N_e\times 1}\\ \left\{p_j^o\right\}_{N_e\times 1}=\dfrac{\pi E'}{2}inv\left(\sum\limits_{layers} k\left[D^o\right]_{N_e\times N_e}\right)\times\left\{\delta_j^o\right\}_{N_e\times 1}\end{cases} \tag{2. 39}$$

In equilibrium loop, geometrical relation is

$$\left\{\delta_j\right\}_{N_e\times 1}=\left\{\delta_j^i\right\}_{N_e\times 1}+\left\{\delta_j^o\right\}_{N_e\times 1} \tag{2. 40}$$

$\left\{\delta_j^i\right\}_{N_e\times 1}$ incorporated in calculation contains two geometrical unknowns (tilting angle θ_t and central deformation Δr).

$$\left\{\delta_j^i\right\}_{N_e\times 1}=\begin{Bmatrix}\Delta r\\ \Delta r+\theta_t\Delta\\ \Delta r+2\theta_t\Delta\\ \vdots\\ \Delta r+(N-1)\theta_t\Delta\end{Bmatrix}\ (\theta_t=\gamma-\gamma_0) \tag{2. 41}$$

In the equilibrium loop, mechanical relations include force balance $\frac{F_i}{F_o}=c$ and moment balance.

According to the scheme of roller end/flange contact in **Figure2. 21**,

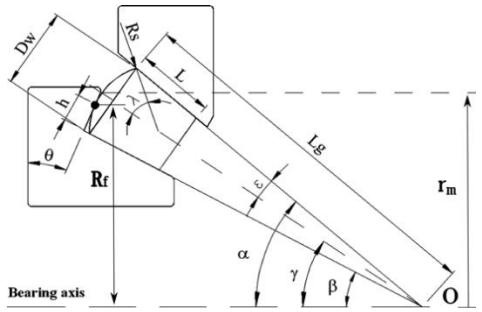

Figure2. 21 Geometric relations of Roller end/Flange Contact (D. Nelias)

Moment equilibrium around roller end/flange contact point is written by

$$(\frac{L}{2}-h\cdot\sin\varepsilon)F_i+M_i=(\frac{L}{2}-(D_w-h)\cdot\sin\varepsilon)F_o+M_o \tag{2. 42}$$

Where,

$$\begin{cases}F_i=\sum_{i=1}^{N}p_i=\sum_{j=1}^{N_e}p_j^i\times 2\Delta\times 2a_j^i\\ F_o=\sum_{i=1}^{N}p_o=\sum_{j=1}^{N_e}p_j^o\times 2\Delta\times 2a_j^o\end{cases}\qquad\begin{cases}M_i=\sum_{i=1}^{N}p_i\cdot(i-\frac{N-1}{2}-1)\cdot L/N\\ M_o=\sum_{i=1}^{N}p_o\cdot(i-\frac{N-1}{2}-1)\cdot L/N\end{cases} \tag{2. 43}$$

Roller end/flange contact position is located by distance *h*.

$$h=\frac{D_w}{2}-R_s\cdot\sin(\gamma-\theta) \tag{2. 44}$$

In this case, the developed equilibrium loop model can recognize relative tilting motion of roller to cone as well as reciprocating motion of rib/roller contact position.

Strictly speaking, tilting equilibrium of roller mainly depends on relative displacements between races. The resultant θ_t and Δr will in turn slightly change overall distributed deformation $\{\delta_j\}_{N_e\times 1}$ between each slice and interacted races in direct bearing model. However, the unique impact on additional deformation proposed in **Paragraph 2.2** can be ignored.

Discussion on Moment Accuracy of Second Approximation Method

In calculation, compared to the forces (F_x, F_y, F_z), the moments (M_y, M_z) are more easily affected by slice number. A more detailed picture depicts the relation between slice number and bearing loads.

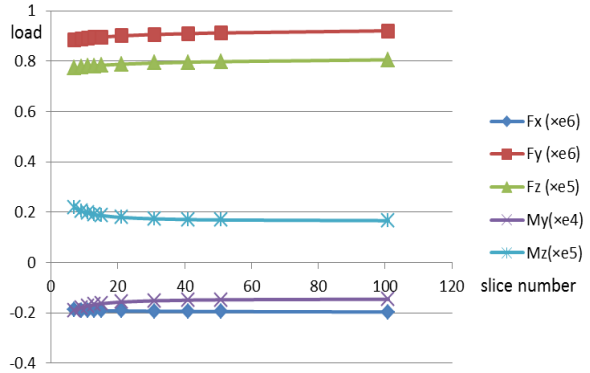

dx=0.8/1000; dy=0.8/1000; dz=0.8/1000; $d\theta z$=0.1/180×π; $d\theta y$=0.1/180×π; phi=5/180×π

Figure2. 22 Slice number-bearing loads relation

In this method, absence of force distribution along slice thickness is the leading error in moment calculation. The more slices are used, the more accurate moments are. When the number of slice is sufficient to fully describe the force distribution, the moments (M_y, M_z) will stay stable. Theoretically speaking, the series $\{Lj\}$ affect the synchronous stability of moment M and force Q calculations. $\{\Delta p\, Lj\}$ decreases to$\{0\}$ in the unique case of adequate slices in calculating stably distributed $\{p\}$. But too many slices in bearing calculation are not realistic.

Semi-empirical method of stabilizing roller moment

A semi-empirical method is suggested to improve the stability of moment calculation. Herein, a constructing function is introduced to simulate pressure distribution along slice thickness. The deformation along the contact length is linear to contact coordinate. As such, the constructing function is linearly related to coordinate.

$$p_{newi}(x)=a_i\square(\pm x)^{1.1}+b_i \quad \begin{cases} - & x<0 \\ + & x>0 \end{cases} \tag{2. 45}$$

Please note, unit of $p_{newi}(x)$ is N/m, not N/m^2 .

Interestingly, any constructing function with a power of 1or 2, etc. cannot ensure the computed moments to stay stable with more slices involved in calculation, expect when a power of 1.1 is chosen. Below gives the constructing idea in depth.

$$p_{n+2} \approx k_{lc}\left[\delta_{n+1}^{1.1}+1.1\delta_{n+1}^{0.1}\Delta\delta_{n+1}\right] \approx k_{lc}\left[\delta_{n}^{1.1}+1.1\delta_{n}^{0.1}\Delta\delta_{n}+1.1\delta_{n+1}^{0.1}\Delta\delta_{n+1}\right]$$

Unequal (non-average) interaction among slices is considered to significantly develop new distributed stiffness along each slice length.

$$\begin{aligned} k_{new-x} &= \frac{\delta p_{new-x_n}}{\delta p_{CST-x_n}} k_{CST-x} \\ &= \frac{p_{n+1}-p_n}{k_{lc}\left[\delta_n^{1.1}+1.1\delta_n^{0.1}\Delta\delta_n\right]-k_{lc}\delta_n^{1.1}} 1.1k_{lc}\delta^{0.1} \\ &= \frac{p_{n+1}-p_n}{\delta_n^{0.1}\Delta\delta_n}\delta^{0.1} \end{aligned} \tag{2. 46}$$

Stiffness for each slice is no more constant, dependent of enhanced pressure values as well as slice deflection distribution. The constructing function in fine proves the correctness of the power 1.1 after integration of **(2. 46)**.

Besides power value 1.1 in constructing function, the integral coefficients a_i, b_i should also be calculated by both load continuity and load conservation inside each slice.

$$\begin{aligned} p_{newi}(x_{i\_slice-center}+\frac{L}{2N}) &= p_{newi+1}(x_{i+1\_slice-center}-\frac{L}{2N}) \qquad x<0 \\ p_{newi}(x_{i\_slice-center}-\frac{L}{2N}) &= p_{newi-1}(x_{i-1\_slice-center}+\frac{L}{2N}) \qquad x>0 \end{aligned} \tag{2. 47}$$

$$\int_{x_{i\_slice-center}-\frac{L}{2N}}^{x_{i\_slice-center}+\frac{L}{2N}} p_{newi}(x)dx = p_{mean,i} \times 2\Delta \times 2a_i \tag{2. 48}$$

Using a simple matrix operation, the coefficients of each slice are calculated recursively and successively, and resultant loads are established.

$$\begin{cases} M_{\varphi y} = \cos\varphi \cos\alpha \sum_{i=1}^{N} \int_{x_{i\_slice-center}-\frac{L}{2N}}^{x_{i\_slice-center}+\frac{L}{2N}} p_{newi}(x) \square x dx \\ M_{\varphi z} = \sin\varphi \cos\alpha \sum_{i=1}^{N} \int_{x_{i\_slice-center}-\frac{L}{2N}}^{x_{i\_slice-center}+\frac{L}{2N}} p_{newi}(x) \square x dx \end{cases} \tag{2. 49}$$

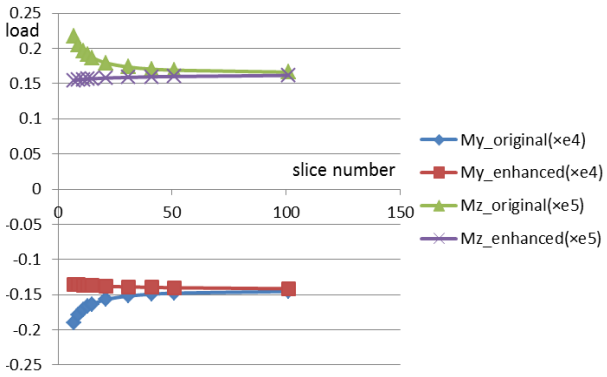

dx=0.8/1000; dy=0.8/1000; dz=0.8/1000; $d\theta z$=0.1/180×π; $d\theta y$=0.1/180×π; phi=5/180×π

Figure2.23 COMPARISONS between original and enhanced moments

Figure2.23 presents updated moments, to find that a small number of slices are sufficient to obtain stable results. The introduction of slice stiffness recalculation is in fine proved to be feasible in bearing engineering. Please note, in roller bearing stiffness and damping matrices, such a relation can replace uniform stiffness formula to perform a better prediction in system vibrating characteristics.

2.3.4 Reduced Roller Contact Calculations (1st and 2nd Mixed Approximation Models)

The first approximation (1/r) suggested by Singh and Paul should be used carefully, since its interacting distance is wide. A more precise work is efficiently performed below.

In Boussinesq work**[46]**, deformation at any point is given by integrating the pressure field $p(x, y)$ over the effective contact area (Sc),

$$\frac{1}{\pi}\left(\frac{1-\nu_1^2}{E_1}+\frac{1-\nu_2^2}{E_2}\right)\iint_{S_C}\frac{p(x,y)dxdy}{\sqrt{(x-x_i)^2+(y-y_i)^2}}dxdy=\delta \tag{2. 50}$$

Using Hertz line-contact theory, $p=p_0\sqrt{1-\left(\frac{x}{a}\right)^2}$ is substituted in (10) to verify 1D reduced interacting relation among load intensity $q=\frac{\pi p_0 a}{2}$, contributed deformation δ and interacting distance r .

$$K\int_{\Delta y=r}\frac{p_0\sqrt{1-\left(\frac{x}{a}\right)^2}dx}{\sqrt{x^2+r^2}}dx=\delta, K=\frac{1}{\pi}\left(\frac{1-\nu_1^2}{E_1}+\frac{1-\nu_2^2}{E_2}\right)=\frac{2}{\pi E'}$$

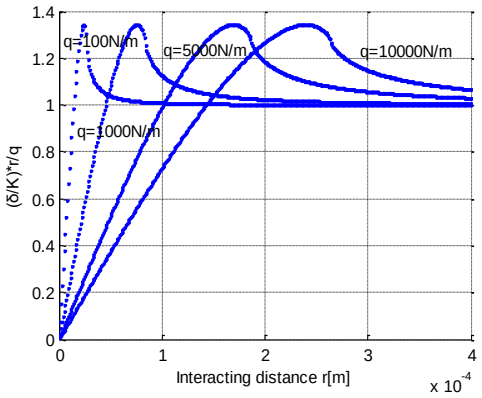

Figure2. 24 1-D Reduced interacting relation dependent of interacting distance

According to 1-D reduced interacting relation,

$$\frac{\delta_{part}}{K}\frac{r}{q}=1$$

1-D reduced contact algorithm is established tentatively,

$$\Sigma\left(q\int_{slice\text{-}width}\frac{1}{r}dr\right)=\frac{1}{K}\delta$$

New influencing coefficients are proposed,

$$w_{j,k}=\begin{cases}\int_{r_{j,k}-0.5L/N}^{r_{j,k}+0.5L/N}\frac{1}{r}dr=\ln\frac{r_{j,k}+0.5L/N}{r_{j,k}-0.5L/N} & j\neq k\\ 2\int_{1/s\times 0.5L/N}^{0.5L/N}\frac{1}{r}dr=2\ln s & j=k\end{cases} \tag{2. 51}$$

Based on this reduced algorithm, the simplified line-contact system involved in tapered roller bearing is architectured in matrix form.

$$\{\delta\}_{N_e\times 1} = K(\left[w^i_{j,k}\right]_{N_e\times N_e}\cdot\{q_i\}_{N_e\times 1}+\left[w^o_{j,k}\right]_{N_e\times N_e}\{q_o\}_{N_e\times 1}) = K(c\left[w^i_{j,k}\right]_{N_e\times N_e}+\left[w^o_{j,k}\right]_{N_e\times N_e})\{q_o\}_{N_e\times 1} \quad (2.52)$$

s-approaching value decides interacting distance incorporated in w_{ii} calculation, and determines availability of new influencing coefficient.

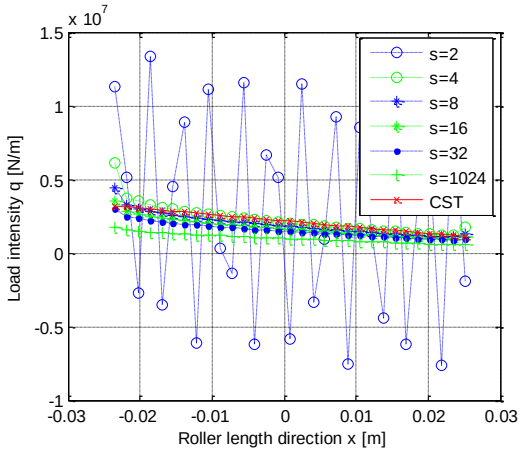

Figure2. 25 Application of 1D reduced contact algorithm in roller load calculation

It is found that w_{ii} is dangerous to calculation and needs a better approximation.

A combined manner below can produce more accurate results by assuming elliptically **(2.53)** or rectangularly **(2.54)** distributed pressure in a slice.

$$w_{j,k} = \begin{cases} \int_{r_{j,k}-0.5L/N}^{r_{j,k}+0.5L/N}\frac{1}{r}dr=\ln\frac{r_{j,k}+0.5L/N}{r_{j,k}-0.5L/N}, & |j\text{-}k|>n \\ & ,r_{j,k}=\Delta \\ \frac{2}{\pi a}\int_{-a\Delta-0.5L/N}^{+a\Delta+0.5L/N}\int\frac{\sqrt{1-\left(\frac{x}{a}\right)^2}\,dxdr}{\sqrt{x^2+r^2}}, & |j\text{-}k|\le n \end{cases} \quad (2.53)$$

$$w_{j,k} = \begin{cases} \int_{r_{j,k}-0.5L/N}^{r_{j,k}+0.5L/N}\frac{1}{r}dr=\ln\frac{r_{j,k}+0.5L/N}{r_{j,k}-0.5L/N}, & |j\text{-}k|>n \\ \frac{P_m}{q}\int_{-a\Delta-0.5L/N}^{+a\Delta+0.5L/N}\int\frac{dxdr}{\sqrt{x^2+r^2}}=\frac{1}{2b}\begin{pmatrix}F(+a_j,\Delta+0.5L/N)+F(-a_j,\Delta-0.5L/N)\\-F(-a_j,\Delta+0.5L/N)-F(+a_j,\Delta-0.5L/N)\end{pmatrix}, & |j\text{-}k|\le n \end{cases} \quad (2.54)$$

Where, $F(X,Y)=\iint\frac{1}{\sqrt{X^2+Y^2}}dXdY=X\ln(Y+\sqrt{X^2+Y^2})+Y\ln(X+\sqrt{X^2+Y^2})$

n refers to coupling value between first and second approximation influencing coefficients. When calculating deformation in slice *j*, 2n more neighbouring cells use second approximation influencing coefficients.

Its iterative calculation is alternatively reduced compared to full second approximation calculation, even less computationally convenient than direct calculation in AST.

To accelerate bearing calculation with an acceptable accuracy, two other works are performed by improving equation (**2.53, 2.54**).

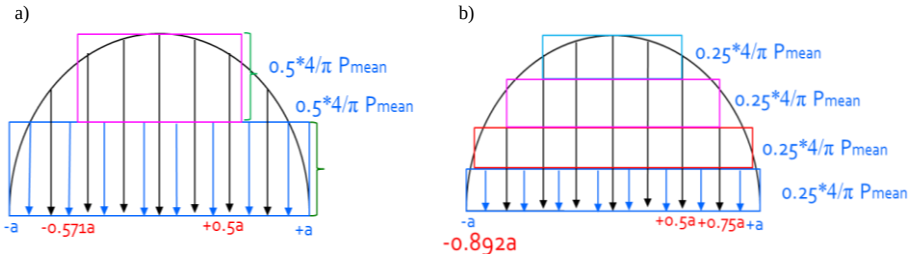

Figure2. 26 Strip Scheme of replacing elliptically distributed pressure

Corresponding to new replacement scheme, analytical governing equations are,

$$w_{j,k}=\frac{1}{q}\frac{P_0}{2}\int_{-a}^{+a}\int_{\Delta-0.5L/N}^{\Delta+0.5L/N}\frac{dxdr}{\sqrt{x^2+r^2}}+\frac{1}{q}\frac{P_0}{2}\int_{-0.571a}^{+0.571a}\int_{\Delta-0.5L/N}^{\Delta+0.5L/N}\frac{dxdr}{\sqrt{x^2+r^2}}$$
$$=\frac{1}{\pi b}\begin{pmatrix}F(+a_j,\Delta+0.5L/N)+F(-a_j,\Delta-0.5L/N)-F(-a_j,\Delta+0.5L/N)-F(+a_j,\Delta-0.5L/N)+\\F(+0.571a_j,\Delta+0.5L/N)+F(-0.571a_j,\Delta-0.5L/N)-F(-0.571a_j,\Delta+0.5L/N)-F(+0.571a_j,\Delta-0.5L/N)\end{pmatrix} \quad (2.55)$$

$$w_{j,k}=\frac{1}{q}\frac{P_0}{4}\begin{pmatrix}\int_{-a}^{+a}\int_{\Delta-0.5L/N}^{\Delta+0.5L/N}\frac{dxdr}{\sqrt{x^2+r^2}}+\int_{-0.892a}^{+0.892a}\int_{\Delta-0.5L/N}^{\Delta+0.5L/N}\frac{dxdr}{\sqrt{x^2+r^2}}+\\\int_{-0.75a}^{+0.75a}\int_{\Delta-0.5L/N}^{\Delta+0.5L/N}\frac{dxdr}{\sqrt{x^2+r^2}}+\int_{-0.5a}^{+0.5a}\int_{\Delta-0.5L/N}^{\Delta+0.5L/N}\frac{dxdr}{\sqrt{x^2+r^2}}\end{pmatrix} \quad (2.56)$$

Discussion on strip scheme and coupling value n in reduced algorithm:

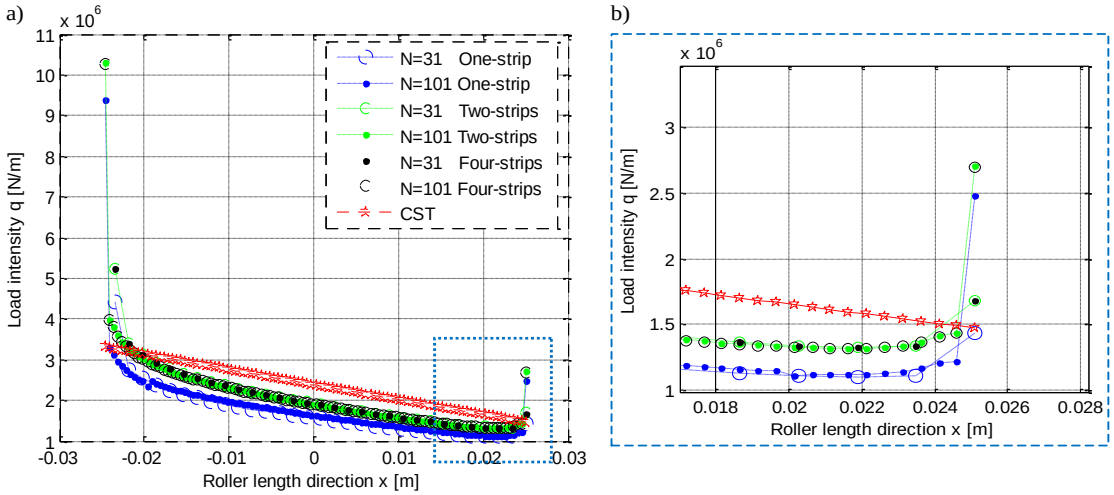

Figure2. 27 Distributed load intensity under different strip schemes

It is observed that two-strips scheme is sufficiently accurate to perform roller contact calculation.

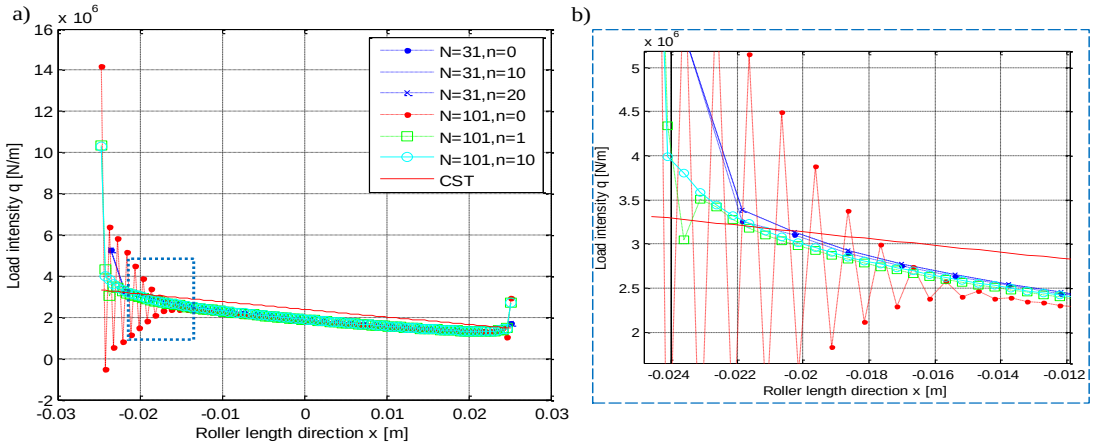

Figure2. 28 Influence of coupling value n on reduced algorithm

It is investigated that a) a very low coupling value n is sufficient to obtain accurate load intensity along roller length; b) in the case of large slice number, use of more second approximation influencing coefficients $w_{j,k}$ (a slightly higher n) will make reduced algorithm more stable.

2.4 Analysis on Bearing Stiffness Matrix

The influence of roller edge effect on bearing transmission lies in angular motion items in stiffness matrix. Under tilting motion, asymmetric pressure concentration will cause considerable moment acting on roller center.

Within two rotations, a tapered roller bearing is calculated, using slice number 31 and setting five inputs:

a) dx=0.8/1000;dy=0.8/1000;dz=0.8/1000;$d\Theta z$=0/180×π;$d\Theta y$=0/180×π;

b) dx=0.8/1000;dy=0.8/1000;dz=0.8/1000;$d\Theta z$=0.1/180×π;$d\Theta y$=0.1/180×π;

c) dx=0.8/1000;dy=0. 8/1000;dz=0.8/1000;$d\Theta z$=0 /180×π;$d\Theta y$=0.4~0.7/180×π;

d) dx=0.8/1000;dy=0.8/1000;dz=0.08/1000;$d\Theta z$=0.1/180×π;$d\Theta y$=0.1/180×π;

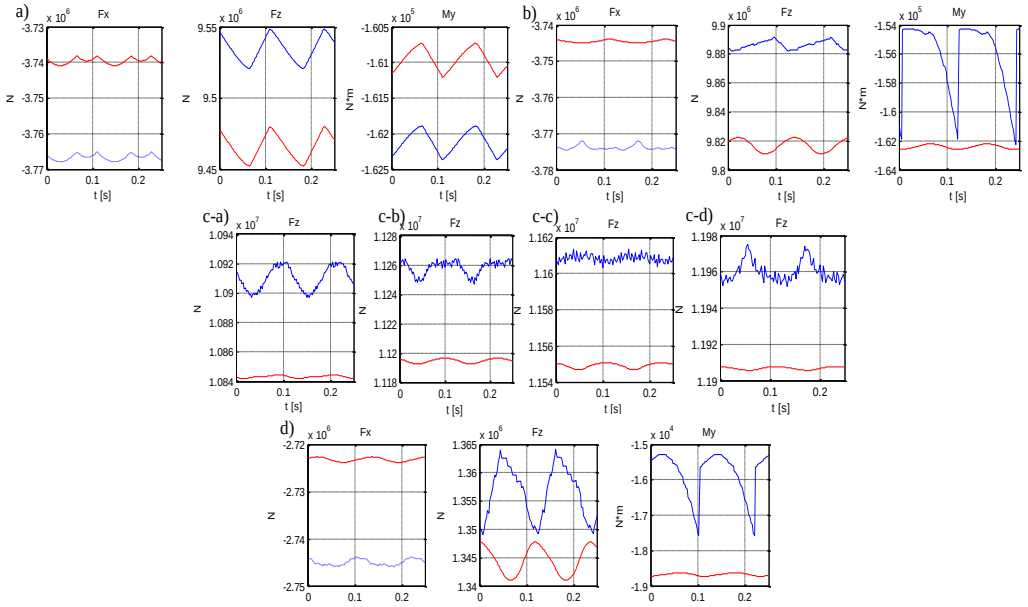

Figure2. 29 Comparisons between CST(red) and AST(blue) results

Much information is behind different inputs. But as for outputs, the possibly different amplitude, phase and period from CST results are of prime interest in study.

a) When $d\Theta y = d\Theta z = 0$, load curves from AST uniquely change in amplitude compared to CST results.

b) Appearance of $d\Theta y$ or $d\Theta z$ in AST will change phase of load curves from CST.

c) Continuously increasing $d\Theta y$ or $d\Theta z$ will gradually produce load curves of opposite phase to CST results, due to growing edge effect. Different combination of $d\Theta y$ and $d\Theta z$ will also lead to different phase changes. This change is in depth explained:

Displaced bearing will be alternatively supported by loaded rollers of an even and an odd number during rotation. The odd case used to produce more supporting load in CST calculation. However, the even case will generate much heavier loads in AST calculation in the case of big tilting motions. Intense edge effect will take

place on one extra roller in the even case compared to the odd one. And this knowledge is acquired by the bearing structure used in this chapter.

d) In the case of non-zero $d\Theta y$ and $d\Theta z$, decrease of dx, dy, dz will respectively give rise to a same phase change of load curve Fx-t, Fy-t and Fz-t as well.

Using finite differential method (incremental value=1% of input), typical linear and angular displacement stiffness of 25 different elements in bearing stiffness matrix are investigated.

$$\begin{bmatrix} K_{xx} & K_{xy} & K_{xz} & K_{x\theta_y} & K_{x\theta_z} \\ K_{yx} & K_{yx} & K_{yx} & K_{y\theta_y} & K_{y\theta_z} \\ K_{zx} & K_{zy} & K_{zz} & K_{z\theta_y} & K_{z\theta_z} \\ K_{\theta_y x} & K_{\theta_y y} & K_{\theta_y z} & K_{\theta_y\theta_y} & K_{\theta_y\theta_z} \\ K_{\theta_z x} & K_{\theta_z y} & K_{\theta_z z} & K_{\theta_z\theta_y} & K_{\theta_z\theta_z} \end{bmatrix}$$

For example,

$$\begin{aligned} K_{\theta_y x} &= \frac{\partial M_y}{\partial(dx)} = \frac{M_y(dx+\Delta dx,dy,dz,d\theta y,d\theta z)-M_y(dx,dy,dz,d\theta y,d\theta z)}{\Delta dx} \\ K_{\theta_y\theta_y} &= \frac{\partial M_y}{\partial(\theta_y)} = \frac{M_y(dx,dy,dz,d\theta y+\Delta d\theta_y,d\theta z)-M_y(dx,dy,dz,d\theta y,d\theta z)}{\Delta d\theta_y} \quad \cdots \quad (2.57) \\ K_{\theta_y\theta_z} &= \frac{\partial M_y}{\partial(\theta_z)} = \frac{M_y(dx,dy,dz,d\theta y,d\theta z+\Delta d\theta_z)-M_y(dx,dy,dz,d\theta y,d\theta z)}{\Delta d\theta_z} \end{aligned}$$

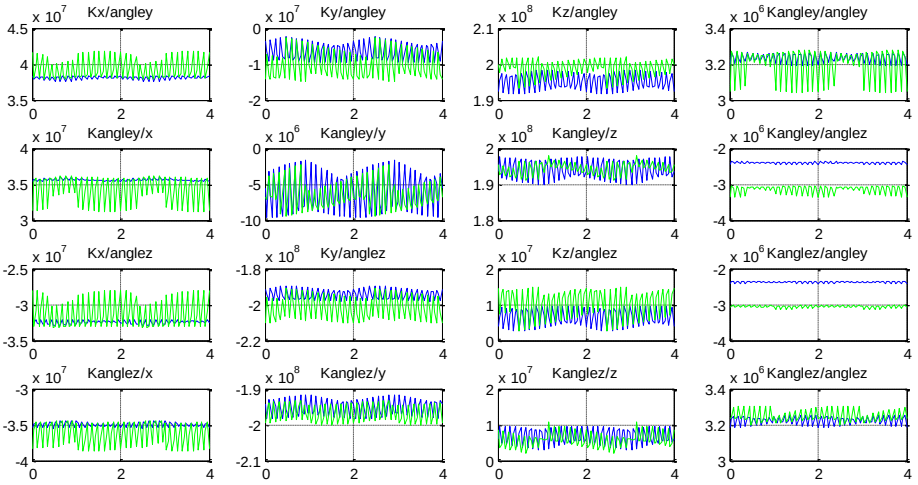

dx=0.8/1000;dy=0.8/1000;dz=0.8/1000;$d\Theta z$=0.1/180×π;$d\Theta y$=0.1/180×π; N=31

(x- time [s] y-stiffness unit blue line-CST results green line-AST results)

Figure2. 30 Comparisons between CST and AST stiffness in rotation

Figure2.30 reveals that phase (distribution of rollers in bearing chamber) will cause more evident periodical fluctuations of stiffness using AST. CST results build up a symmetric stiffness matrix, while AST results produce an asymmetric matrix, but the amount of asymmetry does not deviate very far. Besides, coupled angular stiffness has a more apparent change using AST.

To terminate this chapter, nonlinearity of bearing stiffness coefficients is considered into resonant frequency.

Described under zero phases, nonlinearity of some stiffness terms to inputs:

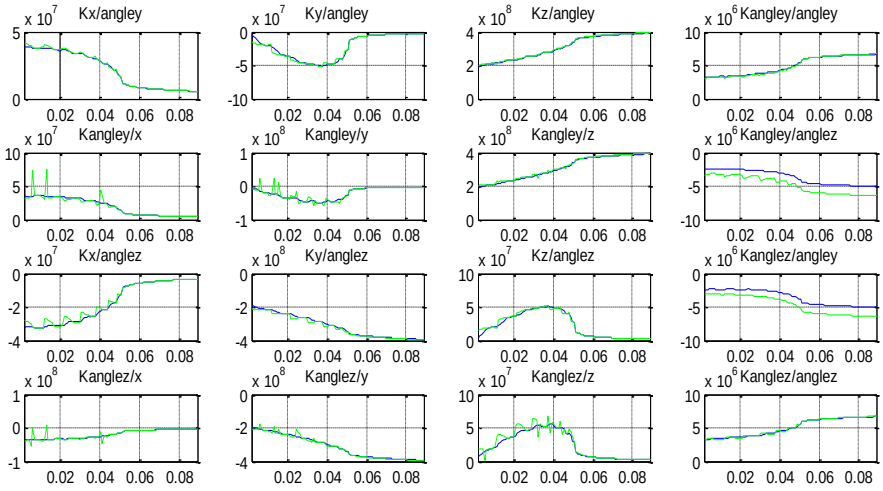

dy=0.8/1000; *dz*=0.8/1000; *dθz*=0.1/180×π; *dθy*= 0.1/180×π; *phi*=0,*N*=31

(*x*- *dx* [m] *y*-stiffness unit blue line- CST results green line-AST results)

Figure2. 31 Comparisons between CST and AST stiffness with d_x changing

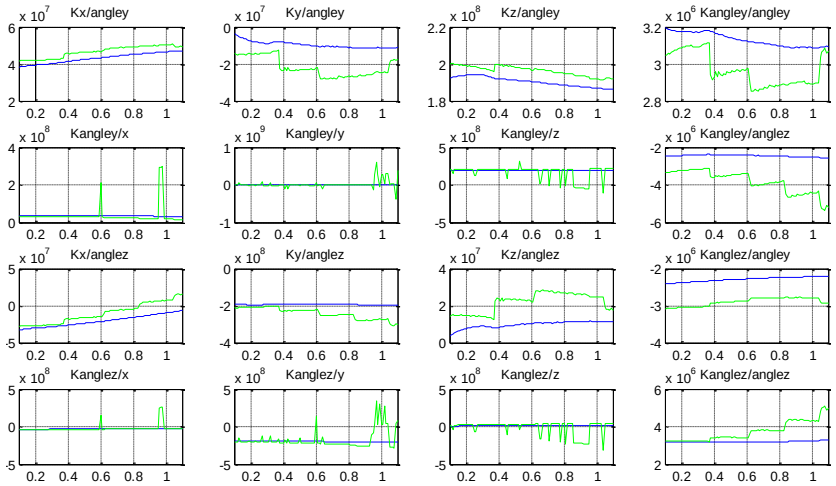

dx=0.8/1000; *dy*=0.8/1000; *dz*=0.8/1000; *dθz*=0.1/180×π; *phi*=0,*N*=31

(*x*- *dθy* [°] *y*-stiffness unit blue line-CST results green line-AST results)

Figure2. 32 Comparisons between CST and AST stiffness with $d_{\Theta y}$ changing

Figure2.31 and **2.32** draw that nonlinear stiffness (AST) is more sensitive to angular displacements compared to linear displacements. AST results imply richer information hidden behind larger angular displacements. It used to be explained by vibration characteristics in engineering.

In some special applications (like axle-box bearing in railways), bearing inputs are of high frequencies but low amplitudes. So that, system resonant frequency *f* can be predicted to understand how these bearings support the excitations, using linearized static stiffness.

$$f \approx \frac{1}{2\cdot\pi}\cdot\frac{\sqrt{\frac{stiffness}{m \ or \ J}}}{\sqrt{1-2\cdot(\alpha')^2}}$$

Where, *m* and *J* are the suspended mass and moment of inertia.

α' is a damping factor, on the amount of 0.05 for example.

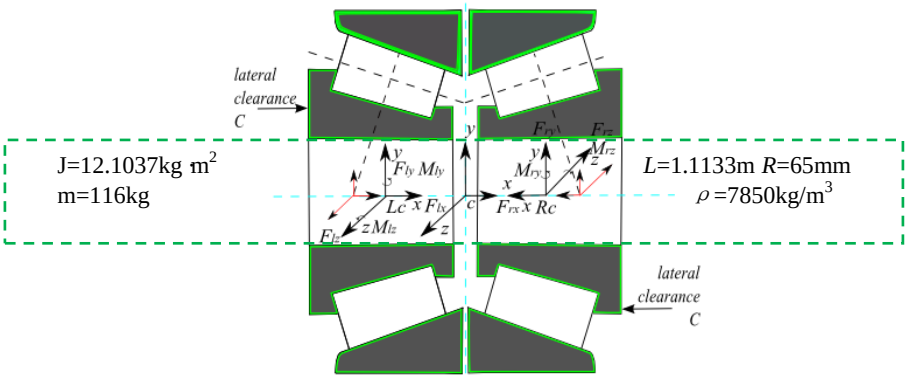

Figure2. 33 Double-row tapered roller bearing supporting a shaft at the centre

Since angular displacements bring about more different nonlinear stiffness, it will be necessary to see how this difference evolves under more varying angular displacements. Below give two waterfall plots of preload(*dx*)-motion(*dθy*)-resonant frequencies and one plot of rotation(*t*)-motion(*dθy*)-resonant frequencies.

Figure 2.34~2.36: *dx*=0.8/1000;*dy*=0.8/1000; *dz*=0.8/1000; *dθz*=0.1/180×π;,*N*=31

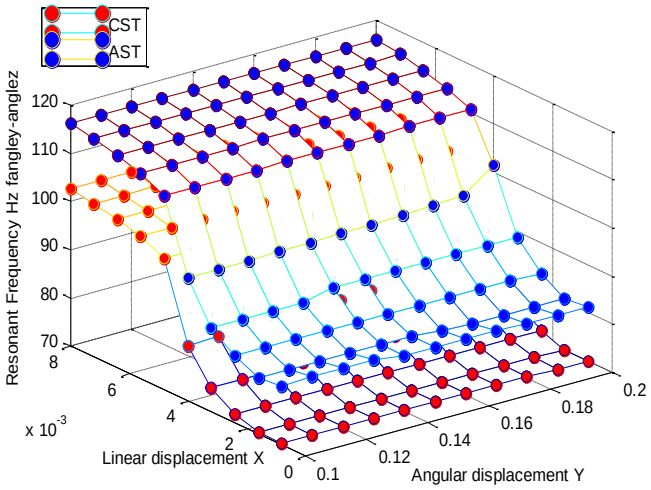

Figure2. 34

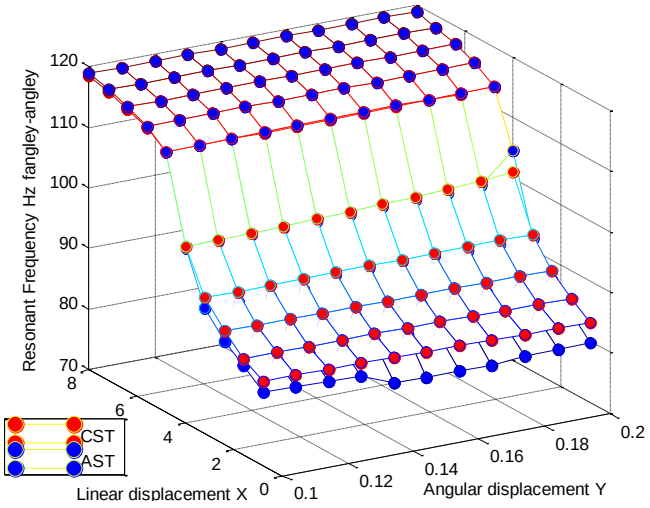

Figure2. 35

Figure 2.34~2.35 Waterfall curves of Preload (dx)-Motion($d\Theta y$)-Resonant frequencies($f_{d\Theta y\text{-}d\Theta z}$, $f_{d\Theta y\text{-}d\Theta y}$)

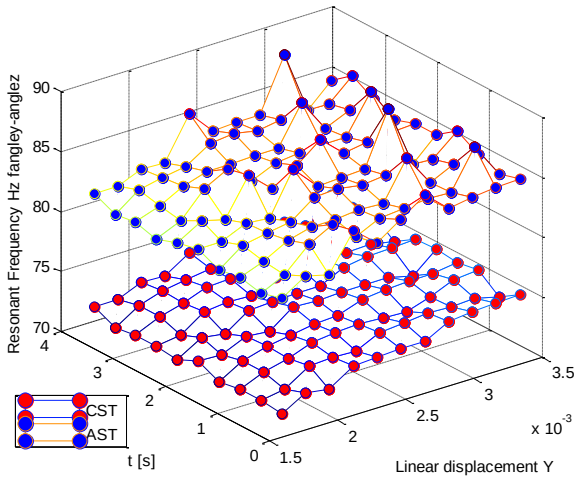

Figure2. 36 Waterfall curves of Time(t)-Motion(d_y)-Resonant frequencies($f_{d\Theta y\text{-}d\Theta z}$)

Figure2.34~2.35 reveals that prediction on coupled vibration ($d\theta y$-$d\theta z$) is more easily affected by calculation techniques(CST or ASC) than self-excited vibration ($d\theta y$-$d\theta_Y$). **Figure2.36** still pictures that rotation causes a fluctuation, but plays less importantly than displacements. The results also predict that resonant frequency changes much more steeply at lighter preload than at heavier preload, so that adequate preload is beneficial to improving stability.

Lots of frequencies exist simultaneously in motion. Some components are unexplainable at times, now the ones resulted from five inputs are more accurately predicted.

2.5 Conclusion

Bearing transmission is better predicted by considering roller edge effect. R.Teutsch's and new developed ASTs are introduced based on first approximation method with their errors explained. Meanwhile, reduced roller contact calculation is also developed by mixing first and second approximation methods. At last, bearing stiffness components and relevant vibrating characteristics are discussed. This paper in fine provides a numerically stable and engineering-adequate bearing model of suitable complexity. Such convenient calculations will be possible to better predict the performances of bearing and its adjacent components by implementing in any non-linear F.E.A package or any complex M.B.S package.

2.6 Nomenclature

D	roller diameter at center	m	ψ	azimuth angle of roller	rad
L	roller length	m	R_i, R_o	mean inner and outer race radius	m
Z	roller number	-	α	half included cup angle	rad
C	lateral clearance	m	δ	contact interference	m
N	slice number	-	γ	half included centre line angle	rad
$dx, dy, dz, d\Theta y, d\Theta z$	displacements	m, rad	w	rotation speed	rad/s
$\Delta dx, \Delta dy, \Delta dz$	displacements due to tilting angles between raceways	m	ϕ_{tilt}, ϕ_{skew}	equivalent tilting and skewing angles of rollers relative to cup	rad
F_x, F_y, Fz, My, Mz	loads	N, N·m			

2.7 References

[24] Reusner, H., 1987, "The Logarithmic Roller Profile-the Key to Superior Performance of Cylindrical and Taper Roller Bearings," Ball Bearing J., Vol. 230, pp. 2–10.

[25] Harris T A. Rolling element analysis [M]. 4th Ed. New York: Wiley-Interscience publication, 2001.

[26] Teutsch R., Sauer B., 2004, "An Alternative Slicing Technique to Consider Pressure Concentrations in Non-Hertzian Contacts", ASME Journal of Tribology, Vol. 126, pp.436-442.

[27] Reusner H. 1960, "Druckflachenbelastung und Oberflachenverschiebung im Walzkon-tact von Rotationskorpern", Ph.D. thesis, Fakultät für Maschinenbau der Universität Karlruhe.

[28] Hartnett M. 1980, "A general numerical solution for elastic body contact problems", ASME, Applied Mechanic Division, 39, pp. 51-66.

[29] De Mul, J. M., Kalker, J. J., Vree J.M., "An orthogonal uniform/parabolic surface pressure Half-space element for the analysis of Non-Hertzian Contact", COMPUTATIONAL MECHANICS, New Trends and Applications, S. Idelsohn, E. Oñate and E. Dvorkin (Eds.) ©CIMNE, Barcelona, Spain, 1998

[30] Bruno Mevel, "Accuracy in Tapered Roller Bearing Equilibrium", STLE Annual Meeting, Detroit, Michigan, USA, May 5-9, 2013.

[31] Bruno Mevel, "Numerical Methods in Bearing Roller Tilt Analysis", Tribology Transactions, 2016, pp. 1-32.

[32] Polonsky I.A., Keer L.M. (1999), "A numerical method for solving rough contact problems based on the multi-level multi-summation and conjugate gradient technique", Wear, 231, pp. 206-219.

[33] Boucly V., Nelias D., Green I. (2007), "Modeling of the rolling and sliding contact Between Two Asperities", Journ. Trib., 129, pp. 235-245.

[34] Palmgren, A., 1959, "Grundlagen der Walzlagertechnik", 2nd ed., Francklische Verlagshandlung, W. Keller & Co.

[35] Kunert, K. (1961), "Spannungsverteilung im Halbraum bei elliptischer Flachenpressungsverteilung über einer rechteckigen Druckflache," Forschung auf dem Gebiete des Ingenieurwesens, 27(6), pp. 165-174.

[36] Houpert, L., 2001, "An Engineering Approach to Hertzian Contact Elasticity-Part I," ASME J. Tribol., 123, pp. 582-588.

[37] Lundberg, G., 1939, "Elastische Berührung zweier Halbraume," Forschung auf dem Gebiete des Ingenieurwesens, 10(5), pp. 201-211.

[38] De Mul, J. M., Kalker, J. J., and Fredriksson, B., 1986, "The Contact between Arbitrarily Curved Bodies of Finite Dimensions,'' ASME J. Tribol., 108, pp. 140–148.

[39] Rothbart, H. A., 1985, Mechanical Design and Systems Handbook, 2nd ed., McGraw-Hill.

[40] Houpert L., 1997, "A Uniform Analytical Approach for Ball and Roller Bearing," ASME J. Tribol., 119, pp. 851–857.

[41] Liu, J., De Mul, J. M., Vree, J. M., and Maas, D. A., "Equilibrium and Associated Load Distribution in Ball and Roller Bearings Loaded in Five Degrees of Freedom While Neglecting Friction-Part I: General Theory and Application to Ball Bearings, Journal of Tribology, Vol. 111, No. 1, pp. 140-148, 1989.

[42] Bercea, I., Nelias, D. and Cavallaro, G. A unified and simplified treatment of the nonlinear equilibrium problem of double-row rolling bearings - Part 1: rolling bearing model. Proc. Instn Mech. Engrs, Part J: J. Engineering Tribology, 2003.
[43] Gupta P.K., "On the dynamics of a Tapered Roller bearing", ASME J. Tribol., 111(2), pp. 278-287.
[44] Houpert, L., 2014, "An Enhanced Study of the Load-Displacement Relationships for Rolling Element Bearings," ASME J. Tribol., 136(1), p. 011105.
[45] Yang Hai-sheng, etc., "Analysis of the roller-race contact deformation of cylindrical roller bearing using an improved slice method", 2011 International Conference on Mechatronic Science, Electric Engineering and Computer August 19-22, 2011, Jilin, China
[46] Boussinesq, J., "Application des Potentiels à l'Etude de l'Equilibre et du Mouvement des Solides Elastiques," Paris : Gauthier-Villars, 1880.
[47] Harris, T. A., and Kotzalas, M. N., 2007, "Essential Concepts of Bearing Technology," Rolling Bearing Analysis, 5th ed., CRC Press, Taylor and Francis, London.
[48] Timoshenko, S. P., Goodier, J. N., "Theory of Elasticity," 3d ed., New York: McGraw-Hill, 1970.
[49] Kleckner R J. High speed cylindrical roller bearing analysis, SKF computer program "CYBEAN", NASA-CR-159460[R]. Washington DC: NASA, 1978.
[50] Lundberg, G., "Elastic Contact between Two Semi-infinite Bodies," Forschung auf dem Gebiete des Engenienswesens, 1961(5), pp. 2-3.
[51] Nelias D., Bercea I., Paleu V. (2008), "Prediction of Roller Skewing in Tapered Roller Bearings", Trib.Trans., 51(2), pp. 128-139

Appendix C Deflection-load relationships for inner and outer race-to- roller contact

Palmgren[34]

$$\delta_i = \delta_o = 3.85 \cdot 10^{-5} \cdot \frac{Q^{0.9}}{L^{0.8}}$$

Kunert[35]

$$\delta_i = \delta_o = 4.05 \cdot 10^{-5} \cdot \frac{Q^{0.925}}{L^{0.85}}$$

Houpert[36]

$$\delta_i = [\frac{Q(1-\nu^2)}{0.2723 \cdot E \cdot L} \cdot d_m^{0.074}]^{1/1.074}$$
$$\delta_o = [\frac{Q(1-\nu^2)}{0.27835 \cdot E \cdot L} \cdot \left(\frac{t}{1+D/d_m}\right)^{0.078}]^{1/1.078}$$

Teutsch[26]

$$\delta_i = 3.17 \cdot (\frac{d_m}{2})^{0.08} \cdot [\frac{Q(1-\nu^2)}{E \cdot L}]^{0.92}$$
$$\delta_o = 2.66 \cdot \left(\frac{t}{1+D/d_m}\right)^{0.09} \cdot [\frac{Q(1-\nu^2)}{E \cdot L}]^{0.91}$$

Lundberg[37]

$$\delta_i = \delta_o = \frac{Q}{\pi} \cdot \frac{2}{L} \cdot (\frac{1-\nu_1^2}{E_1} + \frac{1-\nu_2^2}{E_2}) \cdot (1.8864 + \ln\frac{L}{2 \cdot b})$$

Tripp[38]

$$\delta_i = (\frac{Q}{\pi} \cdot \frac{2}{L}) \cdot [\frac{1-\nu_1^2}{E_1} \cdot (\ln\frac{4R_1}{b} - \frac{1}{2}) + \frac{1-\nu_2^2}{E_2} \cdot (\ln\frac{4R_2}{b} - \frac{1}{2})]$$
$$\delta_o = (\frac{Q}{\pi} \cdot \frac{2}{L}) \cdot [\frac{1-\nu_1^2}{E_1} \cdot (\ln\frac{4R_1}{b} - \frac{1}{2}) + \frac{1-\nu_2^2}{E_2} \cdot (\ln\frac{2t}{b} - \frac{\nu_2}{2(1-\nu_2)})]$$

Dinink[39]

$$\delta_i = (\frac{Q}{\pi} \cdot \frac{2}{L}) \cdot [\frac{1-\nu_1^2}{E_1} \cdot (\frac{1}{3} + \ln\frac{2R_1}{b}) + \frac{1-\nu_2^2}{E_2} \cdot (\frac{1}{3} + \ln\frac{2R_2}{b})]$$
$$\delta_o = (\frac{Q}{\pi} \cdot \frac{2}{L}) \cdot [\frac{1-\nu_1^2}{E_1} \cdot (\frac{1}{3} + \ln\frac{2R_1}{b}) + \frac{1-\nu_2^2}{E_2} \cdot (\frac{1}{3} + \ln\frac{t}{b})]$$

Kowalsky[40]

$$\delta_i = (\frac{Q}{\pi} \cdot \frac{2}{L}) \cdot [\frac{1-\nu_1^2}{E_1} \cdot (0.407 + \ln\frac{2R_1}{b}) + \frac{1-\nu_2^2}{E_2} \cdot (0.407 + \ln\frac{2R_2}{b})]$$
$$\delta_o = (\frac{Q}{\pi} \cdot \frac{2}{L}) \cdot [\frac{1-\nu_1^2}{E_1} \cdot (0.407 + \ln\frac{2R_1}{b}) + \frac{1-\nu_2^2}{E_2} \cdot (0.407 + \ln\frac{t}{b})]$$

Chapter 3

Calculation on nonlinear bearing-rotor system

3.1 Introduction

Bearing technology is a kind of old knowledge, the traditional questions-dynamic interfacial parameters are always welcome in both bearing and relevant transmission applications since accurate and efficient coupling analysis of dynamic relations and subsequent design of structural composition and parameters are required according to diverse demands. Bearing interference characterized by coefficient matrix and its coupling approach with rotor system are of prime interest in this chapter.

From bearing stiffness matrix …

Numerous study efforts have come to bearing stiffness matrix. It has ever been performed by Jones **[52]**, Harris **[53]**, Palmgren **[54]** and others, where either ideal boundary assumption or ignorance of some certain degree of freedom was employed, and failed to simulate the coupled translational and rotational vibrations.

Bearing transmission load is obtained based on a discrete summation method ever used by Lim and Singh **[55]~[57]** or based on an integration method adopted by Hernot **[58]**before formulated into stiffness matrix.

Houpert **[59]** provided a uniform engineering model for both tapered roller and ball bearings in 1997. Later in recent years **[60]~[61]**, a transition from point contact to line contact as load increases has been considered, it chose displacements as model inputs, and a finite differential method was also referred in his work to get stiffness matrix. Like his interest, the authors of this thesis also developed a fast method of calculating bearing stiffness matrix considering roller edge effect in the work **[59]**. However, possible difficulties in finite difference formulation are the selection of differential step size as well as the need of replicated load calculation for several times.

Besides these efforts above, what cannot be also forgotten is a FEM (Finite element method) model used by Guo and parler **[62]** and an experimental approach used by Knaapen

R **[63]**. Although much would be cost, they still well stand for current engineering conceptions.

… **to bearing damping matrix**

On the other hand, bearing applications often occur in high-speed machineries vibrating at high frequency. Strict application conditions also lead to accurate analysis in bearing damping matrix.

Sarangi, M. et al. **[64]~[66]** have proposed two models "Linear spring-damper model of Lubricated Contacts" and "Nonlinear spring-damper model of Lubricated Contacts" for both ball bearing in 2004, 2005 and for roller bearing in 2013, but they were for 2D questions, also based on their former works, in which, they got curve-fitting results by a transition from distributed EHL parameters to lumped parameters, but it was still founded on steady EHL. The authors of this chapter also show a different understanding of transient EHL contact stiffness and damping distributions in the first chapter.

From modeling methods of integrated rotor-bearing system …

Dynamic performances of rotor system depend on different configurations, bearing model can be assumed to be rigid, linear **[69]** or nonlinear, and rotor can be also modeled as rigid system, lumped mass system (with massless beam) or continuous mass system (Euler-Bernoulli beam element, Rayleigh model, Timoshenko beam element **[69],** etc.). At the same time, some effects of stiffness, damping, rotary inertia, gyroscopic moments, or shear deformation of different unit on rotor system have also been studied to different extent. In this chapter, nonlinearity of bearing is emphasized, while rigid rotor is employed.

To mathematically connect sub-models composing rotor-bearing system, transfer matrix method (TMM) and finite element method (FEM) are two mainstream methods. The marching idea in TMM makes the incorporated matrix present at a fixed dimension, beneficial for programming development. FEM should be the earliest method, succeeds in accuracy, but fails in efficiency since the selection of unit needs a careful discussion.

As far as TMM is concerned, since it was first employed in linear bearing-rotor system by Prohl, it has experienced a long-term development, but it still needs a discussion when nonlinear bearing is considered.

… to solving methods of integrated rotor-bearing system

Normally, both time and frequency methods are developed to solve the equations. Compared to frequency methods, not too many arguments are about how to solve nonlinear bearing-rotor equations in a more efficient time-domain way, but higher focus is on parametric influence on system responses as well as discovery of rich nonlinear phenomena in it.

In time integration method **[70]**, periodic, aperiodic, and quasi-periodic solutions can be obtained together with transient responses. However, steady state responses can only be acquired after transient responses. But, it still belongs to a qualitative method by watching the clock of periodic solution's appearance. To perform stability analysis quantitatively, shooting method is often used to get periodic solution, but it requires strict initial values and integration step.

In frequency domain methods, the transient responses are deliberately skipped so that steady state responses of desired frequencies can be directly calculated in a fast way. However, the complexity of non-linear items included in non-linear differential equations determines accessible treatments. Some treatments, like perturbation method, multi-scale method, classical HB method, etc. require application of Taylor expansion or curve-fitting methods, where truncation of high order series does introduce errors and limit periodic solution only obtained around Taylor expansion point. More efficient methods **[71]**,**[72]** for non-linear questions-IHB, HB-AFT, and GHB were later developed. Different from IHB and GHB methods, HB-AFT method performs better technically in nonlinear bearing-rotor system by simultaneously interpreting unknown response and bearing force as combined harmonics.

This chapter undertakes to develop more practical bearing matrices and more reliable model-solving methods in a uniform and economic way.

Practically, we can find a wide usage of analytical model (Lim and Singh, Houpert, etc.) in gear box or other machines, which has been regarded as a fast and enough accurate use. But theoretically, in roller bearing, the integrated load for one roller ignored the high order load term after performing Taylor expansion of Plamgren's roller load relation **[59]**, it would produce errors when slightly gross tilting angle of roller occurs, so that slice technique is intentionally used instead. And in ball bearing, varying contact angle affecting both

deformation value and load transmission is also considered. The two points distinguish and also supplement main diversities in uniform matrices of ball and roller bearings.

Meanwhile, application of roller bearing matrices in time/frequency domain analysis on rotor dynamics system is performed respectively. In time domain analysis, solving method is improved to ensure a convergent result. While in frequency domain analysis, a practically accepted way to periodic solution with less programming effort is manually programmed, using the current popular HB-AFT (Harmonic Balance-Alternating Frequency Time) algorithm to form a uniform 3D code.

3.2 Nonlinear Models of Roller Contact Damping and Stiffness

The dynamic parameters for each lubricated contact in both roller and ball bearings are primarily extracted here. Different from ball bearing, description of both EHL and elastic contact requires an extra usage of slice technique in the roller bearing for analyzing load configuration.

Characteristics of Lubricated Contact

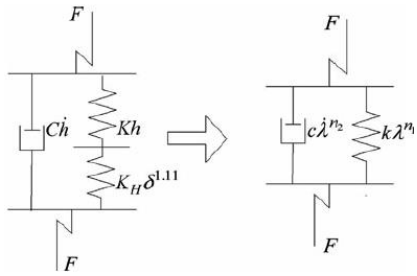

Figure3. 1 Equlivalent stiffness and damping of a lubricated contact

Equivalent contact stiffness at each contact can be simplified by

$$k = \frac{dF}{d\lambda} = \frac{dF}{d\delta - dh} = \frac{K_H K_{EHL}}{K_{EHL} - K_H} \tag{3. 1}$$

According to Harris' relation[73] for line contact, Brewe and Homrock's simplified solution [74] for point contact, Dowson and Higginson's line EHL formula as well as Homrock and Dowson's point EHL formula[75], dynamic contact parameters are derived as (SI units)

$$K_H = \frac{(E')^{0.9}}{2.1054} \frac{l^{0.8}(N \cdot F)^{0.1}}{N} = 1.2037 F\delta^{-1} \qquad \text{For roller slice contact}$$

$$K_H = 1.5\left(\frac{\pi k_e E'}{3\Gamma}\right)^{2/3}\left(\frac{2\Sigma RF}{\Gamma}\right)^{1/3} = 1.5F\delta^{-1}$$ For ball contact

$$K_{EHL} = -\frac{E'R_y^{\,2}}{0.27733N}[\bar{U}^{0.7}G^{0.6}W^{-1.13}]^{-1} = -7.69240Fh_c^{-1}$$ For roller slice contact

$$K_{EHL} = -\frac{E'R_y^{\,2}}{0.18023}[\bar{U}^{0.67}G^{0.53}W^{-1.067}(1-0.61e^{-0.73k_e})]^{-1} = -14.9254Fh_c^{-1}$$ For ball contact

Based on Sommerfeld boundary conditions and simplified integration of Reynolds equation, loads **[76]**, **[77]** supported by inlet oil for roller and ball contact are

$$F_{ef} = \left(\frac{4\eta_0 u_x R_x l}{h_c} + \frac{3\pi\eta_0 R_x^{1.5} l}{h_c^{1.5}} u_z\right)\frac{1}{N}$$ For roller slice contact

$$F_{ef} = \frac{4\eta_0 u_x R_x a}{h_c^{\,2}(k_f/k_c+1)} + \frac{6\pi\eta_0 R_x^{1.5} a}{\sqrt{2}h_c^{1.5}} u_z$$ For ball contact

Central film thicknesses are given by

$$h_c = \frac{4}{3}\cdot 1.6\bar{U}^{0.7}G^{0.6}W^{-0.13}$$ For line contact

$$h_c = 2.69\bar{U}^{0.67}G^{0.53}W^{-0.067}(1-0.61e^{-0.73k_e})$$ For ball contact

Steady squeeze effect at inlet area can pry up the roller, similarly, the transient squeeze effect caused by transient term in Reynolds' equation should also have some effects, resulted from u_z, but relevant to formation of h_c.

Equivalent damping coefficient

$$c = C_{ef} = \frac{dF_{ef}}{du_z} = \frac{3\pi\eta_0 R_x^{1.5} l}{h_c^{1.5}}\frac{1}{N}$$ For roller slice contact

$$c = C_{ef} = \frac{dF_{ef}}{du_z} = \frac{6\pi\eta_0 R_x^{1.5} a}{\sqrt{2}h_c^{1.5}}$$ For ball contact

Inlet squeeze velocity is nearly equal to approaching velocity of two bodies,

$$u_z = \frac{d\lambda}{dt}$$

With given amplitude and initial phase, a harmonic vibration can be described.

$$\frac{d\lambda}{dt}=R_e[i\omega\lambda]$$

Where, $\begin{cases}\lambda(t)=\lambda_0\cos(\omega t+\varphi_0)=R_e[(\lambda_1+i\,\lambda_2)e^{i\omega t}]\\ \lambda_0=\sqrt{\lambda_1{}^2+\lambda_2{}^2}\\ \varphi_0=\arctan\frac{\lambda_2}{\lambda_1}\end{cases}$.

So, individual contact force including damping and elastic loads is

$$\partial F=(k+i\omega c)\partial\lambda \tag{3. 2}$$

Linear Model of damping and stiffness matrices

Finite differential method **[60]** has been used to approach stiffness and damping matrices by comparing bearing load vectors under different similar displacements with only tiny fluctuation for designated differential value. We can see the entire dynamic effect, but not internal transient parametric details.

Herein, stiffness and damping matrices are assembled by transient dynamic parameters from all available contact sources.

In such case, overall stiffness and damping matrices of a roller bearing are derived below,

$$[K]=[\frac{\partial\{Q\}}{\partial\{d\}^T}]=[\sum_{i=1}^{Z}[\sum_{j=1}^{N}(\frac{\partial\{F_{ij}\}}{\partial\{\lambda_{ij}\}^T}\frac{\partial\{\lambda_{ij}\}^T}{\partial\{d\}^T})]] \tag{3. 3}$$

$$[C]=[\frac{\partial\{Q\}}{\partial\{\dot{d}\}^T}]=[\sum_{i=1}^{Z}[\sum_{j=1}^{N}(\frac{\partial\{F_{ij}\}}{\partial\{\dot{\lambda}_{ij}\}^T}\frac{\partial\{\dot{\lambda}_{ij}\}^T}{\partial\{\dot{d}\}^T})]] \tag{3. 4}$$

And for a ball bearing $N=1$, they are

$$[K]=[\frac{\partial\{Q\}}{\partial\{d\}^T}]=[\sum_{i=1}^{Z}[\frac{\partial\{F_i\}}{\partial\{\lambda_i\}^T}\frac{\partial\{\lambda_i\}^T}{\partial\{d\}^T}]]$$

$$[C]=[\frac{\partial\{Q\}}{\partial\{\dot{d}\}^T}]=[\sum_{i=1}^{Z}[\frac{\partial\{F_i\}}{\partial\{\dot{\lambda}_i\}^T}\frac{\partial\{\dot{\lambda}_i\}^T}{\partial\{\dot{d}\}^T}]]$$

To fulfill the above-mentioned matrices, each contact load as well as equivalent contact parameters for one rolling element should be understood at first.

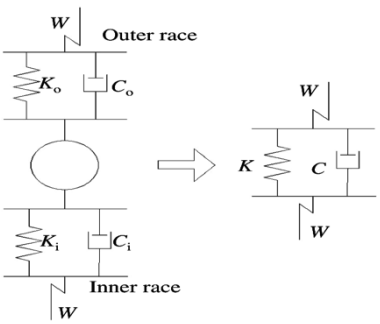

Figure3. 2 Equlivalent stiffness and damping of one rolling element

Equivalent contact parameters for one rolling element are derived here by ignoring roller's mass and assuming linear vibration.

In this case, resultant equivalent frequency-dependent contact parameters for a pair of roller slice's lubricated contacts can be evaluated by means of complex equation (Dietl 1997),

$$k + i\omega c = \left(\frac{s}{k_i + i\omega c_i} + \frac{1}{k_O + i\omega c_O}\right)^{-1} \tag{3. 5}$$

Where, ω is the angular frequency, generally of the inner race, outer race, cage or ball pass frequencies, or combinations of two or more of these **[77]**.

3.3 Load Distributions in Bearing

With five known displacements applied on the bearing as showed in **Figure3.3** and **Figure3.4**, initial and general relative positions of inner and outer races are shown, and the rollers occupied in loading area undergo elastic deformation.

For easy analysis, some initial geometric contact relations are prescribed in advance for the analytical model of tapered rolling bearing.

- When *dy* and *dz* are nil, central lines of both races coincide with each other.
- *dx* equal to zero corresponds to both raceways just touching rolling elements.

Please note, the same "zero" convention still applies when describing a ball bearing.

Geometric relation in tapered roller bearing

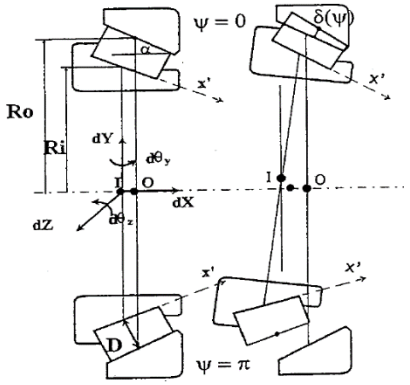

Figure3.3 Deformation distribution in roller bearing (Houpert)

Euler angles are used to demonstrate the relative rotations between raceways. The rotations around *z* axis and updated *y* axis are considered successively. Tilting angles of the cone relative to the cup cause additional displacements at any spatial point.

$$\begin{bmatrix}\Delta d_X\\ \Delta d_y\\ \Delta d_Z\end{bmatrix}=\begin{bmatrix}x\\ y\\ z\end{bmatrix}-\begin{bmatrix}\cos(d\theta_y)\cos(d\theta_Z) & \cos(d\theta_y)\sin(d\theta_Z) & -\sin(d\theta_y)\\ -\sin(d\theta_Z) & \cos(d\theta_Z) & 0\\ \sin(d\theta_y)\cos(d\theta_Z) & \sin(d\theta_y)\sin(d\theta_Z) & \cos(d\theta_y)\end{bmatrix}\begin{bmatrix}x\\ y\\ z\end{bmatrix} \tag{3.6}$$

Arbitrary roller contact position is

$$\begin{bmatrix}x\\ y\\ z\end{bmatrix}=\begin{bmatrix}D\sin\alpha+x'/\cos\gamma\times\cos\alpha\\ (R_O-x'/\cos\gamma\times\sin\alpha)\cos\psi\\ (R_O-x'/\cos\gamma\times\sin\alpha)\sin\psi\end{bmatrix} \tag{3.7}$$

$$\text{With } x'=(j-\frac{N-1}{2}-1)\cdot l/N$$

Total approaching value along contact line at azimuth angle ψ is proposed as

$$\lambda(\psi,x')=(d_X+\Delta d_X)\sin\alpha+\{(d_y+\Delta d_y)\cos\psi+(d_Z+\Delta d_Z)\sin\psi\}\cos\alpha \tag{3.8}$$

Geometric relation in ball bearing

The ball diameter is *D*, the race curvature radii are r_i and r_o with curvature centers *i* and *o* at a distance of R_i', R_o' from rotation axis respectively. Inner and outer race centers are *I* and *O*. the initial contact angle is α_0.

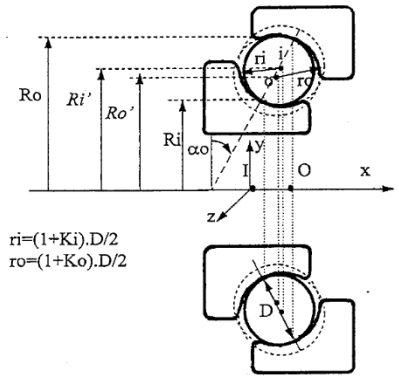

Figure3.4 geometrical parameters in ball bearing(Houpert)

Inner and outer race curvature centers *i*, *o* are respectively located at

$$[x_I \quad y_I \quad z_I]^T = [r_i \sin\alpha_0 \quad R_i' \cos\psi \quad R_i' \sin\psi]^T$$

$$[x_O \quad y_O \quad z_O]^T = [(D - r_o)\sin\alpha_0 \quad R_o' \cos\psi \quad R_o' \sin\psi]^T$$

Different from roller bearing, change of ball-race contact angle brings about different deformation-load relation, while flexible bearing inputs lead to variation of the loaded contact angle α, affecting the paths of load transmission and local elastic deflection.

To pursue a uniform analytical approach, relative displacement between race curvatures centers *i* and *o* is calculated.

Similarly, tilting angles of outer race relative to inner race cause additional relative displacements between race curvature centers and update contact angles for different balls.

$$\begin{bmatrix} \Delta d_x \\ \Delta d_y \\ \Delta d_z \end{bmatrix} = \begin{bmatrix} x_O \\ y_O \\ z_O \end{bmatrix} - \begin{bmatrix} \cos(d\theta_y)\cos(d\theta_z) & \cos(d\theta_y)\sin(d\theta_z) & -\sin(d\theta_y) \\ -\sin(d\theta_z) & \cos(d\theta_z) & 0 \\ \sin(d\theta_y)\cos(d\theta_z) & \sin(d\theta_y)\sin(d\theta_z) & \cos(d\theta_y) \end{bmatrix} \begin{bmatrix} x_O \\ y_O \\ z_O \end{bmatrix} \tag{3. 9}$$

According to a derivation in **Appendix D**, under varying contact angle, resultant interference of ball at azimuth angle ψ owns a uniform expression with tapered type,

$$\lambda(\psi) = -\{(d_x + \Delta d_x)\sin\alpha_0 + [(d_y + \Delta d_y)\cos\psi + (d_z + \Delta d_z)\sin\psi]\cos\alpha_0 \tag{3. 10}$$

And, variation of contact angle is

$$\Delta\alpha = (\tan\alpha_0 + \tan^{-1}\alpha_0)\left(\frac{d_x + \Delta d_x}{x_O - x_I} - \frac{(d_y + \Delta d_y)\cos\psi + (d_z + \Delta d_z)\sin\psi}{(y_O - y_I)\cos\psi + (z_O - z_I)\sin\psi}\right) \tag{3. 11}$$

Load-deformation relation

Approach (λ) of outer race-roller slice (or ball)-inner race is intentionally organized by load term and coefficient term independent of load.

$$\lambda = \delta - h = K_{HC} F^{n_1} - K_{EHLC} F^{n_2} \tag{3. 12}$$

$n_1 = 1/1.11, n_2 = -0.13$ For roller type

$n_1 = 2/3, n_2 = -0.067$ For ball type

Where,

$$K_{HC} = \left(\frac{s}{K_{Hi}}\right)^{n_1} + \left(\frac{1}{K_{Ho}}\right)^{n_1}$$

$s = \frac{Q_i}{Q_o} = \frac{\sin(\theta_o + \theta_f)}{\sin(\theta_i + \theta_f)} \approx 0.99$ For tapered roller contact

$s = 1$ For cylindrical roller or ball contact

$K_{Hi} = K_{Ho} = \frac{E' l^{\frac{8}{9}}}{2.8072N}$ For roller slice contact

$K_{Hi} = K_{Ho} = \pi k_e E' \cdot \left(\frac{R\Sigma}{4.5\Gamma^3}\right)$ For ball contact

And,

$K_{EHLC} = \frac{4}{3} \cdot (1.6 \bar{U}_i^{0.7} G_i^{0.6} s^{n_2} + 1.6 \bar{U}_o^{0.7} G_o^{0.6})$ For roller type

$K_{EHLC} = 2.69 \bar{U}_i^{0.67} G_i^{0.53} (1 - 0.61 e^{-0.73 k_{ei}}) + 2.69 \bar{U}_o^{0.67} G_o^{0.53} (1 - 0.61 e^{-0.73 k_{eo}})$ For ball type

Once load is obtained, each contact parameter in **Part 3.2** will be acquired.

3.4 Formulations of Bearing Stiffness and Damping Matrices

Load Transmission through tapered roller Bearing

The force along the roller with N slices will be obtained. The total transmission load at roller contact center that the cup applies on at azimuth angle ψ is given by

$$\begin{cases} F_{\varphi x}=\sin\alpha \sum_{i=1}^{N} p_i \\ F_{\varphi y}=\cos\varphi\cos\alpha \sum_{i=1}^{N} p_i \\ F_{\varphi z}=\sin\varphi\cos\alpha \sum_{i=1}^{N} p_i \end{cases} \quad \begin{cases} M_{\varphi y}=-\sin\varphi\cos\alpha \sum_{i=1}^{N} p_i\cdot(i-\frac{N-1}{2}-1)\cdot L/N \\ M_{\varphi z}=\cos\varphi\cos\alpha \sum_{i=1}^{N} p_i\cdot(i-\frac{N-1}{2}-1)\cdot L/N \end{cases} \tag{3. 13}$$

Where, $p_i = k_i\delta_i^n > 0$ acting on outer race, $p_i = -k_i\delta_i^n < 0$ acting on inner race.

Along roller length, the force acting on a roller will be replaced by an equivalent force and moment at contact center (Houpert, T.C. Lim (ignores additional moment)).

Load transfer to roller contact center helps to concentrate all the forces at $R_i\tan\alpha$ point of inner race's central line, and additional roller moments in rollers can also be transplanted to $R_i\tan\alpha$ point of inner race's central line directly within the scope of theoretical mechanics.

Hence, total load that the outer race applies on the inner race assembly is given by

$$\begin{cases} Q_x=\sum_{\varphi=\varphi_0}^{\varphi_N} F_{\varphi x} \\ Q_y=\sum_{\varphi=\varphi_0}^{\varphi_N} F_{\varphi y} \\ Q_z=\sum_{\varphi=\varphi_0}^{\varphi_N} F_{\varphi z} \end{cases} \quad \begin{cases} M_y=+R_i\cdot\tan\alpha\cdot Q_z+\sum_{\varphi=\varphi_0}^{\varphi_N} M_{\varphi y} \\ M_z=-R_i\cdot\tan\alpha\cdot Q_y+\sum_{\varphi=\varphi_0}^{\varphi_N} M_{\varphi z} \end{cases} \tag{3. 14}$$

The deformation values are far smaller than R_i, and can be neglected when getting total moments.

Organized into Overall stiffness and damping matrices

$$[K]=[\sum_{i=1}^{Z}\{\begin{bmatrix}\sin\alpha & 0\\ \cos\varphi\cos\alpha & 0\\ \sin\varphi\cos\alpha & 0\\ R_i\sin\varphi\sin\alpha & -\sin\varphi\cos\alpha\\ -R_i\cos\varphi\sin\alpha & \cos\varphi\cos\alpha\end{bmatrix}\sum_{j=1}^{N}[\begin{bmatrix}1\\ (j-\frac{N-1}{2}-1)\cdot l/N\end{bmatrix}\begin{bmatrix}\frac{\partial\lambda_{ij}}{\partial d_x}\\ \frac{\partial\lambda_{ij}}{\partial d_y}\\ \frac{\partial\lambda_{ij}}{\partial d_z}\\ \frac{\partial\lambda_{ij}}{\partial d\theta_y}\\ \frac{\partial\lambda_{ij}}{\partial d\theta_z}\end{bmatrix}^T\cdot\frac{\partial F_{ij}}{\partial\lambda_{ij}}]\}] \tag{3. 15}$$

According to geometric and motion relations,

$$\frac{\partial F_{ij}}{\partial\lambda_{ij}}=k=\frac{s\cdot k_i(k_o{}^2+w^2c_o{}^2)+k_o(k_i{}^2+w^2c_i{}^2)}{(s\cdot k_o+k_i)^2+(s\cdot c_o+c_i)^2w^2}$$

$$\frac{\partial\lambda_{ij}}{\partial d_x}=\sin\alpha \qquad \frac{\partial\lambda_{ij}}{\partial d_y}=\cos\varphi\cos\alpha \qquad \frac{\partial\lambda_{ij}}{\partial d_z}=\sin\varphi\cos\alpha$$

$$\frac{\partial\lambda_{ij}}{\partial d\theta_{y(\text{or }z)}}=\begin{bmatrix}\sin\alpha\\ \cos\varphi\cos\alpha\\ \sin\varphi\cos\alpha\end{bmatrix}^T\frac{\partial}{\partial d\theta_{y(\text{or }z)}}\begin{bmatrix}\Delta d_x\\ \Delta d_y\\ \Delta d_z\end{bmatrix}$$

$$\frac{\partial}{\partial d\theta_y}\begin{bmatrix}\Delta d_x\\ \Delta d_y\\ \Delta d_z\end{bmatrix}=-\begin{bmatrix}-\sin(d\theta_y)\cos(d\theta_z) & -\sin(d\theta_y)\sin(d\theta_z) & -\cos(d\theta_y)\\ 0 & 0 & 0\\ \cos(d\theta_y)\cos(d\theta_z) & \cos(d\theta_y)\sin(d\theta_z) & -\sin(d\theta_y)\end{bmatrix}\begin{bmatrix}x\\ y\\ z\end{bmatrix}=-\begin{bmatrix}-d\theta_y & 0 & -1\\ 0 & 0 & 0\\ 1 & d\theta_z & -d\theta_y\end{bmatrix}\begin{bmatrix}x\\ y\\ z\end{bmatrix}$$

$$\frac{\partial}{\partial d\theta_z}\begin{bmatrix}\Delta d_x\\ \Delta d_y\\ \Delta d_z\end{bmatrix}=-\begin{bmatrix}-\cos(d\theta_y)\sin(d\theta_z) & \cos(d\theta_y)\cos(d\theta_z) & 0\\ -\cos(d\theta_z) & -\sin(d\theta_z) & 0\\ -\sin(d\theta_y)\sin(d\theta_z) & \sin(d\theta_y)\cos(d\theta_z) & 0\end{bmatrix}\begin{bmatrix}x\\ y\\ z\end{bmatrix}=-\begin{bmatrix}-d\theta_z & 1 & 0\\ -1 & -d\theta_z & 0\\ 0 & d\theta_y & 0\end{bmatrix}\begin{bmatrix}x\\ y\\ z\end{bmatrix}$$

The same derivation is also employed for damping matrix,

$$[C]=[\sum_{i=1}^{Z}\{\begin{bmatrix}-\sin\alpha & 0\\ \cos\varphi\cos\alpha & 0\\ \sin\varphi\cos\alpha & 0\\ R_i\sin\varphi\sin\alpha & -\sin\varphi\cos\alpha\\ -R_i\cos\varphi\sin\alpha & \cos\varphi\cos\alpha\end{bmatrix}\sum_{j=1}^{N}[\begin{bmatrix}1\\ (j-\frac{N-1}{2}-1)\cdot l/N\end{bmatrix}\begin{bmatrix}\frac{\partial\delta\dot{\lambda}_{ij}}{\partial\dot{d}_x}\\ \frac{\partial\dot{\lambda}_{ij}}{\partial\dot{d}_y}\\ \frac{\partial\dot{\lambda}_{ij}}{\partial\dot{d}_z}\\ \frac{\partial\dot{\lambda}_{ij}}{\partial\dot{d}\theta_y}\\ \frac{\partial\dot{\lambda}_{ij}}{\partial\dot{d}\theta_z}\end{bmatrix}^T\cdot\frac{\partial F_{ij}}{\partial\dot{\lambda}_{ij}}]\}] \tag{3.16}$$

$$\frac{\partial F_{ij}}{\partial\dot{\lambda}_{ij}}=c=\frac{s\cdot c_i(k_o^2+w^2c_o^2)+c_o(k_i^2+w^2c_i^2)}{(s\cdot k_o+k_i)^2+(s\cdot c_o+c_i)^2w^2}$$

$$\frac{\partial\dot{\lambda}_{ij}}{\partial\dot{d}_x}=\sin\alpha \qquad \frac{\partial\dot{\lambda}_{ij}}{\partial\dot{d}_y}=\cos\varphi\cos\alpha \qquad \frac{\partial\dot{\lambda}_{ij}}{\partial\dot{d}_z}=\sin\varphi\cos\alpha$$

Due to $\frac{\partial\dot{\lambda}_{ij}}{\partial\dot{d}\theta_{y(z)}}=\begin{bmatrix}\sin\alpha\\ \cos\varphi\cos\alpha\\ \sin\varphi\cos\alpha\end{bmatrix}^T\frac{\partial}{\partial\dot{d}\theta_{y(z)}}\begin{bmatrix}\Delta\dot{d}_x\\ \Delta\dot{d}_y\\ \Delta\dot{d}_z\end{bmatrix}$ $\qquad \begin{bmatrix}\Delta\dot{d}_x\\ \Delta\dot{d}_y\\ \Delta\dot{d}_z\end{bmatrix}=\frac{\partial}{\partial d\theta_y}\begin{bmatrix}\Delta d_x\\ \Delta d_y\\ \Delta d_z\end{bmatrix}d\dot{\theta}_y+\frac{\partial}{\partial d\theta_z}\begin{bmatrix}\Delta d_x\\ \Delta d_y\\ \Delta d_z\end{bmatrix}d\dot{\theta}_z$

$$\frac{\partial}{\partial d\dot{\theta}_y}\begin{bmatrix}\Delta\dot{d}_x\\ \Delta\dot{d}_y\\ \Delta\dot{d}_z\end{bmatrix}=\frac{\partial}{\partial d\theta_y}\begin{bmatrix}\Delta d_x\\ \Delta d_y\\ \Delta d_z\end{bmatrix} \qquad \frac{\partial}{\partial d\dot{\theta}_z}\begin{bmatrix}\Delta\dot{d}_x\\ \Delta\dot{d}_y\\ \Delta\dot{d}_z\end{bmatrix}=\frac{\partial}{\partial d\theta_z}\begin{bmatrix}\Delta d_x\\ \Delta d_y\\ \Delta d_z\end{bmatrix}$$

Load Transmission through ball Bearing

According to **Appendix E**, contact angle affects load transmission and deformation fluctuation.

$$\begin{cases}Q_x=\sum_{i=\varphi_0}^{\varphi_N}(\sin\alpha_0F_i+\Delta\alpha\cos\alpha_0F_i)\\ Q_y=\sum_{i=\varphi_0}^{\varphi_N}(\cos\varphi\cos\alpha_0F_i-\Delta\alpha\sin\alpha_0\cos\varphi F_i)\\ Q_z=\sum_{i=\varphi_0}^{\varphi_N}(\sin\varphi\cos\alpha_0F_i-\Delta\alpha\sin\alpha_0\sin\varphi F_i)\end{cases} \tag{3.17}$$

$$\begin{cases} M_y = -\sum_{\varphi=\varphi_0}^{\varphi_N} R_i \sin\varphi \sin\alpha_0 F_i - \sum_{\varphi=\varphi_0}^{\varphi_N} \sin\varphi \Delta\alpha (R_i \cos\alpha_0 + r_i) F_i \\ M_z = \sum_{\varphi=\varphi_0}^{\varphi_N} R_i \cos\varphi \sin\alpha_0 F_i + \sum_{\varphi=\varphi_0}^{\varphi_N} \cos\varphi \Delta\alpha (R_i \cos\alpha_0 + r_i) F_i \end{cases} \quad (3.18)$$

Organized into Overall stiffness and damping matrices

$$[K] = [\sum_{i=1}^{Z} \{ \begin{bmatrix} \sin\alpha_0 & \cos\alpha_0 \\ \cos\varphi\cos\alpha_0 & -\sin\alpha_0\cos\varphi \\ \sin\varphi\cos\alpha_0 & -\sin\alpha_0\sin\varphi \\ R_i\sin\varphi\sin\alpha_0 & -\sin\varphi(R_i\cos\alpha_0 + r_i) \\ -R_i\cos\varphi\sin\alpha_0 & \cos\varphi(R_i\cos\alpha_0 + r_i) \end{bmatrix} \begin{bmatrix} \frac{\partial F_i}{\partial \lambda_i} \\ \frac{\partial(\Delta\alpha F_i)}{\partial \lambda_i} \end{bmatrix} \begin{bmatrix} \frac{\partial \lambda_i}{\partial d_x} \\ \frac{\partial \lambda_i}{\partial d_y} \\ \frac{\partial \lambda_i}{\partial d_z} \\ \frac{\partial \lambda_i}{\partial d\theta_y} \\ \frac{\partial \lambda_i}{\partial d\theta_z} \end{bmatrix}^T \}] \quad (3.19)$$

$$[C] = [\sum_{i=1}^{Z} \{ \begin{bmatrix} \sin\alpha_0 & \cos\alpha_0 \\ \cos\varphi\cos\alpha_0 & -\sin\alpha_0\cos\varphi \\ \sin\varphi\cos\alpha_0 & -\sin\alpha_0\sin\varphi \\ R_i\sin\varphi\sin\alpha_0 & -\sin\varphi(R_i\cos\alpha_0 + r_i) \\ -R_i\cos\varphi\sin\alpha_0 & \cos\varphi(R_i\cos\alpha_0 + r_i) \end{bmatrix} \begin{bmatrix} \frac{\partial F_i}{\partial \dot{\lambda}_i} \\ \frac{\partial(\Delta\alpha F_i)}{\partial \dot{\lambda}_i} \end{bmatrix} \begin{bmatrix} \frac{\partial \dot{\lambda}_i}{\partial \dot{d}_x} \\ \frac{\partial \dot{\lambda}_i}{\partial \dot{d}_y} \\ \frac{\partial \dot{\lambda}_i}{\partial \dot{d}_z} \\ \frac{\partial \dot{\lambda}_i}{\partial \dot{d}\theta_y} \\ \frac{\partial \dot{\lambda}_i}{\partial \dot{d}\theta_z} \end{bmatrix}^T \}] \quad (3.20)$$

All related partial differential terms have the same formats as those in tapered roller bearing, except for $\frac{\partial(\Delta\alpha F_i)}{\partial \lambda_i} = \Delta\alpha \frac{\partial(F_i)}{\partial \lambda_i} + F_i \frac{\partial(\Delta\alpha)}{\partial \lambda_i}$

$$\frac{\partial(\Delta\alpha)}{\partial \lambda_i} = \frac{\partial(\Delta\alpha)}{\partial dx}\frac{\partial dx}{\partial \lambda_i} + \frac{\partial(\Delta\alpha)}{\partial dy}\frac{\partial dy}{\partial \lambda_i} + \frac{\partial(\Delta\alpha)}{\partial dz}\frac{\partial dz}{\partial \lambda_i} + \frac{\partial(\Delta\alpha)}{\partial d\theta_y}\frac{\partial d\theta_y}{\partial \lambda_i} + \frac{\partial(\Delta\alpha)}{\partial d\theta_z}\frac{\partial d\theta_z}{\partial \lambda_i}$$

Where, $\frac{\partial(\Delta\alpha)}{\partial dx} = (\tan\alpha_0 + \tan^{-1}\alpha_0)\frac{1}{x_O - x_I}$

$$\frac{\partial(\Delta\alpha)}{\partial dy} = (\tan\alpha_0 + \tan^{-1}\alpha_0)\frac{-\cos\psi}{(y_O - y_I)\cos\psi + (z_O - z_I)\sin\psi}$$

$$\frac{\partial(\Delta\alpha)}{\partial dz} = (\tan\alpha_0 + \tan^{-1}\alpha_0)\frac{-\sin\psi}{(y_O-y_I)\cos\psi+(z_O-z_I)\sin\psi}$$

$$\frac{\partial(\Delta\alpha)}{\partial d\theta_{y(\text{or z})}}=(\tan\alpha_0+\tan^{-1}\alpha_0)\begin{bmatrix}\frac{1}{x_O-x_I}\\ \frac{-\cos\psi}{(y_O-y_I)\cos\psi+(z_O-z_I)\sin\psi}\\ \frac{-\sin\psi}{(y_O-y_I)\cos\psi+(z_O-z_I)\sin\psi}\end{bmatrix}^T\frac{\partial}{\partial d\theta_{y(\text{or z})}}\begin{bmatrix}\Delta d_x\\ \Delta d_y\\ \Delta d_z\end{bmatrix}$$

also for $\frac{\partial(\Delta\alpha F_i)}{\partial\dot{\lambda}_i}=\Delta\alpha\frac{\partial(F_i)}{\partial\dot{\lambda}_i}+F_i\frac{\partial(\Delta\alpha)}{\partial\dot{\lambda}_i}$ and $\frac{\partial(\Delta\alpha)}{\partial\dot{\delta}_i}=0$

In roller bearing, slicing technique used meets with uneven distributions of EHL and Hertz behaviors in each misaligned roller. In ball bearing, variation of contact angle described agrees with essential fluctuations of deformation and load transmission. Bearing transmission matrices are in fine derived with five relative displacements (d_x, d_y, d_z, $d\theta_y$, $d\theta_z$) between raceways acknowledged.

3.5 Application in Nonlinear Bearing-Rigid rotor dynamics

Apart from the model configurations and modeling methods referred in the introduction, another very important part concerns how to solve models as well as to discover the hidden information between solutions and models.

Nonlinearity of bearing unit included in mathematical model used to be in the form of nonlinear force **(3.21)**, mainly characterized by Hertz deformation-force relation, at times, also considering bearing clearance and element waviness.

$$M\ddot{X}(t)+C\dot{X}(t)+KX(t)=f(t)+f_{b\to rotor}(X(t),\dot{X}(t)) \qquad (3.21)$$

To boil down to format of linear equation, it can be also found in some publications that transient bearing stiffness and damping matrices participate in bearing-rotor dynamic calculation, instead of varying mean bearing matrices of coefficients **(3. 22)**, using finite differential method.

$$M\ddot{X}(t)+(C+\overline{C_{bearing}(X(t),\dot{X}(t))})\dot{X}(t)+(K+\overline{K_{bearing}(X(t),\dot{X}(t))})X(t)=f(t) \qquad (3.22)$$

$$K_{bearing}(X(t),\dot{X}(t))=\frac{\partial f_{bearing}(X(t),\dot{X}(t))}{\partial X}=-\frac{\partial f_{b\to rotor}(X(t),\dot{X}(t))}{\partial X}\overset{replace}{\approx}\overline{K_{bearing}(X(t),\dot{X}(t))}$$

…

Using incremental linear equation to preform nonlinear relation, it will be more persuasive in application. Differential format **(3. 23), (3. 24)** of equation **(3. 21)** is employed.

$$M\Delta\ddot{X}(t)+C_1\Delta\dot{X}(t)+K_1\Delta X(t)+(C_2(X(t-\tau))\Delta\dot{X}(t)+K_2(X(t-\tau))\Delta X(t))=\Delta f(t) \quad (3.23)$$

$$\Delta X(t) = X(t) - X(t-1) \quad (3.24)$$

Where, C_1, K_1 are constant coefficients, C_2, K_2 are nonlinear bearing coefficients.

Better solutions with less programming effort are explored to understand how bearing interacts with rotor, using a most simplified rotor system described in **Figure3.5**, where a rigid rotor is symmetrically supported by a bearing.

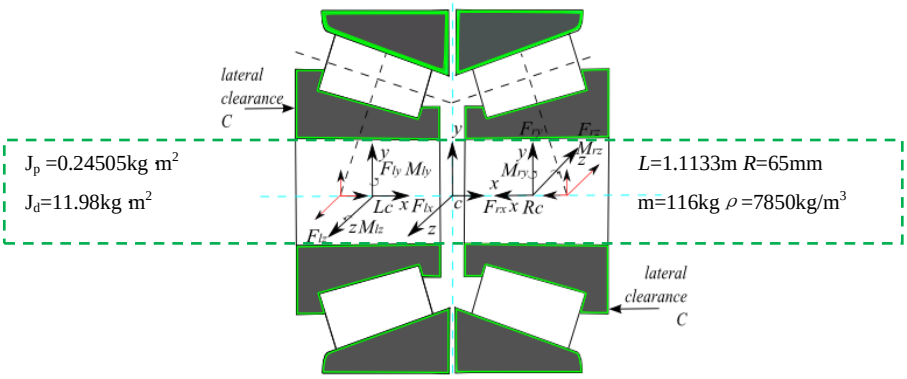

Figure3.5 A symmetric rigid rotor-nonlinear bearing System

The matrices included are given here.

$$f(t)=\begin{bmatrix} Q_x \\ m\omega^2[e\cos(\omega t+\varphi)]-mg+Q_y \\ m\omega^2[e\cos(\omega t+\varphi)]+Q_z \\ M_y \\ M_z \end{bmatrix}$$

$$M=\begin{bmatrix} m & & & & & \\ & m & & & & \\ & & m & & & \\ & & & J_d & & \\ & & & & J_d & \end{bmatrix}, C_1=\begin{bmatrix} 0 & & & & & \\ & 0 & & & & \\ & & 0 & & & \\ & & & 0 & -\omega J_p & \\ & & & \omega J_p & 0 & \end{bmatrix}, K_1=0,\ X(t)=\begin{bmatrix} x & y & z & \theta_y & \theta_z \end{bmatrix}^T$$

In this 5-DOF system, the matrices M, $C_1$are on behalf of mass and gyroscopic matrices; Q_x,Q_y,Q_z,M_y,M_z stand for preloads or varying external excitations acting on the rotor center equivalently; and e represents eccentricity value. Parameter-varying bearing coefficients K_2 C_2 are derived in **Part 3.4**. Below, two novel solvers are respectively developed for both time and frequency domains analysis.

3.5.1 Study on rotor responses considering nonlinear bearing in time domain

Using Four-order Adams Method given in **Appendix F**, in the manner of bearing matrices, the governing equation **(3.23)** can be easily solved to recognize incremental variables $\Delta X(t)$. Four-order Adams method performs perfectly in calculation efficiency and convergence of $\Delta X(t)$. However, the error from $\Delta X(t)$ will be continuously accumulated for $X(t)$, its fragile accuracy and convergence ask for a comprehensive solver.

3.5.1.1 A new solver of Incremental nonlinear dynamic equation

The error from $\Delta X(t)$ must be seriously considered after a lot of simulation failures, using current numerical methods (like Four-order Adams Method). Incremental governing equation **(3.23)** totally dominated by $\Delta X(t)$ (like parameter-varying bearing coefficients e.g. $K_2=f(x_0+\sum\Delta x)$), should also consider each parameter-varying coefficient's fluctuation and its robustness at each integration step.

This chapter specifically proposes a new constructing function. $K_2^i=K(x_0+\sum_1^{i-1}\Delta x)$ is suggested to be replaced by $K_2^i=\frac{1}{2}[K(x_0+\sum_1^{i-1}\Delta x)+K(x_0+\sum_1^{i}\Delta x)]$. It is qualitatively explained that generation of Δx_i considers effects of preceding states x_{i-3},x_{i-2},x_{i-1} and Δx_i itself on dynamic equation. This effect mainly reflects on varying bearing coefficients, and adoption of mean value between $K_2^{i+1}=K(x_0+\sum_1^{i}\Delta x)$ and $K_2^i=K(x_0+\sum_1^{i-1}\Delta x)$ in the solver is one essential manner considering this effect.

However, the story does not end yet, since how the relationship is quantitatively established is still not clear. Interestingly, all other settings of coefficients before $K(x_0+\sum_{1}^{i-1}\Delta x)$ and $K(x_0+\sum_{1}^{i}\Delta x)$ fail to work except 1/2. Explanation below.

In static balance of bearing, simple newton iterative method can help to get accurate displacement under known loads as left picture shows. However, it is different in dynamic balance. Before reaching balance point, load of $M\ddot{X}(t)+C\dot{X}(t)+KX(t)$ participating in balance is changing due to fake inertial effect (simulation error). Correspondingly, the point solved at each iterative step will become unsure, e.g. $Xi\ (2)$ in left picture will turn into $Xi\ (2)_{error1}$ or $Xi\ (2)_{error2}$ in right picture.

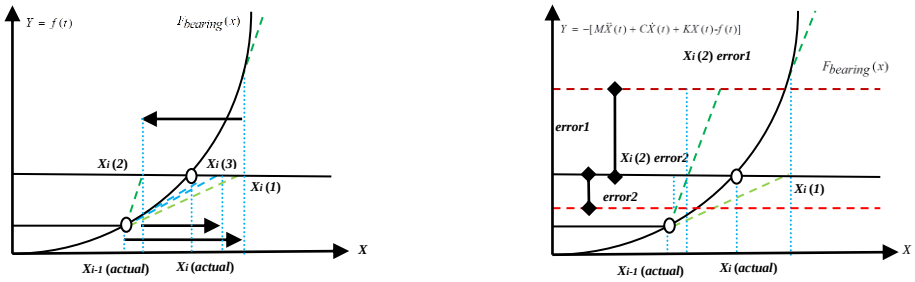

Figure3.6 Newton iteration path for nonlinear contact question

(Unsure converged load deviates from target load in right picture)

To eliminate this error inaccurate $X(t)$ introduces to $M\ddot{X}(t)+C\dot{X}(t)+KX(t)$, new governing equation is rebuilt.

$$M\Delta\ddot{X}(t)+C_1\Delta\dot{X}(t)+K_1\Delta X(t)-\Delta f(t)+(C_2(X(t-\tau))\Delta\dot{X}(t)+K_2(X(t-\tau))\Delta X(t))...$$
$$...+M\Delta\ddot{X}(t)+C_1\Delta\dot{X}(t)+K_1\Delta X(t)-\Delta f(t)+(C_2(X(t))\Delta\dot{X}(t)+K_2(X(t))\Delta X(t))=0 \quad (3.25)$$

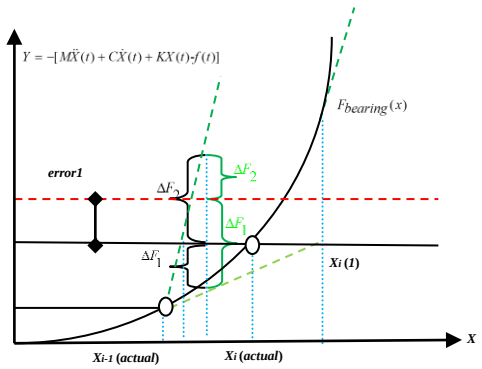

Figure3.7 Newton iteration strategy for incremetnal nonlinear bearing question

It is found that for arbitrary displacement, $\Delta F_1+\Delta F_2$ won't be influenced by

movement of red dash line. It is equal to the following equation.

$$M\Delta\ddot{X}_{actual}(t)+C_1\Delta\dot{X}_{actual}(t)+K_1\Delta X_{actual}(t)-\Delta f(t)+(C_2(X(t-\tau))\Delta\dot{X}(t)+K_2(X(t-\tau))\Delta X(t))$$
$$...+M\Delta\ddot{X}_{actual}(t)+C_1\Delta\dot{X}_{actual}(t)+K_1\Delta X_{actual}(t)-\Delta f(t)+(C_2(X(t))\Delta\dot{X}(t)+K_2(X(t))\Delta X(t))=0 \quad (3.26)$$

No convergent drawback is in fine overcome by bridging to an equivalent question of the same convergence as static bearing mechanic balance question, where 0.5 is proved to be the right coefficient. And, obviously, other setting of unequal coefficients fails to get rid of the influence of the error inaccurate $X(t)$ introduces to $M\ddot{X}(t)+C\dot{X}(t)+KX(t)$ (demonstrated by red dash line). Meanwhile, it also well corresponds to simulation findings.

$$M\Delta\ddot{X}(t)+C_1\Delta\dot{X}(t)+K_1\Delta X(t)-\Delta f(t)+\frac{C_2(X(t-\tau))+C_2(X(t))}{2}\Delta\dot{X}(t)+\frac{K_2(X(t-\tau))+K_2(X(t))}{2}\Delta X(t)=0 \quad (3.27)$$

These nonlinear variables are in fine predicted implicitly instead of explicitly, since it becomes a combination of dynamic marching procedure and static balance procedure. Now, by assuming boundary conditions, solutions are obtained.

$$t=-2\Delta t,\quad -\Delta t,\quad 0,\quad \Delta\ddot{X}(t)=\Delta\dot{X}(t)=\Delta X(t)=0$$

$$\begin{bmatrix}Q_x & Q_y & Q_z & M_y & M_z\end{bmatrix}=0$$

Fundamental results on nonlinear bearing-rotor system

The different manners in which undamped or damped bearing and balanced or unbalanced rotor perform in healthy rotor vibration responses are studied. Although much focus has been put on numerical solver, more explanations about possible simulation results are also given to make proposed solver persuasive.

3.5.1.2 Undamped conditions

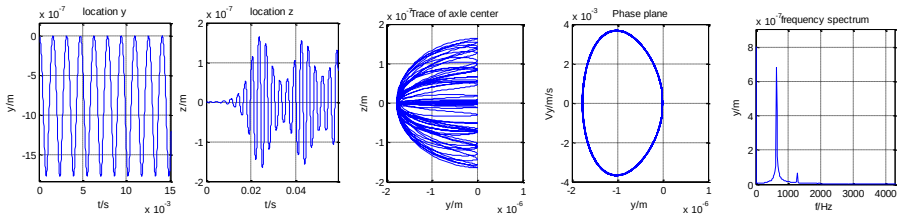

Figure3.8 Responses of balanced rotor starting at Zero point

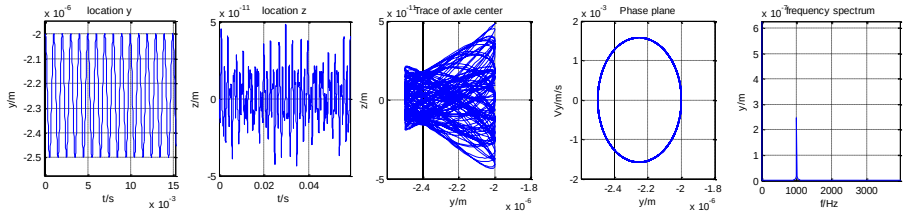

Figure3.9 Responses of balanced rotor starting at Non-zero point

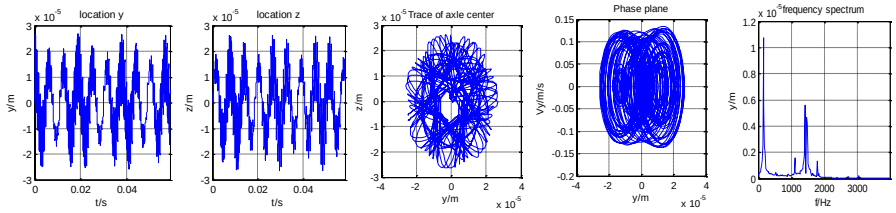

Figure3.10 Responses of unbalanced rotor starting at Zero point

In a simplest linear conservative system under gravity and other preloads **(3.28)**, besides balance point $\frac{G+F_{preload}}{KM}$, the response **(3.29)** is still dependent of initial states. Initial states mean initial distribution of transferable potential and kinetic energies. They stand for a disposable energy (consumable in case of damping) distributed in two different forms at one moment, but preload represents a permanent and untransferable potential energy.

$$M\ddot{X}(t)+KX(t)=G+F_{preload} \tag{3.28}$$

$$X(t)=\frac{G+F_{preload}}{KM}+A\sin(\sqrt{\frac{K}{M}}t+\varphi) \tag{3.29}$$

fgdgsd

Similarly, in nonlinear conservative system, it is found as well that bearing vibrations in **Figure3.8** and **Figure3.9** are also influenced by initial conditions $\ddot{X}(t), \dot{X}(t), X(t)$ $(t=-2\Delta t,\ -\Delta t,\ 0)$.

In **Figure3.8**, initial states at $t=-2\Delta t,\ -\Delta t,\ 0$ are all set as zero, and vibration highest peak is located at zero point. It points out that if no gravity and preload are considered, the rotor is well balanced at $t=-2\Delta t,\ -\Delta t,\ 0$ and has zero initial transferable potential energy.

In **Figure3.9**, different vibration scope and different balance point are found, it is because the setting of $\ddot{X}(t), \dot{X}(t), X(t)$ at $t=-2\Delta t,\ -\Delta t,\ 0$ contains more information than initial transferable potential energy, preloads hidden inside represent untransferable potential energy and constrain the motions at $t=-2\Delta t,\ -\Delta t,\ 0$. Moreover, different initial untransferable (preload) or transferable potential energy (the extent of compressing bearing "spring") result in different vibration frequencies.

How influences of untransferable and transferable potential energies are distributed in responses is not clear using a random initial setting, however, in application, $\dot{X}(0)$ can be given by a non-zero value to represent the initial kinetic energy, which, in essence, is an equivalent potential energy. To further confirm them, preload and initial kinetic energy can be carefully calculated using first two groups of state equations. Here, no more discussion is performed.

Below give two situations uniquely changing initial potential energies. Combined with the findings on rotor dynamic characteristics from **Figure3.9**, it is again evidenced that initial transferable potential energy affects vibration amplitude and natural resonant frequencies, while preload affects vibration balance point and natural resonant frequencies.

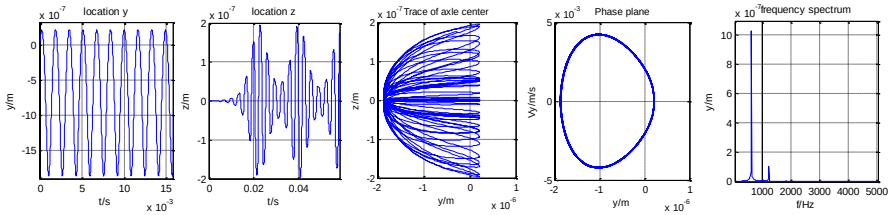

Figure3.11 Responses of balanced rotor starting at Zero point

$(\dot{X}(0)=0.002m/s)$

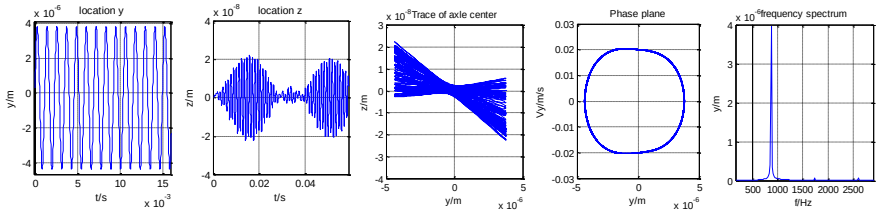

Figure3. 12 Responses of balanced rotor starting at Zero point

$(\dot{X}(0)=0.02m/s)$

Therein, different from preload, the impact of initial transferable potential energy at most times will be invisible and turn into insignificant as **Figure3.10** shows, if other important factors dominate it. E.g., if the unbalance value $m\omega^2[e\cos(\omega t+\varphi)]$ weighs more, the influence of initial states will be hidden in the unbalance motions. The same effect can also be taken by other external excitations.

Furthermore, the impact of initial transferable potential energy will even become reduced due to damping, so, in practical engineering, it seldom takes many difficulties of getting rid of initial states' influence in identifying system as well as external excitations. In fact, if the damping is considered, the initial potential energy and even some small excitations (like VC vibration) will disappear.

3.5.1.3 Damped conditions

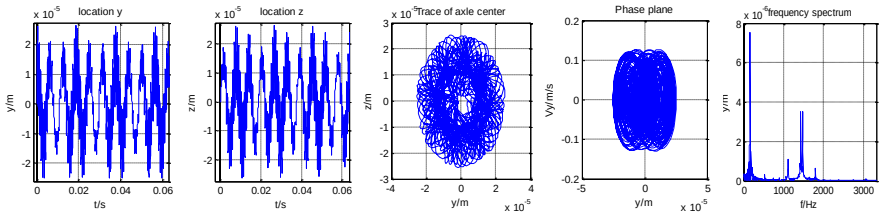

Figure3.13 Responses of unbalanced rotor using constant damping

(C_{yy}=C_{yz}=C_{zz}=C_{zy}=200 $N/m\cdot s$)

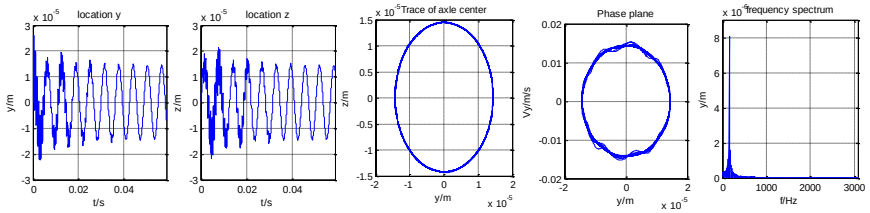

Figure3.14 Responses of unbalanced rotor using proposed damping

(Simplified steady-state damping coefficients in an integrated manner)

It is noticed that damping dispersive behavior does suppress some vibration. In **Figure3.13**, vibration amplitude is reduced compared to **Figure3.10**, using constant damping values. In **Figure3.14**, VC (varying compliance) vibration is nearly totally suppressed, when adopting simplified steady-state damping coefficients in an integrated manner.

The amount of bearing damping available has been theoretically in doubt, but is especially important near the resonant regions. This dissipation comes from buffer of

viscous-elastic materials and lubrication. More accurate damping coefficients expect more work. At the stage of present knowledge, a most complex lubricating damping function is the curve-fitted relation developed by Chippa and Sarangi **[64]**.

The inlet force prying up the rollers will experience fluctuations, once contact vibration happens. This fluctuation forms an additional damping force. It is admitted that formulations proposed by Chippa and Sarangi are numerically excellent, but

- The perturbation method used is based on a synchronous perturbed value of film thickness along contact width. Synchronous perturbation of film thickness distribution, in essence, trusts robustness of steady-state EHL under transient conditions. A consideration of asynchronous film thickness variation along contact width is taken by the authors in the first chapter.

- Linear superposition of the lubricant film stiffness, damping forces and Hertz force is still a bolder hypothesis, since distributed lubricant force nonlinearly reconstructs Hertz deformation and force distributions.

In conclusion, two points rarely emphasized are specifically studied in this chapter.

1. Use of incremental differential equation delivers a uniform but also persuasive engineering interpretation in case of nonlinear stiffness/damping coefficients.

2. The Runge-Kutta method used to perform a better convergence in nonlinear stiff equations, since the integration step in this one-step method can be changed as accuracy requires, however it also naturally produces an unpredictable convergence time. The four-order Adams method used in this chapter is a multi-step method with unchanged integration step, but easily diverges in nonlinear questions. The success herein is mainly profitable with the specific treatment for varying simulation error shared by inertial loads and gyroscopic moments (for which part, no safe method in the past, like Jacobian matrix in static equation, can help to converge it, unless step-varying control of dynamic accuracy). Although several iterative times are taken in static calculation included at each integration step, less integration steps out of a max motion period are wasted in the whole convergence. Only when damping exists, some more periods are needed. The described enhancement can be observed from all preceding results.

The proposed time method has a short convergent period, only a small number of periods are needed to observe system behavior. However, initial states still need a discussion on distribution of initial transferable potential and kinetic energies, as well as constant preloads. The authors in this thesis also believe that a combination of the Runge-Kutta method and proposed constructing function can be a good choice to settle it.

3.5.2 Study on Rotor responses considering nonlinear bearing in frequency domain

The dynamic relationship between local parameters with global rotor working behaviors is the core of designs and the destination of simulation predictions, and inversely important to identify and control each element in bearing-rotor system.

More than what we have observed from the preceding pictures, global working behaviors reflected in transient and steady state responses are much richer in reality. However, it is sure that periodic solutions and stability are technically important for a nonlinear system.

Again, local parameters consist of those describing each internal element (disk, supporting or suspending bearings, etc.), and those depicting external excitations (rotor gravity, rotor unbalance, environmental vibrations, etc.), so that parametric influence on systematic stability is a diverse question. Accordingly, acquisition of periodic and non-asymptotic solution needs a more direct path in frequency domain.

3.5.2.1 HB-AFT applied in nonlinear bearing-rotor system using uniform matrix format

Using truncated Fourier series to describe unknown displacements, bearing forces and other external loads acting on rotor,

$$X = A_0 + \sum_{j=1}^{K} [A_j \cos(jwt) - B_j \sin(jwt)] \tag{3.30}$$

$$F = C_0 + \sum_{j=1}^{K} [C_j \cos(jwt) - D_j \sin(jwt)] \tag{3.31}$$

$$F_{external} = E_0 + \sum_{j=1}^{K} [E_j \cos(jwt) - H_j \sin(jwt)] \tag{3.32}$$

$$X=\begin{bmatrix} x \\ y \\ z \\ \theta_y \\ \theta_z \end{bmatrix}, A_j=\begin{bmatrix} a_{xj} \\ a_{yj} \\ a_{zj} \\ a_{\theta_y j} \\ a_{\theta_z j} \end{bmatrix}, B_j=\begin{bmatrix} b_{xj} \\ b_{yj} \\ b_{zj} \\ b_{\theta_y j} \\ b_{\theta_z j} \end{bmatrix}, F=\begin{bmatrix} Fx \\ Fy \\ Fz \\ M\theta_y \\ M\theta_z \end{bmatrix}, C_j=\begin{bmatrix} c_{xj} \\ c_{yj} \\ c_{zj} \\ c_{\theta_y j} \\ c_{\theta_z j} \end{bmatrix}, D_j=\begin{bmatrix} d_{xj} \\ d_{yj} \\ d_{zj} \\ d_{\theta_y j} \\ d_{\theta_z j} \end{bmatrix} \dots$$

Harmonic coefficients of diplacements and nonlinear bearing forces are proposed.

$$\begin{bmatrix} P \\ Q \end{bmatrix}=\begin{bmatrix} A_0{}^T & A_1{}^T & B_1{}^T & A_2{}^T & B_2{}^T & \cdots & A_K{}^T & B_K{}^T \\ C_0{}^T & C_1{}^T & D_1{}^T & C_2{}^T & D_2{}^T & \cdots & C_K{}^T & D_K{}^T \end{bmatrix}$$

Substituting $\begin{cases} \frac{d}{dt}X=\sum_{j=1}^{K} jw[-A_j\sin(jwt)-B_j\cos(jwt)] \\ \frac{d^2X}{dt^2}=\sum_{k=1}^{K}(jw)^2[-A_j\cos(jwt)+B_j\sin(jwt)] \end{cases}$ into dynamic equations, the same harmonic compositions in Q and P are balanced with a Galerkin projection. The resultant format in frequency domain is yielded in general way.

$j=0$

$$0\cdot A_0=C_0+\begin{bmatrix} 0 & -mg & 0 & 0 & 0 \end{bmatrix}^T+E_0$$

$j \geq 1$

$$\begin{bmatrix} -(jw)^2\mathrm{M} & -jw\mathrm{C}_G \\ jw\mathrm{C}_G & -(jw)^2\mathrm{M} \end{bmatrix}\begin{bmatrix} A_j \\ B_j \end{bmatrix}=\begin{bmatrix} C_j \\ D_j \end{bmatrix}+\begin{bmatrix} E_j \\ H_j \end{bmatrix}$$

Where, $w=w_{cage}$ is the fundamental angular frequency.

If external forces participate, the Fourier coefficients of all harmonic items involved should be written into the vectors E_0 (on behalf of preload), E_j and H_j respectively.

Now, in order to search a constant vector P constituting periodic solution, how to solve such a group of nonlinear algebraic equations is of another interest in this chapter. Two direct iterative strategies are commonly used for general nonlinear algebraic question.

Strategy 1: $P_l \rightarrow X \rightarrow F_{bearing} \overset{FFT}{\rightarrow} Q_{FFT}(P_l) \overset{dynamic}{\rightarrow} P_{l+1}$

Strategy 2: $Q_i \rightarrow F_{bearing} \rightarrow X \xrightarrow{FFT} P_{FFT}(Q_i) \xrightarrow{dynamic} Q_{i+1}$

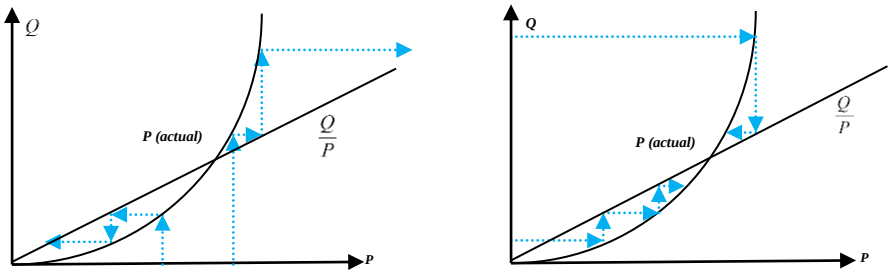

Figure3.15 Iterative paths of fixed point P included in frequency method

The straight lines in the pictures describe the relation between P and Q hidden in systematic dynamic relation as linear relation. (Remember, when k=0, the elements in Q have nothing to do with those in P. This linearity will not be influenced). This finding reflects that a function as rebuilt in time domain is not necessary. In strategy 1, direct iterative procedure apparently fails to get a converged P vector according to the trends of blue arrows in **Figure3.15** (left one). While in strategy 2, iterative relation seems to have a convergence. But we doubt that: 1, whether it is right that the bearing mechanics relation also performs an exponential function relation with exponent greater than 1(near 1.1 or 1.5) in frequency domain; 2, each calculation in strategy 2 contains lots of time-consuming bearing static balance operations, where iterative step involved is very sensitive to different load combinations. The step-size control coefficient in **(3. 33)** is very elusive even although it just needs to be programmed once for all.

$$\begin{bmatrix} x \\ y \\ z \\ \theta y \\ \theta z \end{bmatrix}_{i+1} = \begin{bmatrix} x \\ y \\ z \\ \theta y \\ \theta z \end{bmatrix}_{i} - coeff \times inv(K(\begin{bmatrix} x \\ y \\ z \\ \theta y \\ \theta z \end{bmatrix}_{i}))(\begin{bmatrix} Fx \\ Fy \\ Fz \\ M\theta_y \\ M\theta_z \end{bmatrix}_{bearingi} - \begin{bmatrix} Fx \\ Fy \\ Fz \\ M\theta_y \\ M\theta_z \end{bmatrix}_{bearingi-1}) \quad (3.33)$$

In our study, strategy 2 is performed in advance, it is found to be very time-wasting, and given different conditions, iterative step should be changed frequently. Also, whether such a direct strategy will work is uncertain, because not all situations are considered to prove the correctness of the preceding exponential function relation.

As introduced in recent literatures, systematic dynamics relation and bearing mechanics relation are mixed together, where assumed preceding exponential function relation is replaced by a new one using HB-AFT.

$$f(Q,P)=0$$

$$P_{i+1}=P_i-\frac{f(Q,P)}{f'(Q,P)}$$

$$f'(Q,P)=\frac{\partial f(Q,P)}{\partial P}+\frac{\partial f(Q,P)}{\partial Q}\frac{\partial Q}{\partial P}$$

$\frac{\partial Q}{\partial P}$, as main work, should be derived based on bearing mechanics relation and alternative time-frequency relation of P. Considering that the complexity will increase with the numbers of harmonics used and degrees of freedom involved increasing, a uniform matrix relation is suggested in this chapter.

The acknowledgment of all Fourier coefficients can directly tell an arbitrary-time output using equations **(3.30)~(3.32)**. However, reverse question should be answered differently. A simple idea below performs an inverse calculation of each hidden Fourier coefficient using time signals within a time period.

$$F(t)=\sum_{j=0}^{k}(C_j cos(jwt)-D_j sin(jwt)) \quad \overset{t=\frac{2\pi n}{wN}}{\Rightarrow} \quad F(n)=\sum_{j=0}^{k}(C_j cos(\frac{2\pi jn}{N})-D_j sin(\frac{2\pi jn}{N}))$$

$$\sum_{n=0}^{N-1}[F_n]=\int_0^{\frac{2\pi}{w}}F(t)dt=\int_0^{\frac{2\pi}{w}}\{\sum_{j=0}^{k}(C_j cos(jwt)-D_j sin(jwt))\}dt=\frac{2\pi}{w}C_0=NC_0$$

$$\sum_{n=0}^{N-1}[F_n]\cos(\frac{2\pi in}{N})=\int_0^{\frac{2\pi}{w}}F(t)\cos(iwt)dt=\int_0^{\frac{2\pi}{w}}\{\sum_{j=0}^{k}(C_j\cos(jwt)-D_j\sin(jwt))\cos(iwt)\}dt=\frac{\pi}{w}C_i=\frac{N}{2}C_i$$

$$\sum_{n=0}^{N-1}[F_n]\sin(\frac{2\pi in}{N})=\int_0^{\frac{2\pi}{w}}F(t)\sin(iwt)dt=\int_0^{\frac{2\pi}{w}}\{\sum_{j=0}^{k}(C_j\cos(jwt)-D_j\sin(jwt))\sin(iwt)\}dt=-\frac{\pi}{w}D_i=-\frac{N}{2}D_i$$

So that, C_i and D_i are described using $[F_{t_n}]$.

$$C_0=\frac{1}{N}\sum_{n=0}^{N-1}[F_{t_n}] \tag{3.34}$$

$$C_i=\frac{2}{N}\sum_{n=0}^{N-1}[F_{t_n}]\cos(\frac{2\pi in}{N}) \tag{3.35}$$

$$D_i=-\frac{2}{N}\sum_{n=0}^{N-1}[F_{t_n}]\sin(\frac{2\pi in}{N}) \tag{3.36}$$

Integration result can be analytical, for as each harmonic wave involved performs a multi-period integral.

$$j+i>1,|j-i|\geq 1, j\neq i$$

$$\sin(jwt)\sin(iwt)=-\frac{\cos((j+i)wt)-\cos((j-i)wt)}{2}$$
$$\sin(iwt)\sin(iwt)=\frac{1-\cos(2iwt)}{2}$$
$$\cos(jwt)\cos(iwt)=\frac{\cos((j+i)wt)+\cos((j-i)wt)}{2}$$
$$\cos(iwt)\cos(iwt)=\frac{\cos(2iwt)+1}{2}$$
$$\sin(jwt)\cos(iwt)=\frac{\sin((j+i)wt)+\sin((j-i)wt)}{2}$$

Consequently, each sub matrix included in the overall Jacobian matrix is obtained.

$$\frac{\partial Q}{\partial P}\Big|_{0\sim K}=\begin{bmatrix} \frac{\partial C_0}{\partial A_0} & \frac{\partial C_0}{\partial A_1} & \frac{\partial C_0}{\partial B_1} & \cdots & \frac{\partial C_0}{\partial A_K} & \frac{\partial C_0}{\partial B_K} \\ \frac{\partial C_1}{\partial A_0} & \frac{\partial C_1}{\partial A_1} & \frac{\partial C_1}{\partial B_1} & & \frac{\partial C_1}{A_K} & \frac{\partial C_1}{\partial B_K} \\ \frac{\partial D_1}{\partial A_0} & \frac{\partial D_1}{\partial A_1} & \frac{\partial D_1}{\partial B_1} & & \frac{\partial D_1}{\partial A_K} & \frac{\partial D_1}{\partial B_K} \\ \vdots & & & \ddots & & \vdots \\ \frac{\partial C_K}{\partial A_0} & \frac{\partial C_K}{\partial A_1} & \frac{\partial C_K}{\partial B_1} & & \frac{\partial C_K}{\partial A_K} & \frac{\partial C_K}{\partial B_K} \\ \frac{\partial D_K}{\partial A_0} & \frac{\partial D_K}{\partial A_1} & \frac{\partial D_K}{\partial B_1} & \cdots & \frac{\partial D_K}{\partial A_K} & \frac{\partial D_K}{\partial B_K} \end{bmatrix}$$

Where,

$$\frac{\partial C_0}{\partial A_0}=\frac{1}{N}\sum_{n=0}^{N-1}[\frac{\partial F_{t_n}}{\partial X}\frac{\partial X}{\partial A_0}]=\frac{1}{N}\sum_{n=0}^{N-1}[K_{t_n}]$$
$$\frac{\partial C_0}{\partial A_j}=\frac{1}{N}\sum_{n=0}^{N-1}[\frac{\partial F_{t_n}}{\partial X}\frac{\partial X}{\partial A_j}]=\frac{1}{N}\sum_{n=0}^{N-1}[[K_{t_n}]\cos(jwt)]$$
$$\frac{\partial C_0}{\partial B_j}=\frac{1}{N}\sum_{n=0}^{N-1}[\frac{\partial F_{t_n}}{\partial X}\frac{\partial X}{\partial B_j}]=-\frac{1}{N}\sum_{n=0}^{N-1}[[K_{t_n}]\sin(jwt)]$$

$$\frac{\partial C_i}{\partial A_0} = \frac{2}{N}\sum_{n=0}^{N-1}[\frac{\partial F_{t_n}}{\partial X}\frac{\partial X}{\partial A_0}]\cos(\frac{2\pi in}{N}) = \frac{2}{N}\sum_{n=0}^{N-1}[K_{t_n}]\cos(\frac{2\pi in}{N})$$

$$\frac{\partial C_i}{\partial A_j} = \frac{2}{N}\sum_{n=0}^{N-1}[\frac{\partial F_{t_n}}{\partial X}\frac{\partial X}{\partial A_j}]\cos(\frac{2\pi in}{N}) = \frac{2}{N}\sum_{n=0}^{N-1}[K_{t_n}]\cos(jwt)\cos(\frac{2\pi in}{N})$$

$$\frac{\partial C_i}{\partial B_j} = \frac{2}{N}\sum_{n=0}^{N-1}[\frac{\partial F_{t_n}}{\partial X}\frac{\partial X}{\partial B_j}]\cos(\frac{2\pi in}{N}) = -\frac{2}{N}\sum_{n=0}^{N-1}[K_{t_n}]\sin(jwt)\cos(\frac{2\pi in}{N})$$

$$\frac{\partial D_i}{\partial A_0} = -\frac{2}{N}\sum_{n=0}^{N-1}[\frac{\partial F_{t_n}}{\partial X}\frac{\partial X}{\partial A_0}]\sin(\frac{2\pi in}{N}) = -\frac{2}{N}\sum_{n=0}^{N-1}[K_{t_n}]\sin(\frac{2\pi in}{N})$$

$$\frac{\partial D_i}{\partial A_j} = -\frac{2}{N}\sum_{n=0}^{N-1}[\frac{\partial F_{t_n}}{\partial X}\frac{\partial X}{\partial A_j}]\sin(\frac{2\pi in}{N}) = -\frac{2}{N}\sum_{n=0}^{N-1}[K_{t_n}]\cos(jwt)\sin(\frac{2\pi in}{N})$$

$$\frac{\partial D_i}{\partial B_j} = -\frac{2}{N}\sum_{n=0}^{N-1}[\frac{\partial F_{t_n}}{\partial X}\frac{\partial X}{\partial B_j}]\sin(\frac{2\pi in}{N}) = \frac{2}{N}\sum_{n=0}^{N-1}[K_{t_n}]\sin(jwt)\sin(\frac{2\pi in}{N})$$

Where, $t = \frac{2\pi n}{wN}$, $N = \frac{2\pi}{w}/\Delta t$.

Some applications of frequency domain method in bearing system

3.5.2.2 Parametric influence on system stability

Even for the steady state responses, not all periodic responses included are stable, so that, some laws of stability have ever been studied, among which, Floquet theory is the most popular one.

As found in **Part 3.5.1** (time method), initial states, damping, unbalance, and others strongly influence steady-state responses, it is very visible but needs post-treatment (like error, period identification, etc.) in quantitative analysis, and acquisition of more information also needs to burden expensive computations.

In the frequency domain method, direct output of system responses irrelevant to time bridges a more direct access to stability analysis, using the Floquet multipliers. Normally, monodromic matrix $A(t)$ is extracted from state-space equation.

$$\begin{bmatrix}\ddot{X}(t)\\ \dot{X}(t)\end{bmatrix} = A(t)\begin{bmatrix}\dot{X}(t)\\ X(t)\end{bmatrix}$$

Here, due to complex nonlinearity, partial differential relation is used.

$$A(t)=\frac{\partial\begin{bmatrix}\ddot{X}(t)\\ \dot{X}(t)\end{bmatrix}}{\partial\begin{bmatrix}\dot{X}(t)\\ X(t)\end{bmatrix}}=\begin{bmatrix}-M^{-1}(C_G+C_2(t)+C_1) & -M^{-1}(K_2(t)+K_1)\\ I & 0\end{bmatrix} \quad (3.37)$$

Derived from $M\Delta\ddot{X}(t)+C_G\Delta\dot{X}(t)+(C_2(X(t-\tau))\Delta\dot{X}(t)+K_2(X(t-\tau))\Delta X(t))=0$

It is obvious that the system stability is parameter-varying. To further perform it, the discrete state transition matrix developed by Hsu **[78]** is used.

$$\begin{cases} C_k=\frac{1}{\Delta_k}\int_{t_{k-1}}^{t_k}A(t)dt, k=1,2,... \\ \Theta=\prod_{k=1}^{N}\exp(\Delta_k C_k)\end{cases} \Rightarrow \Theta=\prod_{k=1}^{N}\exp(\frac{T}{N}A(t_{k-1}))\approx\prod_{k=1}^{N}(\mathrm{I}+\sum_{j=1}^{n}\frac{(\frac{T}{N}A(t_{k-1}))^j}{j!}) \quad (3.38)$$

Proposed frequency method makes direct use of time domain matrix $K_2(t), C_2(t)$, so that matrix Θ is much more easily determined to search the instability regions by calculating its eigenvalues.

Under gravity, a response at *y* direction is obtained using 3D cylindrical bearing to support a rotor rotating at speed of 1000 rad/s.

$$\begin{aligned} y(t)=10^{-8}\times[&-16.45858-0.2219\cos(w_{VC}t)-0.0109\sin(w_{VC}t)\\ &-0.0030\cos(2w_{VC}t)-0.0003\sin(2w_{VC}t)-0.0006\cos(3w_{VC}t)-0.001\sin(3w_{VC}t)\\ &-0.0003\cos(4w_{VC}t)-0.0001\sin(4w_{VC}t)-0.0002\cos(5w_{VC}t)-0.0001\sin(5w_{VC}t)\\ &-0.0001\cos(6w_{VC}t)-0.0001\cos(7w_{VC}t)-0.0001\cos(8w_{VC}t)-0.0001\cos(9w_{VC}t)]\end{aligned}$$

The corresponding Floquet multipliers can be calculated.

0.9874 + 0.1583i 0.9961 + 0.0887i -0.9671 + 0.2545i -0.3990 + 0.9169i 1.0000 + 0.0000i

0.9874 - 0.1583i 0.9961 - 0.0887i -0.9671 - 0.2545i -0.3990 - 0.9169i 1.0000 + 0.0000i

It is found that the system is critically stable. Although now no constraint (preload) is set at *x* direction to increase stability of system, a slight disturbance still will not easily destroy the stability of system at speed of 1000 rad/s.

Speed is inevitably the main inspected parameter to control running conditions. Now, take the impact of speed on stability as an example. In equation **(3.38)**, $N=10^4, n=5$ is assumed.

Normally, T_{VC}-1 solutions can be searched between w_{vc1} and w_{vc2}, therein, 10 rad/s as a step-size, afterwards, 1 rad/s as a finer step-size around unstable region.

However, a full-parameter tracking simulation as demanded above encounters a robustness question of frequency-domain method.

1. Around unstable regions, multi-solutions make initial iterative position and iterative step-size more elusive compared to general regions (even for single solution, it is also hard to locate initial position around accurate solution). To deal with the problem, especially around the turning points, solution experiences a dramatic change. The arc-length continuation method which delegates a continuous version reformulating from the homotopy **[79]** can be well embedded.

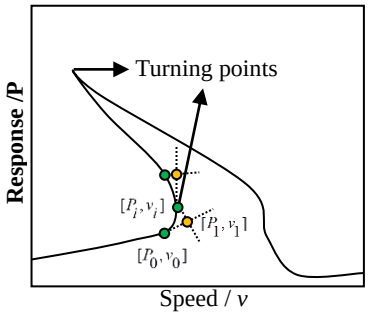

Figure3. 16 Arc-length continuation method

At turning point, the spatial coordinate corresponding to continuation parameter v (also called “natural continuation” or “sequential”) makes iterative Jacobian matrix singular. Its failure requires a new continuation parameter α (arc-length), so that a brilliant strategy is to transform original equation into a differential equation about α, which is usually normalized to guarantee a unitary tangent predictor $[\frac{\partial P^T}{\partial \alpha}, \frac{\partial v}{\partial \alpha}]$.

$$\begin{cases} \frac{\partial f}{\partial \alpha} = \frac{\partial f}{\partial P}\frac{\partial P}{\partial \alpha} + \frac{\partial f}{\partial v}\frac{\partial v}{\partial \alpha} = 0 = [\frac{\partial f}{\partial P}, \frac{\partial f}{\partial v}] \times [\frac{\partial P}{\partial \alpha}, \frac{\partial v}{\partial \alpha}]^T \\ \frac{\partial P}{\partial \alpha}\frac{\partial P^T}{\partial \alpha} + (\frac{\partial v}{\partial \alpha})^2 = 1 \end{cases} \quad (3.39)$$

Then, solution track follows a predictor-corrector order.

At predictor stage, it is calculated on basis of an accurate neighboring point (P_0, v_0). The direction perpendicular to tangential direction of previous solution determines next initial guess. The curvature of solution line also determines the size of iterative step **[80]**.

$$(P_1, v_1) = (P_0, v_0) + [\frac{\partial P^T}{\partial \alpha}, \frac{\partial v}{\partial \alpha}]_0 \cdot \Delta \tag{3.40}$$

$$g = \overrightarrow{Vector_{0\to 1}} \cdot \overrightarrow{Vector_{i\to 1}} = \begin{bmatrix} \frac{\partial P^T}{\partial \alpha}, \frac{\partial v}{\partial \alpha} \end{bmatrix} \cdot \begin{bmatrix} P_i - P_1 \\ v_i - v \end{bmatrix} = \frac{\partial P^T}{\partial \alpha}(P_i - P_1) + \frac{\partial v}{\partial \alpha}(v_i - v_1) = 0 \tag{3. 41}$$

At corrector stage, the global Newton-Raphson iterative method is employed to calculate the extended system **(3.42)**, where, both $f = 0$ and $g = 0$ should be satisfied. In the global Jacobian matrix, $\frac{\partial f}{\partial v}$ can be approximated by finite difference method, a way different from that performed in **[81]**, where other forces (bearing forces partly dependent of rotating speed) are not taken into consideration except inertial forces.

$$\begin{bmatrix} P_{i+1} \\ v_{i+1} \end{bmatrix} = \begin{bmatrix} P_i \\ v_i \end{bmatrix} - \begin{bmatrix} \frac{\partial f}{\partial P} & \frac{\partial f}{\partial v} \\ \frac{\partial P^T}{\partial \alpha} & \frac{\partial v}{\partial \alpha} \end{bmatrix}^{-1} \cdot \begin{bmatrix} f(P_i, v_i) \\ \frac{\partial P^T}{\partial \alpha}(P_i - P_1) + \frac{\partial v}{\partial \alpha}(v_i - v_1) \end{bmatrix} \tag{3.42}$$

Where, $\frac{\partial g}{\partial P} = \frac{\partial P^T}{\partial \alpha}$ and $\frac{\partial g}{\partial v} = \frac{\partial v}{\partial \alpha}$ are employed to accurately perform next initial guess and avoid singularity of Jacobian matrix.

Referring to **[80]**,**[82]**, the tangential vector $[\frac{\partial P}{\partial \alpha}, \frac{\partial v}{\partial \alpha}]$ can be calculated as follows, using equations **(3. 39)**.

$$\begin{cases} \frac{\partial P}{\partial \alpha} = (-1)^i C(P,v) \cdot \det[DH_{[-i]}(P,v)] \\ \frac{\partial v}{\partial \alpha} = (-1)^{N+1} C(P,v) \cdot \det[DH_{[-(N+1)]}(P,v)] \end{cases}$$

Deleting i^{th} column from $DH(P,v) = [\frac{\partial f}{\partial P}, \frac{\partial f}{\partial v}]$,

$$DH_{[-i]}(P,v) = (DH(P,v)(:,1,i-1), DH(P,v)(:,i+1,N+1))$$

and

$$C(P,v)=\frac{(-1)^{N+1}\,\mathrm{sgn}\left[\det[\left(\frac{\partial f}{\partial P}\right)_0]\right]}{\sqrt{\sum_{i=1}^{N+1}(\det[DH[-i](P,v)])^2}}$$

2. Around turning regions, even singularity of Jacobian matrix is mathematically avoided; it is still physically near singularity and fails to globally converge towards local minima. We think, it has a solution of same relative error ($\Delta P_i / P_{actual}$), but of bigger absolute error (ΔP_i), the convergence turns bad, especially when a lot of variables are involved. To improve convergence rate and calculation stability when approaching its regime, the criteria used in convergence of Newton iterative method and selection of step size should be understood.

- Either absolute and relative accuracies of independent variable or absolute accuracies of independent and dependent variables should be satisfied.

$$q_{i+1} = q_i + \Delta q_i = q_i + (J_i)^{-1} \cdot f(q_i)$$

$$\frac{\Delta q_i}{1+q_i} < \varepsilon, \qquad \mathrm{Residual}_i(q_i, v) = J\Delta q_i - f(q_i) < \varepsilon$$

- On the other hand, iterative times counted at last integration step can be also used to consider whether reduced step size should be used or even iterative process should be stopped.

- Unfortunately, either accuracy control or step-size reduction still doesn't work. The solution asks for more efficient method of linear search technique for Newton's Method, developed in **[83]** and performed in **[84]**.

If it is necessary to locate precisely the dangerous points, supplementary equations are sometimes needed to locate system singularity.

$$\det\left(\frac{\partial f}{\partial P}\right) = 0$$

$\frac{\partial f}{\partial P}\Phi = 0$ is a variant which has been well recognized in **[81][85][86]** as a parallel equation, and also a replacement of $g = 0$ combined with $f = 0$ to directly identify bifurcation points.

Since Φ is defined as the eigenvector corresponding to $\text{eigenvalue}\left(\frac{\partial f}{\partial P}\right)=0$, the eigenvector associated with $\text{Min}(\text{eigenvalue}\left(\frac{\partial f}{\partial P}\right))$ naturally becomes as an initial iterative vector of bifurcation point-identifying algorithm.

For a good parameter-varying track, $\det\left(\frac{\partial f}{\partial P}\right)$ can also help to inform algorithm to use reduced step size.

Results

Results of using 3D cylindrical bearing to support a rotor are plotted at a bigger range of speeds.

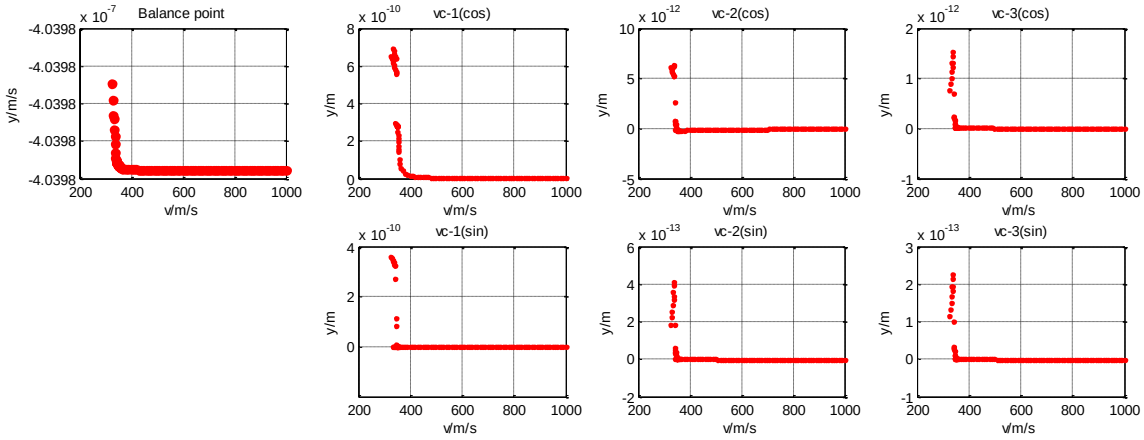

Figure3.17 Multi-Harmonic waves appearing at **y** direction

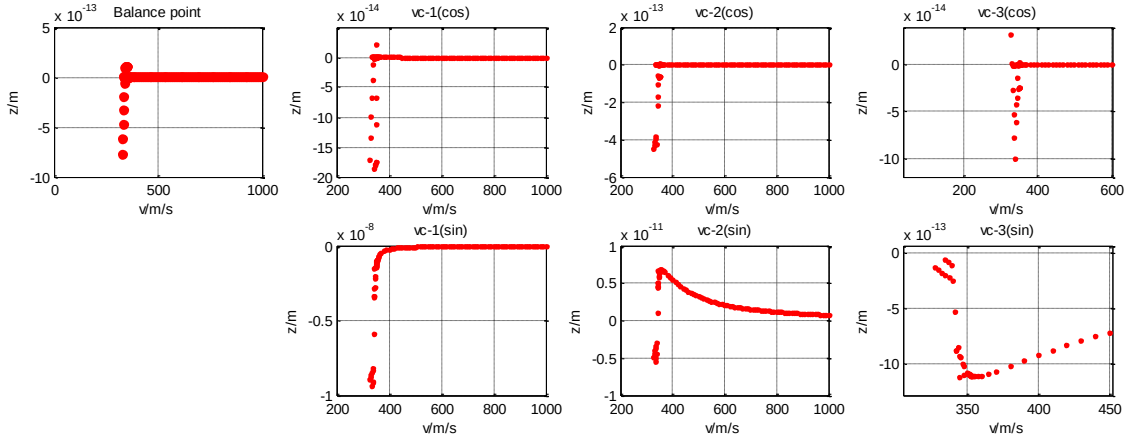

Figure3.18 Multi-Harmonic waves appearing at **z** direction

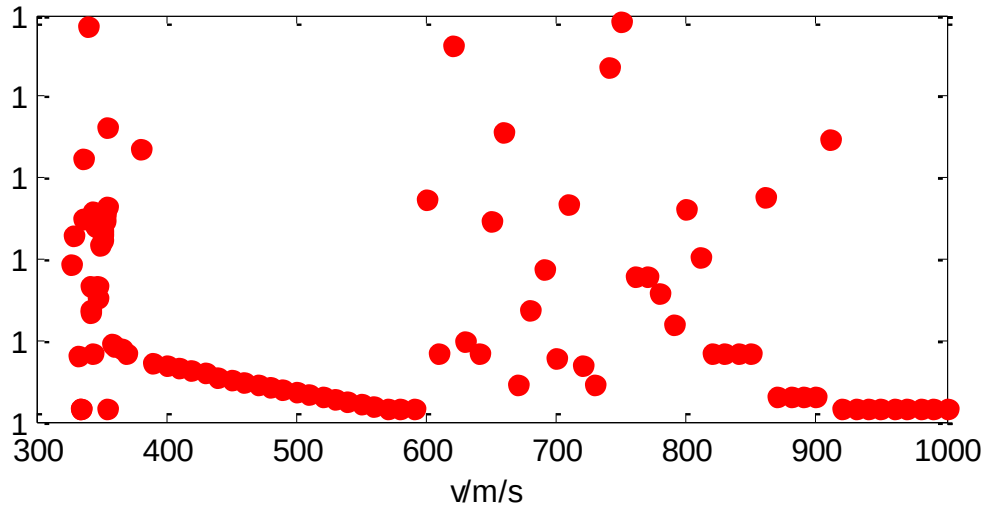

Figure3.19 Distribution of instability region

It can be found from **Figure3.19** that the stability analysis is more difficult for 3D condition and shows a more irregular distribution. Since the model used is cylindrical bearing-rotor model and no horizontal preload is imposed, all situations present slight instability, but some tendencies can still imply that the ranges of 380m/s~600m/s and 910m/s~1000m/s look much tenderer.

Further works on bifurcation, like the factors of bifurcation, period doubling, hysteresis, and the routes to chaos, can be found in the book **[79]**.

3.5.2.3 Parametric influence on system responses

System responses include vibration amplitude, frequency as well as balance position etc. at output stage. Using frequency domain method, some information hidden in responses caused by internal and external excitations can be discovered. Here, influences of both internal and external excitations are briefly discussed.

- Internal excitation is still caused by varying rotating speed.
- External excitation acting on bearing-rotor dynamic system is described in an alternative but simpler manner.

$$M\ddot{X}(t) + C\dot{X}(t) + KX(t) = f(t) + f_{b\rightarrow rotor}(X(t), \dot{X}(t))$$

$$X(t) = X_{rotor}(t) - X_{housing}(t)$$

If $X_{housing}(t) = 0$, $M\ddot{X}(t) + C\dot{X}(t) + KX(t) = f(t) + f_{b\to rotor}(X(t), \dot{X}(t))$

If $X_{housing}(t) \neq 0$, $M(\ddot{X}(t) + \ddot{X}_{housing}(t)) + C\dot{X}(t) + KX(t) = f(t) + f_{b\to rotor}(X(t), \dot{X}(t))$

To reproduce engineering facts, excitation harmonic load here can be explained as external displacement excitation.

$$\Delta f(t) = -M\ddot{X}_{housing}(t) \tag{3.43}$$

Displacement excitation of outer race is in essence an inertial load excitation of rotor, which will interfere the balanced rotor and reset new balance. In such a case, the influence of external excitation can be easily mathematically investigated.

$$X_{housing}(t) \xrightarrow{\text{How to influence}} X(t) \quad (\text{ or } X_{rotor}(t))$$

This is conveniently analyzed not only in the programming manner (in **Chapter 3**), but also in the experimental manner (It appeals to the exploitation of First generation bearing test bench proposed in **Chapter 4**). In the latter case, the desired structural parameters or dynamic relations in nonlinear bearing-rotor system can all be found.

Results

Since each composition in alternative external load is $Ma_k(kw)^2\cos(kwt) - Mb_k(kw)^2\sin(kwt)$, two discussions about different exciting frequencies and amplitudes are performed.

- $w = w_{vc}, k = 1, a_k = 0.001, \text{or } 0.0001, \ b_k = 0$ are input to see the results.
- $w = w_{vc}, k = 1, \text{or } 2, a_k = 0.0001, b_k = 0$ are input to see the results;

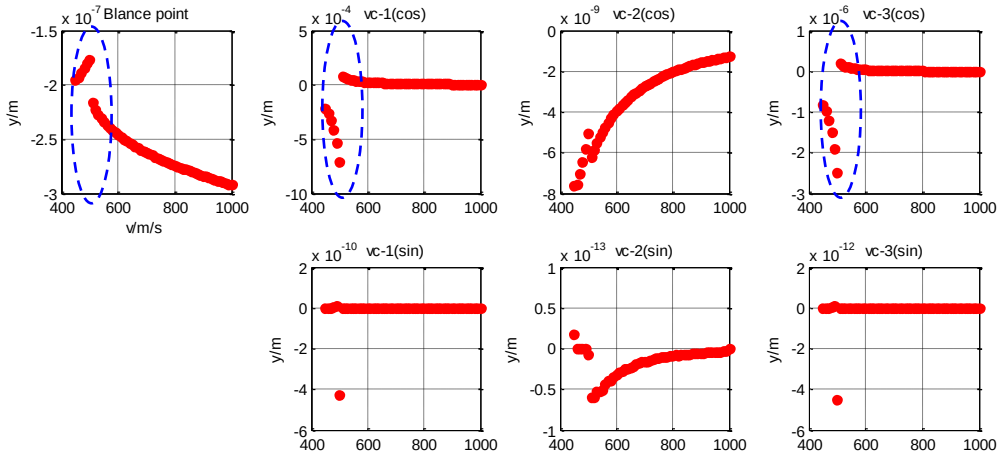

Figure3.20 Multi-Harmonic waves appearing at **y** direction $k=1, a_k = 0.001$

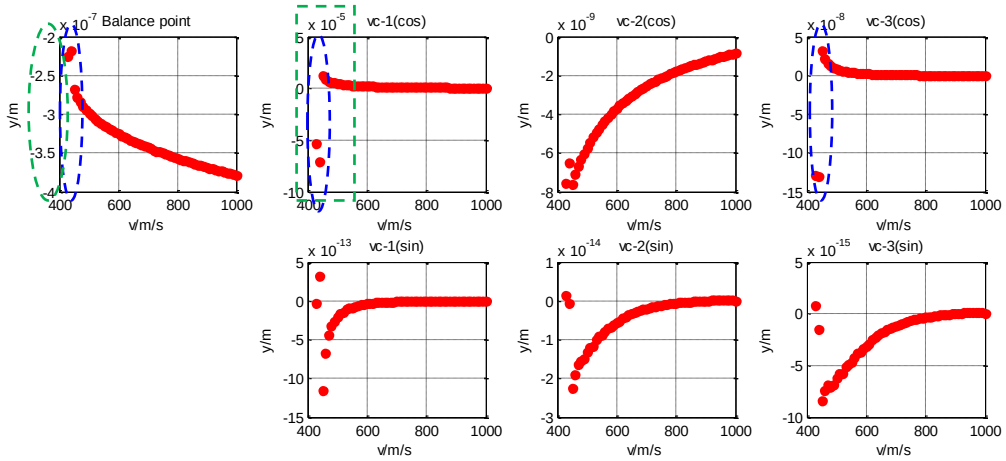

Figure3.21 Multi-Harmonic waves appearing at **y** direction $k=1, a_k = 0.0001$ ($>10^{-8}$ is discussed)

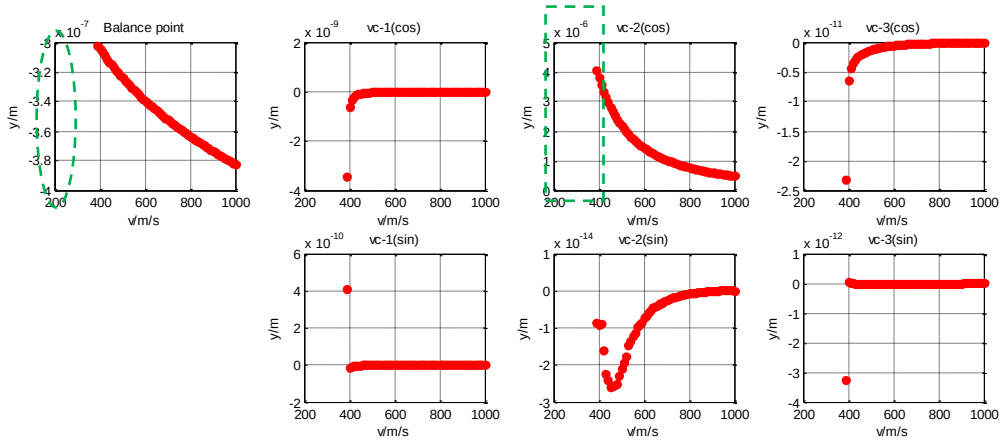

Figure3.22 Multi-Harmonic waves appearing at **y** direction $k=2, a_k = 0.0001$

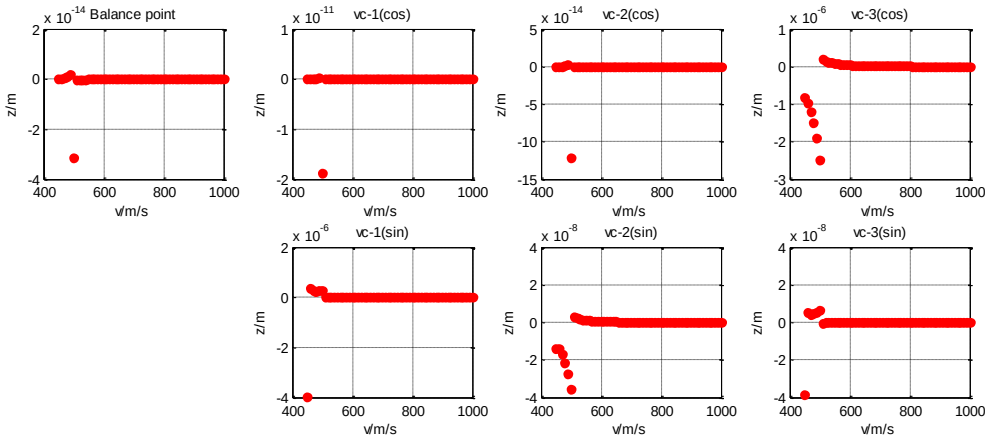

Figure3.23 Multi-Harmonic waves appearing at **z** direction $k=1, a_k = 0.001$

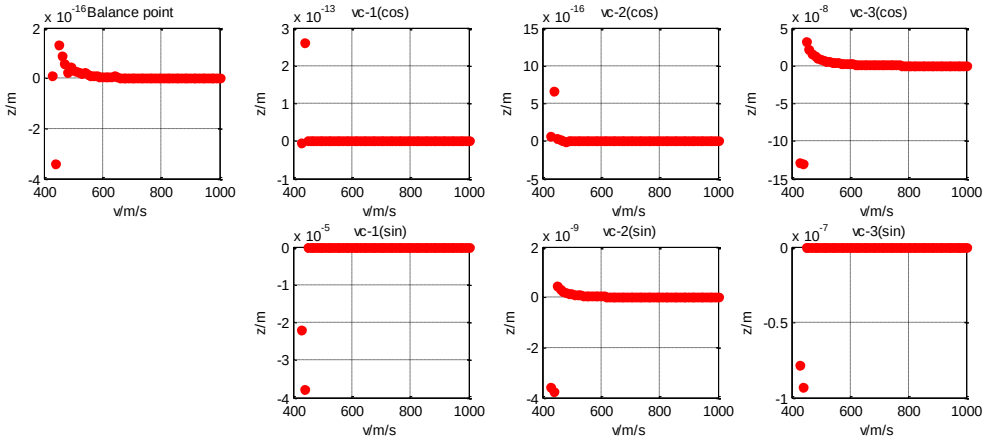

Figure3.24 Multi-Harmonic waves appearing at **z** direction $k=1, a_k = 0.0001$

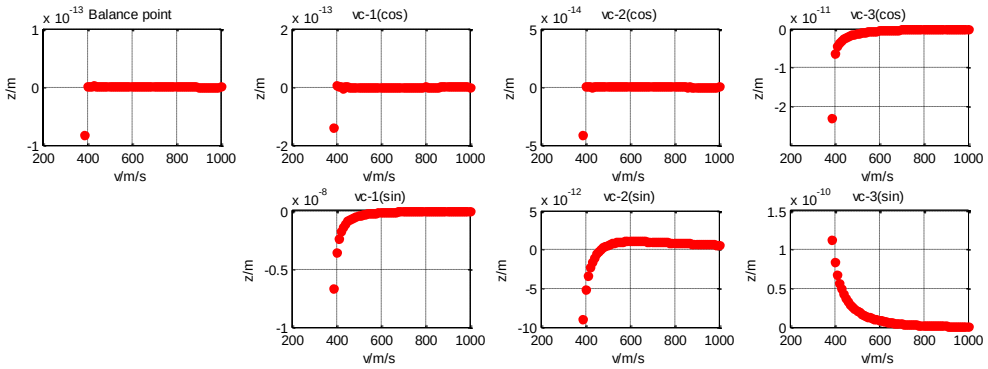

Figure3.25 Multi-Harmonic waves appearing at **z** direction $k=2, a_k = 0.0001$

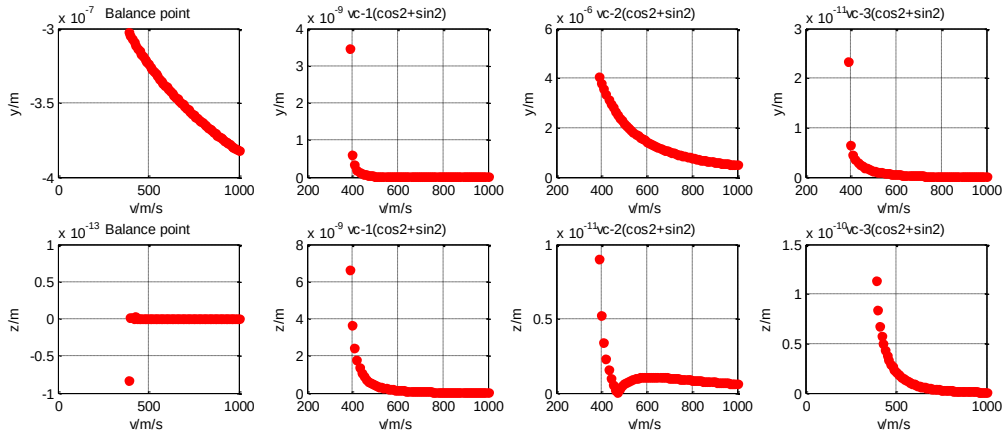

Figure3.26 Multi-Harmonic waves appearing at **radial** direction $k = 2, a_k = 0.0001$

The balance position is influenced by both internal and external excitations.

For internal excitation, the change of balance position is the main reason that dominates bearing stiffness and influences rotor resonant regions and unstable regions.

If preload is largely imposed, resonant point can be predicted, using linear vibration theory. Even resonant frequency is also found to be time-varying, but larger the preload is applied, more accurate the prediction is.

$$w(t)=\sqrt{\frac{K(t)}{M}}$$

For high-amplitude bearing resonance resulted from external excitation, normally no prior estimation for approximate regions can be made, since balance point takes less effect on entire bearing stiffness. Only full track simulation can help to predict the resonant regions.

For same external excitation, speed rise will decrease vibrating amplitude in **Figure3.26**. For same exciting frequency, different amplitude used has a similar distribution of resonant regions; the difference is that unstable area is enlarged at bigger amplitude (Blue dash lines in **Figure3.20** and **Figure3.21**). For same exciting amplitude, higher frequency imposed benefits to stabilize balance position (Green dash lines in **Figure3.21** and **Figure3.22**). This once again evidences that the anti-correlation exists between system stability and system vibrating intensity.

Besides, super-harmonic vibration occurs, and odd order-harmonic waves look more active in **Figure3.21**. Jumping phenomenon can be found under first two conditions. And same information about other degrees of freedom can be observed from **Figure3.23** to **Figure3.26**.

There should be a more accurate analysis on resonant regions and system bifurcation, but the accessible speed scope incorporated still needs to be increased by a more advanced and efficient mathematical solver. Currently, arc-length continuation method, accuracy control, step-size control, even simple linear search technique for Newton's method are used, but some problems of convergence in 3D question still occur, with more different singularity phenomena taking place at certain speed for more degrees of freedom, even they are proved to work very well in 2D questions.

3.6 Conclusion

Proposed bearing model of uniform format is engineering-convenient. It will therefore be possible to do such calculations to predict easily the performances of bearing and its adjacent components by implementing in any non-linear F.E.A package or any complex M.B.S package.

Both the new time-domain solver and the uniform frequency-domain method HB-AFT for calculating nonlinear bearing-rotor system can work to find some hidden information and to guide bearing engineering design and application.

3.7 Nomenclature

Symbols	Explanations
$G' = \alpha E'$	Dimensionless material parameter, α proportional modulus
$W = F/(E'R^2)$	Dimensionless load parameter
$\bar{U} = \frac{\eta_0 u}{E'R}$	Dimensionless material parameter
k_e=1.0339$\left(\frac{R_y}{R_x}\right)^{0.636}$	Ellipticity parameter
$\Gamma = 1.5277 + 0.6023\ln\left(\frac{R_y}{R_x}\right)$	Complete elliptic integral of the second kind
Σ=1.0003+0.5968$\frac{R_x}{R_y}$	Complete elliptic integral of the first kind
$1/R_x$=$1/r_{x1}$+$1/r_{x2}$	effective radius of curvature in the principal x-plane

$1/R_y=1/r_{y1}+1/r_{y2}$	effective radius of curvature in the principal y-plane
$R=\frac{R_1 \cdot R_2}{R_1 \pm R_2}$	Equivalent radius in rolling direction (for principal x or y plane or sum radius)
$R_i'=r_i\cos\alpha_0+R_i$	-
$R_o'=(D-r_o)\cos\alpha_0+R_i$	-
$u=(u_1+u_2)/2$	Entraining surface velocity, and 1,2 for two contact bodies
η_0	Lubricant viscosity in the inlet area
$E'=\frac{2}{(1-\upsilon_1^2)/E_1+(1-\upsilon_2^2)/E_2}$	Reduced Young's modulus
l	roller length
F	Normal applied load
e	Rotor eccentricity
m	Rotor mass
J_d , J_p	Rotor inertial moment

3.8 References

[52] JonesA.B. New departure engineering data: analysis of stresses and deflections. New Departure Division, General Motors Corporation, Vol. 2, 1946.

[53] Harris T. A. Rolling Bearing Analysis. Wiley, New York, 1984.

[54] Palmgren A. Ball and Roller Bearing Engineering. SKF Industries Inc., Philadelphia, 1959.

[55] Lim T. C., Singh R. Vibration transmission through rolling element bearings, part I: bearing stiffness formulation. Journal of Sound and Vibration, Vol. 139, Issue 2, 1990, p. 179-199.

[56] Lim T. C., Singh R. Vibration transmission through rolling element bearings, part II: system studies. Journal of Sound and Vibration, Vol. 139, Issue 2, 1990, p. 201-225.

[57] Lim T. C., Singh R. Vibration transmission through rolling element bearings, part V: effect of distributed contact load on roller bearing stiffness matrix. Journal of Sound and Vibration, Vol. 169, Issue 4, 1994, p. 547-553

[58] Hernot X., Sartor M., Guillot J. Calculation of the stiffness matrix of angular contact ball bearings by using the analytical approach. Journal of Mechanical Design, Vol. 122, Issue 1, 2000, p. 83-90.

[59] Houpert L., 1997, "A Uniform Analytical Approach for Ball and Roller Bearing," ASME J. Tribol., 119, pp. 851–857.

[60] Houpert, L., 2014, "An Enhanced Study of the Load-Displacement Relationships for Rolling Element Bearings," ASME J. Tribol., 136(1), p. 011105.

[61] Houpert, L., 2015, "Load-Displacement Relationships for Ball and Spherical Roller Bearings," ASME J. Tribol., 137(1), p. 021102.

[62] Guo Y., Parker R. G. Stiffness matrix calculation of rolling element bearings using a finite element/contact mechanics model. Mechanism and Machine Theory, Vol. 51, 2012, p. 32-45.

[63] Knaapen R., Kodde L. Experimental Determination of Rolling Element Bearing Stiffness. Ph.D. Thesis, Eindhoven University of Technology, Eindhoven, The Netherlands, 1997.

[64] Sarangi, M., Majumdar, B. C., and Sekhar, A. S. On the dynamics of EHD mixed lubricated ball bearings. Part I: formulation of stiffness and damping coefficients. Proc. Instn Mech. Engrs, Part J: J. Engineering Tribology, 2005, 219 (J6), 411–421.

[65] Sarangi, M., Majumdar, B.C., and Sekhar, A.S. "Stiffness and damping characteristics of lubricated ball bearings. Part 1: theoretical formulation" Proc. Instn Mech. Engrs, Part J: J. Engineering Tribology, 218(6), 529~538, 2004.

[66] Chippa, S.P. and Sarangi, M., "On the Dynamics of Lubricated Cylindrical Roller Bearings, Part I: Evaluation of Stiffness and Damping Characteristics", Tribology Transactions, 56, 1087~1096, 2013.

[67] Chippa, S. P. and Sarangi, M., "On the Dynamics of Lubricated Cylindrical Roller Bearings, Part ii: linear and nonlinear vibration analysis", Tribology Transactions 56 (6), 1097~1108, 2013.

[68] S.Zhu, D.Nélias, W.Zhang, "A fast analytical technique of transient EHL based on acquisition of contact stiffness and damping distributions," RW2016.

[69] Lund J.W., Stability and Damped Critical Speeds of a Flexible Rotor in Fluid Film Bearings, Journal of Engineering for Industry, May 1974: 509-517.

[70] X.D.Huang, Z.G.Zeng, Y.N.Ma, The Theory and Methods for Nonlinear Numerical Analysis, Wuhan University Press, Wuhan, 2004.
[71] Loic Peletan, Sebastien Baguet, et al.. “A comparison of stability computational methods for periodic solution of nonlinear problems with application to rotordynamics”, Nonlinear Dynamics, 72, 3 (2013) 671-682.
[72] T. Detroux, L. Renson, G. Kerschen, The Harmonic Balance Method for Advanced Analysis and Design of Nonlinear Mechanical Systems
[73] Harris, T. A., and Kotzalas, M. N., 2007, “Essential Concepts of Bearing Technology,” Rolling Bearing Analysis, 5th ed., CRC Press, Taylor and Francis, London.
[74] David E.Brewe and Bernard J.Hamrock, 1976, “Simplified solution for point contact deformation between two elastic solids,” NASA, Washington, D.C..
[75] Bernard J.Hamrock and Duncan Dowson, “Isothermal elasto-hydrodynamic lubrication of point contact,” NASA, Washington, D.C. (Part 1, 1975 and Part 3, 1976).
[76] Walford T.L.H., Stone B., J. “The sources of damping in rolling element bearings under oscillating conditions”, Proc. Instn Mech. Engrs, Part C: J. Mechanical Engineering Science, 197, 225~232, 1983.
[77] G.D.Hagiu, M.D.Gafitanu. “Dynamic characteristics of high speed angular contact ball bearings”, wear, 211, 22~29, 1997.
[78] C.S.Hsu. “On Approximating a General Linear Periodic System”, Journal of mathematical analysis and applications, 45,234~251,1974.
[79] Rudiger Seydel. Practical Bifurcation and Stability Analysis, third edition, published by Springer, 2009.
[80] Zhiyong Zhang, Yushu Chen, et al. “Bifurcations and hysteresis of varying compliance vibrations in the primary parametric resonance for a ball bearing”, Journal of Sound and Vibration, 350, 171~184, 2015.
[81] L. Xie, S. Baguet, et al. “Bifurcation tracking by Harmonic Balance Method for performance tuning of nonlinear dynamical systems”, Mechanical Systems and Signal Processing, May 2017.
[82] Zhiyong Zhang, Yushu Chen. “Harmonic balance method with alternating frequency/time domain technique for nonlinear dynamical system with fractional exponential”, Appl. Math. Mech. -Engl. Ed., 35(4), 423~436, 2014.
[83] L. Grippo, F. Lamparillo, et al. “A Nonmonotone Line Search Technique for Newton's Method”, Journal on Numerical Analysis, 23(4):707-716, 1986.
[84] Yi Guo, Jonathan Keller, Robert G. Parker. “Dynamic Analysis of Wind Turbine Planetary Gears Using an Extended Harmonic Balance Approach”, International Conference on Noise and Vibration Engineering, Leuven, Belgium, September 17~19, 2012.
[85] Lihan Xie, Sébastien Baguet, et al. “Numerical Tracking of Limit Points for Direct Parametric Analysis in Nonlinear Rotor-dynamics”, Journal of Vibration and Acoustics, January 2016.
[86] T. Detroux, L. Renson, et al. “The Harmonic Balance Method for Bifurcation Analysis of Large-Scale Nonlinear Mechanical Systems”, Computer Methods in Applied Mechanics and Engineering, November 2015.

Appendix D Ball deformation and Contact angle

$$\lambda(\psi) = A(\psi) - A_0 = \left\| \begin{bmatrix} x_O \\ y_O \\ z_O \end{bmatrix} + \begin{bmatrix} d_x+\Delta d_x \\ d_y+\Delta d_y \\ d_z+\Delta d_z \end{bmatrix} - \begin{bmatrix} x_I \\ y_I \\ z_I \end{bmatrix} \right\| - \left\| \begin{bmatrix} x_O \\ y_O \\ z_O \end{bmatrix} - \begin{bmatrix} x_I \\ y_I \\ z_I \end{bmatrix} \right\|$$

$$=-\{(x_O+d_x+\Delta d_x-x_I)\sin\alpha+[(y_O+d_y+\Delta d_y-y_I)\cos\psi+(z_O+d_z+\Delta d_z-z_I)\sin\psi]\cos\alpha\}...$$

$$...-\{(x_I-x_O)\sin\alpha_0+[(y_I-y_O)\cos\psi+(z_I-z_O)\sin\psi]\cos\alpha_0\}$$

$$=-\{(d_x+\Delta d_x)\sin\alpha+[(d_y+\Delta d_y)\cos\psi+(d_z+\Delta d_z)\sin\psi]\cos\alpha\}...$$

$$...\underbrace{-\{(x_I-x_O)(-\Delta\alpha\cos\alpha_0)+[\frac{x_I-x_O}{\tan\alpha_0}](\Delta\alpha\sin\alpha_0)\}}_{\text{zero}}$$

$$= -\{(d_x + \Delta d_x)\sin\alpha_0 + [(d_y + \Delta d_y)\cos\psi + (d_z + \Delta d_z)\sin\psi]\cos\alpha_0\} - ...$$

$$...\underbrace{\Delta\alpha\{(d_x+\Delta d_x)\cos\alpha_0-[(d_y+\Delta d_y)\cos\psi+(d_z+\Delta d_z)\sin\psi]\sin\alpha_0\}}_{\text{second order small term}}$$

$$= -\{(d_x + \Delta d_x)\sin\alpha_0 + [(d_y + \Delta d_y)\cos\psi + (d_z + \Delta d_z)\sin\psi]\cos\alpha_0\}$$

Where, $\sin\alpha = \sin\alpha_0 + \Delta\alpha\cos\alpha_0$

$$\cos\alpha = \cos\alpha_0 - \Delta\alpha\sin\alpha_0$$

$$\tan\alpha = \frac{x_O+d_x+\Delta d_x-x_I}{(y_O+d_y+\Delta d_y-y_I)\cos\psi+(z_O+d_z+\Delta d_z-z_I)\sin\psi}$$

$$\tan\alpha_0 = \frac{x_I-x_O}{(y_I-y_O)\cos\psi+(z_I-z_O)\sin\psi}$$

Variation of contact angle $\Delta\alpha = \dfrac{\frac{A+\Delta A}{B+\Delta B}-\frac{A}{B}}{1+\frac{A+\Delta A}{B+\Delta B}\frac{A}{B}} = \dfrac{\Delta AB-\Delta BA}{B^2+\Delta BB+A^2+\Delta AA}$

Where

$$A = x_O - x_I$$
$$\Delta A = d_x+\Delta d_x$$
$$B = (y_O-y_I)\cos\psi+(z_O-z_I)\sin\psi$$
$$\Delta B = (d_y + \Delta d_y)\cos\psi + (d_z + \Delta d_z)\sin\psi$$

For simplification, second order small terms $\Delta\alpha\Delta BB$ and $\Delta\alpha\Delta AA$ are neglected compared with other terms, and it turns out

$$\Delta\alpha = (\tan\alpha_0 + \tan^{-1}\alpha_0)(\frac{d_x+\Delta d_x}{x_O-x_I} - \frac{(d_y+\Delta d_y)\cos\psi+(d_z+\Delta d_z)\sin\psi)}{(y_O-y_I)\cos\psi+(z_O-z_I)\sin\psi})$$

Appendix E Moment of Ball bearing with consideration of varying Contact angle

Due to $\begin{cases}\sin\alpha=\sin\alpha_0+\Delta\alpha\cos\alpha_0\\ \cos\alpha=\cos\alpha_0-\Delta\alpha\sin\alpha_0\end{cases}$, resultant load of ball bearing is,

$$\begin{cases}F_{\varphi x}=-\sin\alpha_0 F_i-\Delta\alpha\cos\alpha_0 F_i\\ F_{\varphi y}=\cos\varphi\cos\alpha_0 F_i-\Delta\alpha\sin\alpha_0\cos\varphi F_i\\ F_{\varphi z}=\sin\varphi\cos\alpha_0 F_i-\Delta\alpha\sin\alpha_0\sin\varphi F_i\end{cases}\qquad \begin{cases}Q_x=\sum_{\varphi=\varphi_0}^{\varphi_N}F_{\varphi x}\\ Q_y=\sum_{\varphi=\varphi_0}^{\varphi_N}F_{\varphi y}\\ Q_z=\sum_{\varphi=\varphi_0}^{\varphi_N}F_{\varphi z}\end{cases}$$

$$\begin{aligned}M_y&=-(R_i'\cdot\tan\alpha-r_i\cdot\sin\alpha_0)\cdot Q_z\\ &=-\sum_{\varphi=\varphi_0}^{\varphi_N}(R_i'\cdot\tan\alpha-r_i\cdot\sin\alpha_0)\sin\varphi\cos\alpha F_i\\ &=-\sum_{\varphi=\varphi_0}^{\varphi_N}R_i'\cdot\sin\varphi\sin\alpha F_i+\sum_{\varphi=\varphi_0}^{\varphi_N}r_i\cdot\sin\alpha_0\sin\varphi\cos\alpha F_i\\ &=-\sum_{\varphi=\varphi_0}^{\varphi_N}R_i'\cdot\sin\varphi(\sin\alpha_0+\Delta\alpha\cos\alpha_0)F_i+\sum_{\varphi=\varphi_0}^{\varphi_N}r_i\cdot\sin\alpha_0\sin\varphi(\cos\alpha_0-\Delta\alpha\sin\alpha_0)F_i\\ &=-\sum_{\varphi=\varphi_0}^{\varphi_N}(R_i'-r_i\cos\alpha_0)\cdot\sin\varphi\sin\alpha_0F_i-\sum_{\varphi=\varphi_0}^{\varphi_N}\sin\varphi\Delta\alpha(R_i'\cdot\cos\alpha_0+r_i\cdot\sin\alpha_0\sin\alpha_0)F_i\\ &=-\sum_{\varphi=\varphi_0}^{\varphi_N}(R_i'-r_i\cos\alpha_0)\sin\varphi\sin\alpha_0F_i-\sum_{\varphi=\varphi_0}^{\varphi_N}\sin\varphi\Delta\alpha(R_i'\cdot\cos\alpha_0+r_i-r_i\cos^2\alpha_0)F_i\\ &=-\sum_{\varphi=\varphi_0}^{\varphi_N}R_i\sin\varphi\sin\alpha_0F_i-\sum_{\varphi=\varphi_0}^{\varphi_N}\sin\varphi\Delta\alpha(R_i\cos\alpha_0+r_i)F_i\end{aligned}$$

Similarly,

$$\begin{aligned}M_z&=+(R_i'\cdot\tan\alpha-r_i\cdot\sin\alpha_0)\cdot Q_y\\ &=\sum_{\varphi=\varphi_0}^{\varphi_N}(R_i'\cdot\tan\alpha-r_i\cdot\sin\alpha_0)\cos\varphi\cos\alpha F_i\\ &=\sum_{\varphi=\varphi_0}^{\varphi_N}R_i\cos\varphi\sin\alpha_0F_i+\sum_{\varphi=\varphi_0}^{\varphi_N}\cos\varphi\Delta\alpha(R_i\cos\alpha_0+r_i)F_i\end{aligned}$$

Appendix F Four-order linear multistep numerical Method (Four-order Adams Method)

Using polynomial of third degree, these nonlinear variables are implicitly predicted,

$$\ddot{X}(t+\Delta t) = \ddot{X}(t) + a_1\Delta t + a_2(\Delta t)^2 + a_3(\Delta t)^3$$

$$\dot{X}(t+\Delta t) = \dot{X}(t) + \ddot{X}(t)\Delta t + \frac{1}{2}a_1(\Delta t)^2 + \frac{1}{3}a_2(\Delta t)^3 + \frac{1}{4}a_3(\Delta t)^4$$

$$X(t+\Delta t) = X(t) + \dot{X}(t)\Delta t + \frac{1}{2}\ddot{X}(t)(\Delta t)^2 + \frac{1}{6}a_1(\Delta t)^3 + \frac{1}{12}a_2(\Delta t)^4 + \frac{1}{20}a_3(\Delta t)^5$$

Participating coefficients are accordingly calculated based on accelerations selected at continuous simulating points in a recursive manner.

$$a_1 = \frac{1}{\Delta t}\left[\frac{1}{3}\ddot{X}(t+\Delta t) + \frac{1}{2}\ddot{X}(t) - \ddot{X}(t-\Delta t) + \frac{1}{6}\ddot{X}(t-2\Delta t)\right]$$

$$a_2 = \frac{1}{2(\Delta t)^2}\left[\frac{1}{3}\ddot{X}(t+\Delta t) - 2\ddot{X}(t) + \ddot{X}(t-\Delta t)\right]$$

$$a_3 = \frac{1}{6(\Delta t)^3}\left[\ddot{X}(t+\Delta t) - 3\ddot{X}(t) + 3\ddot{X}(t-\Delta t) - \ddot{X}(t-2\Delta t)\right]$$

Introducing relevant variables into governing equation, acceleration is in fine derived explicitly.

$$\ddot{X}(t+\Delta t) = \left\{M + \frac{3}{8}\Delta t(C_1+C_2) + \frac{19}{180}(\Delta t)^2(K_1+K_2)\right\}^{-1} \times \ldots$$
$$\left\{\begin{array}{l}\Delta F(t+\Delta t) + M\ddot{X}(t) - (C_1+C_2)\left[\frac{19}{24}\Delta t\ddot{X}(t) - \frac{5}{24}\Delta t\ddot{X}(t-\Delta t) + \frac{1}{24}\Delta t\ddot{X}(t-2\Delta t)\right] - \ldots \\ \ldots (K_1+K_2)\left[\Delta t\dot{X}(t) + \frac{19}{40}(\Delta t)^2\ddot{X}(t) - \frac{1}{10}(\Delta t)^2\ddot{X}(t-\Delta t) + \frac{7}{360}(\Delta t)^2\ddot{X}(t-2\Delta t)\right]\end{array}\right\}$$

$$X(t) = X(t-1) + \Delta X(t)$$

Chapter 4
An alternative bearing test bench reproducing contact loads

4.1 Research challenge for vibrating bearing -Powerful bench

As running speed increases, the dynamic interaction between environment and transmission system will deteriorate bearings incorporated in rotor system. These bearings will experience a long-term dynamic external loading. Once they are broken, the system will lose stability and safety. Normally little different dynamic response outside bearings will be aroused only due to initial bearing failures, since other suspension elements installed outside bearing box used to isolate some influences of bearing vibration on other components. Thus, it is more important to detect bearing states than others at most times, to avoid further bearing degradation and to reduce financial cost.

Different bearing responses caused by different external loads do send some hidden alarming signals of bearing life-span and update period. These warnings may come from **(a)** experimental descriptions of bearings, like shorten time of temperature increase, haste of relative vibration intensities between races, louder noise, and so on (they are useful) or **(b)** from analytical prediction of undetectable element (when relative motions cannot be detected directly, absolute motion of outer race can be detected instead), since rotor motion can be estimated by varying vibration intensities of bearing box. For detectable element, not all lower vibrations can ensure no failure. E.g. zero vibration may represent infinite bearing stiffness, which means that some part associated to rotation is broken and cannot move; Moreover, not all higher vibrations necessarily trigger off higher possibility of failure, it mainly depends on the factors arousing relative motions.

On one hand, bearing entire vibration does relate to bearing failure. Relative vibrations between races that, the thesis thinks, have direct relation with failures, should be caught at different degrees of freedom and under different excitations.

On the other hand, complex failure conditions always mix together, but in general, cage deformation, roller or race materials loss, and radial diameter expansion of raceway due to temperature rise, etc. all influence dynamic relations in original design. It sounds clear to distinguish them with design results.

As a modern strategy, using a nonlinear mathematics relation to characterize it is the most economical way to promote future design, perform fault diagnosis and maintenance.

One major manner in which bearing feels the vibrations is so called resonance, it points out that the balance of rotor is broken, vibration mode reset, and relative vibration intensities changed once different external excitations or failure excitations are imposed. The contact force between rotor and housing dominated by their relative displacement will change due to absolute housing motions or failure excitations introducing rotor inertial forces **(3. 43)**.

As a practical strategy, a powerful bench is also required either to verify computer-aided theory calculation or to better guide relevant structure to escape from some intense vibration regions.

Some resonance mechanism can be tested, using the first generation bearing test bench proposed in this chapter. However, bearing failures are always accelerated due to more intense relative vibrations and larger contact loads between races. Now, it is more elusive to make clear of failure mechanism: resonance, abnormal failure, or other fatigue failures with different conditions mixed. How to use the bench to reproduce them has powerful meaning. However, searching from most of current techniques, only simulation and entire vehicle test can replay extreme conditions. But reliability and cost are still what we are concerned about. To deal with it, an alternative bearing test bench is proposed as the second generation one, which directly reproduces the resonant results or other similar vibration conditions of races, but does not ensure the environments' reproduction of rotor or bearing box. The fatigue scenarios under different vibrations inside a bearing are expected to be discovered before reaching its life end or failing to work properly.

Due to

- All simulation results are not compatible to be reproduced by test bench. Some single stable solution can be found, but some double-stable solutions or unstable solutions cannot be found.
- Elements like rollers, cage are more easily ruined, so that if the dynamic behaviors of axle box and rotor are not very significant, in study, we can skip reproducing their environments, but directly to copy the dynamic bearing contact loads (or reproduce

absolute motions of races), and then observe bearing non-dynamic parameters' change.

- Using the first-generation bench, the maximum dynamic load scope the vibrator can reach and the max motion acceleration reproduced in races are constrained due to neighboring rotor and supporting frame synchronically vibrating and consuming energy.

$$\text{Step 1: } \overset{reproduce}{\Rightarrow} \text{ Contact load } \overset{reproduce}{\Rightarrow} \text{ Relative motion}$$

$$\text{Step 2: } \overset{reproduce}{\Rightarrow} \text{ Inner race motion } \overset{reproduce}{\Rightarrow} \text{ Outer race motion}$$

In the alternative bearing bench, effective dynamic loads are recreated, and the motions of tested bearing are accelerated, while ineffective dynamic loads are reduced.

Test benches from different bearing manufacturers **[89][90][91]**differ in main structure, loading technique, testing technique and control technology. Test benches in this chapter are enhanced alternatively in loading technique and control technique. With tests conducted on the electromagnetic vibrator, this scheme can not only reproduce heavy loads, but it can also reproduce high-frequency vibration, which is rarely involved in bearing researches in the history and relevant for train bearing tests.

Since external loads acting on train bearing are very complex and include a wide range of frequencies and amplitudes, which makes it of considerable impact to reproduce dynamic vibrations of the train axle box bearings to investigate failure mechanism under different vibration conditions. The bearing test bench proposed in this chapter meets this industrial demand.

4.2 First generation bearing test bench

First generation bearing test bench is composed of electromagnetic vibrator, moving coil, expansion table, and bench platform. Bench platform design is the main job in developing dynamic bearing test technology.

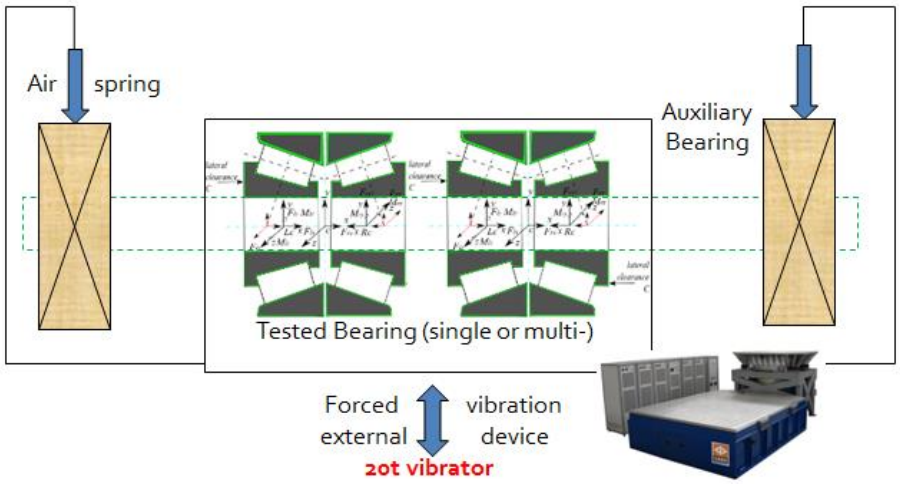

Figure4. 1 Entire Test Job

Figure4. 2 First Generation Bearing Test Bench

The maximum mass that the electromagnetic vibrator can support is 20 Tons, meaning that the electromagnetic vibrator can generate a maximum thrust force of 200,000 N, which will be responsible for all static and dynamic forces occurring above vibrator. Given a maximum vibrator power, the mass above the vibrator will constrain the max acceleration (frequency or amplitude), so that there should be a compromise among the platform mass and max acceleration. Given a minimum platform mass, a maximum acceleration must be strictly designed, considering other static and dynamic loads generated by moving coil and expansion table, and vice versa.

$$\left(M_{\text{moving coil}}+M_{\text{expansion table}}+M_{\text{bearing platform}}\right)\times a\leq 200000N \quad (4.\ 1)$$

$$M_{\text{moving coil}}+M_{\text{expansion table}}=510kg,\ M_{\text{bearing platform}}\geq 500kg \quad (4.\ 2)$$

$$a \leq \frac{200000\,N}{510kg+500kg} \approx 20g$$

The calculation shows that if the bench platform weighs over 500kg, the vibrator will generate an acceleration of less than 20g. In practice, the accessible or reachable acceleration of vibrator is very sensitive to mass, since acceleration decrease/increase performs a faster step than mass increase/decrease. Therefore, the test bench mass should be carefully designed. In first generation bench design, light material and simplified structure are used if they matter little to test requirements.

Using first generation bearing test bench, rotor behaviors caused by nonlinear bearing can be more focused. E.g.,

- Amplitude-frequency curve can be detected to investigate the resonant regions. How different factor from either internal or external excitation arouse hysteresis phenomenon, jumping phenomenon, or stable and unstable regions?
- The resonance behaviors can be further analyzed by recognizing the harmonics involved can be using FFT technique.

4.3 Conception of 2nd generation bearing test bench

Bearing test bench reproduces bearing forces and bearing motions. This equipment (**Figure4. 1**) can load inertia force and static spring force. Static force adjusted by different spring pre-compression can ensure a basic bearing application condition with approximate stiffness preset, while dynamic force imposed by different inertia forces, generated in manner of carrying different rotor masses or programming vibrator with different amplitudes or frequencies, can meet different bearing vibration conditions.

However, in application, these forces are shared by both effective and ineffective masses. Considering a great amount of electricity needed to drive bearing test bench, ineffective mass or force shall be eliminated to improve usage of vibrator. In the first-generation bench, ineffective mass has been reduced as much as possible; now this part looks for another way.

Mark spring force as F_0, vibration acceleration as a, mass of bearings, suspension boxes, and rotor as m, the effective force can be approximated: $F_{dy} = F_0 + ma$.

As stated in introduction, if bench platform fails to reproduce bearing-rotor motions, an alternative proposition is just to reproduce dynamic bearing contact force as versatile as possible if we care little about rotor and housing. As exercised, only entire vehicle is capable to comprehensively reproduce dynamic behaviors of large-scale bearing machine. However, proposed simplified bearing test bench can also reproduce the main components of bearing contact force by loading inertial force. However, both procedures require some inevitable energies to synchronically push moving coil, expansion table, housing and supporting frame of bench platform. All will produce ineffective loads, contributing little to dynamic bearing contact force, but reducing usage of vibrator.

In application of train bearings, even for axle box, the acceleration tested on the scene reaches 20g~50g, far beyond the capacity of the present vibrator. Using proposed bench, important components of bearing contact force can be versatilely reproduced to perform alternative tests.

Below gives a more economic bench, especially aimed for heavy-bearing load reproduction case, where the power shared by ineffective masses is reduced.

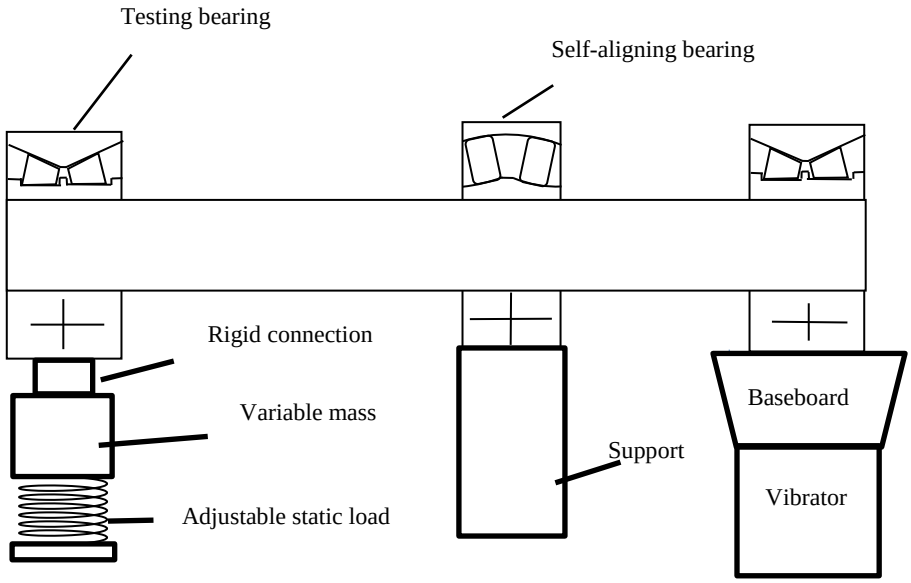

Figure4. 3 Conception of Second Generation Bearing Test Bench

As plotted above, by setting tested bearing outside vibrator and bridging a lever between tested bearing and vibrator, acceleration of vibrator can be reduced to get a same bearing motion. The multiplier can be modified by moving the supporting point. The acceleration and power wasted on moving coil and baseboard are reduced. To reproduce dynamic load acting on tested bearing, besides higher acceleration, variable mass showed in figure is still required.

The variable mass is connected rigidly to the tested bearing, while it is elastically connected to the ground with pre-compressed spring used to ensure an approximate range of static force. Since high vibration acceleration and low vibration amplitude are performed in test, the dynamic bearing contact load is approximated.

Assuming that: Bearing contact force $F_{dy}=25kN\sim50kN$

Bearing vibration acceleration $a_{\max}=50g$

Leverage amplification ratio $b <= 2$

Capacity calculation: Static spring force $F_0=\frac{20kN+50kN}{2}=37.5kN$

Maximum inertia force $ma=12.5kN$

Vibrator acceleration $a_{\max}'=25g$

Effective load acting on vibrator $F_{1\max}=(37.5kN+12.5kN)\times 2=100kN$

Final vibrator pushing force

$$\left(M_{\text{moving coil}}+M_{\text{expansion table}}\right)a_{\max}'+F_{1\max}=227500N\approx200000N$$

It can be found that both dynamic bearing force and motions of rolling elements inside bearing can be well copied in the alternative method.

4.4 Input signals of train bearing bench test

Bearing test bench acquires motions from vibrator.

$$a(t)=\frac{F_{dy}(t)-F_o}{m},\left\{a_{bearing}(t)\right\}\in a(t) \qquad (4.3)$$

$F_{dy}(t)$ and $a_{bearing}(t)$ can be determined by simulation or online test.

As far as train bearing is concerned, using multi-body dynamic software SIMPACK, loads and motions of axle box bearings in the train model can be differently predicted according to different bearing model participated. Although normally bearing is rigidly modeled, it still has little effect on predicting dynamic bearing contact loads, due to low

suspension stiffness and correspondingly unchanged dynamic loads of neighboring components (except axle box). However, the evaluation on dynamic bearing motions would be more complicated. Only precise bearing model used can find it.

Using online test, both race motions and contact loads of bearing can be acquired. The motions of components in a bearing differ from each other. Motions of the weakest elements, like roller, cage, etc. can be practiced by setting similar motion boundaries of bearing in test bench with boundary motions set under specific frequency and amplitude.

4.5 Development on 2nd bearing test bench conception

The bench test elaborated in **Part 4.3** is reachable theoretically, but there are two technical problems. First, the spring used to load static force will have a slight deformation during bearing vibration. Second, supporting point in the lever moves on the raceway of self-aligning bearing, bringing error to leverage amplification ratio. To solve them, an optimized design is used with sliding mode control method adopted.

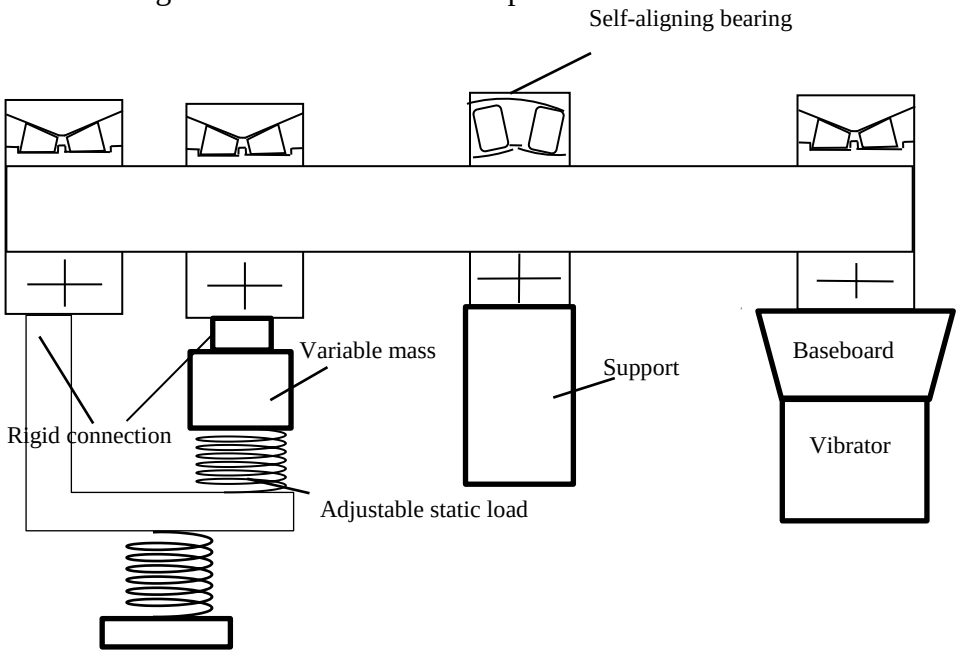

Figure4.4 Second Generation Bearing Test Bench

In order to ensure no relative motion between the downside of loading spring and housing, this chapter also uses the design in **Figure4.4**. Another bearing is added on the rotating shaft so that two bearings on the left side interact with each other, using same radial static spring force. Meanwhile, to ensure bearings on the left side to synchronically work

along with rotating shaft, this design deliberately settles a spring of small stiffness at the bottom of left part, which matters little to system load, but helps to guide frame motion.

In this method, it results in that the load transmitted from the left to the right will be further reduced, since bearing static loads acting on both bearings at the left side are almost canceled. It means that more energy will be saved and higher vibrator ratio can be obtained.

Following the topic, the error caused by supporting point is also mathematically explained.

The dynamic bearing contact force is expected,

$$F_{dy}=\ddot{x}_{dy}m+kx_0,\ddot{x}_{dy}=ba \tag{4. 4}$$

Considering error in $\ddot{x}_{dy}$, b , bearing contact force is updated,

$$F=m\ddot{x}+kx_0,\ddot{x}=ba$$

As required, motion state $\ddot{x}$ follows $\ddot{x}_{dy}$, and bearing load F follows F_{dy}. In improved design, a simple variable structure control (sliding control **[92],[93]**) is performed to predetermine a “sliding mode”.

Since system structure parameter changes with state changing, the system has to input a differently in accordance with the state trajectory of the predetermined “sliding mode”.

The uncertainty of system caused by b is reduced below. Bearing acceleration is obtained by vibrator through the “lever”. Considering sliding range of fulcrum on the raceway of self-aligning bearing, acceleration coefficient b varies within a certain range.

To meet bearing acceleration value $\ddot{x}$ with the designed $\ddot{x}_{dy}$, the initial value should fit,

$$x_{dy}(0)=x(0) \tag{4. 5}$$

Define $$\ddot{x}=f+ba, f=0$$

Where, f represents other interference (neglected), and b has a range of, i.e.,

$$0<b_{\min}\le b\le b_{\max}$$

Since control input a involved in governing equation is a multiplier, gain b can be estimated, using the geometric mean value of the above-mentioned boundaries.

$$\hat{b}=\sqrt{b_{\min}b_{\max}}$$

And meanwhile, define $$\beta^{-1}\leq\frac{\hat{b}}{b}\leq\beta,\beta=\sqrt{\frac{b_{\max}}{b_{\min}}}$$

To track $x(t)=x_{dy}(t)$, the trajectory must remain on the sliding surface $S(t)$, $t>0$

$$s=(\frac{d}{dt}+\lambda)\tilde{x}=\dot{\tilde{x}}+\lambda\tilde{x} \tag{4. 6}$$

$$\dot{s}=\ddot{x}-\ddot{x}_{dy}+\lambda\dot{\tilde{x}}=ba-\ddot{x}_{dy}+\lambda\dot{\tilde{x}} \tag{4. 7}$$

The best approximation $\hat{a}$ meets continuous control law $\dot{s}=0$.

$$\hat{b}\hat{a}=\ddot{x}_{dy}-\lambda\tilde{x}$$

And the control law is

$$a=\hat{b}^{-1}\left[\hat{b}\hat{a}-k\,\mathrm{sgn}(s)\right] \tag{4. 8}$$

Constituting the above formula into $\dot{s}$

$$\dot{s}=\left(1-b\hat{b}^{-1}\right)\left(-\ddot{x}_{dy}+\lambda\dot{\tilde{x}}\right)-b\hat{b}^{-1}k\,\mathrm{sgn}(s) \tag{4. 9}$$

To reach the sliding condition $\frac{1}{2}\frac{d}{dt}s^2\leq-\eta|s|$, k must meet

$$k\geq\left|\left(\hat{b}b^{-1}-1\right)\left(-\ddot{x}_{dy}+\lambda\dot{\tilde{x}}\right)\right|+\eta\hat{b}b^{-1} \tag{4. 10}$$

In operation, an appropriate k is selected in real time by detecting unknowns required in the equation. a incorporating k is in fine input into vibrator controller, using sensor-feedback system.

The test system is asymptotically stable owing to its quick response to simple signals and its robustness under conditions of unstable system parameters and external disturbances. However, the drawbacks of sliding mode control are still this asymptote or slight fluctuation of stability, as well as the necessity of understanding boundaries of uncertain parameters.

4.5 Conclusion

This chapter proposes an alternative bearing test bench, from the first generation bench to the second generation bench, due to the increasing demands on high speed and heavy load, as well as inducing enhanced requirements on vibrator capacity and more expensive test cost, original test on nonlinear bearing-rotor dynamic behaviors is replaced by an alternative test on bearing contact behaviors by reproducing dynamic bearing contact load and dynamic roller motion of some main components, like resonant components. It does not reproduce rotor behaviors, but economically considers the endurance or failure questions of weakest contact bodies inside a bearing. Compared to current bearing tests, this method is advanced, since the conditions performed not only include reproduction of dynamic loads, but also reproduction of absolute motions of both races, even under heavy load situation. This reproduction can consider the impact of internal and external excitations on bearing contact load and roller motion or roller inertia load. Even although roller inertia load is low, roller motion does also impact its contact behaviors at unloaded areas and the ways of temperature rise, etc.

In conclusion, to understand more contact information inside a bearing under different application situations, the resultant change needs to be discovered numerically and experimentally. Some simple results can be mentioned in **Part 3.5**; working parameters at a range of as wide as possible can be considered in a very simple manner in this bench. And meanwhile, fatigue or so-called longevity test can be also economically performed by accelerating vibrations.

4.6 References

[87] Zhang Gen-bei, Zang Chao-ping. The influence of weakly nonlinearities and uncertainties on the structural dynamic analysis [J], Journal of Vibration Engineering, 2012, 25(4):365-372.
[88] X.D. Huang, Z.G. Zeng, Y.N. Ma. The Theory and Methods for Nonlinear Numerical Analysis, Wuhan University Press, Wuhan, 2004.
[89] Zhang Jin-jiang. Optimal design of structural dynamics under multiple frequencies and mode shapes. Northwestern Polytechnical University. Master degree thesis. 2007.
[90] Xie Ronghua, Luo Guihuo. Failure analysis of high speed rolling bearing for aviation [J]. ROTDYN.2008.
[91] Liu Suya. Bearing testing machine and testing technology. Bearing. 2011 (8):55-59.
[92] Jean-Jacques E.Slotine, Li Weiping. Applied Nonlinear Control [M]. Beijing: Machinery Industry Press, 2006, 4.186-207.
[93] Liu Jinkun, Sun Fugui. Research and development on theory and algorithms of sliding mode control [J]. Control Theory and Application.,2007,24(3):407-418

General conclusions and prospects

This thesis explains in Chapter 1:

How the distributed damping and stiffness coefficients of oil film correspond to the distributed oil film thickness under steady and transient states?

Perturbation method is extended to prove that steady-state EHL contact damping and stiffness distributions should not be used to analyze the transient conditions, let alone acquire equivalent total contact damping and stiffness coefficients for dynamic analysis.

The distributions of EHL oil film damping and stiffness are tentatively proposed. By regarding the steady-state solution of EHL as initial state, and continuously acquiring EHL stiffness and damping distributions, dynamic mechanical behaviors of oil film are predicted.

This chapter in fine gives new but simple insights into what is happening to rolling contact of bearing roller. It can be also extended for transient point EHL problem. The idea proposed can be easily delivered to any engineer.

This thesis explains in Chapter 2:

Whether edge effect of roller/race contact affects load and motion transmissions? How to numerically interpret this effect in a simpler manner?

Bearing, as a key part of vibration system, participates in vibration transmission. A better prediction of bear transmission is introduced by taking account of pressure concentration.

To interpret pressure concentration easily, below are performed:

- Deformation calculation in direct bearing model;
- Calculation of roller force and moment distributions based on first and second approximation methods;
- Development of approximation model for higher loads accuracy and better calculation efficiency;

To involve pressure concentration into bearing transmission easily, others are performed:

- An engineering-adequate way of bearing calculation by combining normalization process and advantages of both approximation models;
- The influence of new algorithm on bearing stiffness components and relevant vibrating characteristics;

This chapter in fine provides a better description of longitudinal contact between roller and raceways, which might be involved in any non-linear F.E.A package or any complex M.B.S package with a very simple code.

This thesis also explains in Chapter 3:

How to develop more practical bearing matrices and more reliable methods of solving nonlinear bearing-rotor model in a uniform and economic way? Whether frequency-domain method performs a better computer-aided identification capacity than time-domain method?

A uniform derivation for overall stiffness and damping matrices of both roller and ball bearings is conducted, using the pioneer work of Luc-Houpert (1997). Slicing technique and varying contact angle respectively considered in roller and ball bearings can lead to a more accurate prediction. Bearing matrices formulated with simplified EHL and Hertz relations can be analytical, however, the contact descriptions incorporated are still in doubt.

Nonlinear bearing-rotor system is modeled with a better linear mathematical equation and solved in simpler enhanced numerical manner of Adams. Meanwhile, nonlinear bearing-rotor system is also remodeled and resolved with analytical method of HB-AFT. It performs a faster efficiency and an easier system behavior-identifying capacity, especially when considering 3D condition. After modeling and solving nonlinear bearing-rotor system, some factors participated can be well considered qualitatively and quantitatively, including initial states, damping, and eccentricity, internal and external excitations.

This chapter in fine provides a good interface between raceways, which can be involved in any non-linear F.E.A package or any complex M.B.S package. The solving methods can also be extended and then applied in more complex bearing-rotor system.

This thesis at last introduces in Chapter 4:

How to build up an alternative bearing test bench to reproduce contact behaviors inside a bearing under large loading and high-frequency vibration?

This chapter proposes an alternative bearing test bench. From the first-generation bench to the second-generation bench, due to the increasing demands on high speed and heavy load, as well as increasing requirements on vibrator capacity and increasing test cost, original test on nonlinear bearing-rotor dynamic behaviors is replaced by an alternative test on bearing contact behaviors by reproducing dynamic bearing contact load and dynamic roller motion of some main components, like resonant components. This reproduction can consider the impact of internal and external excitations on bearing contact load and roller motion (or roller inertia load). Even although roller inertia load is small, roller motion does also impact its contact (impact) behaviors at unloaded areas and the ways of contact manner, temperature rise, and others at loaded areas.

To understand more contact information inside a bearing under different application situations, the differences can be mathematically or experimentally. Besides mathematical manner in **Chapter 3**, which is economic; the experimental method is also developed in **Chapter 4**, furthermore, working parameters at a range of as large as possible can be also replayed in a very simple manner in this bench. And meanwhile, fatigue or so-called longevity test can be also economically performed by accelerating vibrations.

Prospects:

From contact model to bearing model, and from bearing-rotor model to bench reproduction technique, the four chapters deliver the author's understandings in bearing engineering application. However, a lot of relevant ideas are still there and waiting for some clearer solutions.

- Complex calculations performed in Chapter 1 and Chapter 2 attempt to describe distributed roller contact parameters in rolling and roller length directions, and to explain some resultant vibration characteristics of rotor, and so on. However, due to calculation cost, a simple and lumped parameter is more preferred in dynamic calculation of multi-EHL contacts. But, the extraction of accurate Transient EHL parameters is still very difficult.

- The perturbation method used is based on a synchronously perturbed value of film thickness along contact width. Synchronous perturbation of film thickness distribution, in essence, trusts robustness of steady-state EHL solution under transient conditions. A consideration of asynchronous film thickness variation along contact width is taken by the authors in the first chapter. But compared to distributed parameters, the corresponding lumped parameters are still unknown.
- Linear superposition of the lubricant film stiffness, damping forces and Hertz force is a bolder hypothesis, since distributed lubricant force nonlinearly reconstructs Hertz deformation and force distributions. So that it will be more persuasive to perform that in other more complicated manners.
- The proposed method for line EHL problem can be applied in Point EHL problem.
- The transition from line contact to point contact can be well considered when bearing is applied in rotor system. The selection of slice number can be further confirmed by comparing numerical bearing moment with experimental bearing moment.
- More information hidden in bearing-rotor system can be studied by considering edge effect, using linear vibration theory or non-linear rotor theory.
- The proposed slice load can be further introduced into bearing damping and stiffness matrices before performing dynamic analysis.
- More complex bearing-rotor system can be modeled using TTM or FEM. And a versatile code can be developed to solve TTM model of complex bearing-rotor system, using frequency domain method.
- The corresponding experimental results will be compared with theoretical solutions, with the construction of bearing test bench.

FOLIO ADMINISTRATIF

THESE DE L'UNIVERSITE DE LYON OPEREE AU SEIN DE L'INSA LYON

NOM : Shaocheng DATE de SOUTENANCE : le xx novembre 2017

Prénom: Zhu

TITRE: **Contribution to the modeling of rolling element bearing – rotor system for railway application**

NATURE : Doctorat Numéro d'ordre : 2017LYSEI136

Ecole doctorale : MECANIQUE, ENERGETIQUE, GENIE CIVIL, ACOUSTIQUE

Spécialité : Mécanique -Génie Mécanique - Génie Civil

RESUME:

Some developments on bearing applications are emphasized in this thesis, from contact model to bearing model, and from bearing-rotor model to bench reproduction technique.

First, perturbation method is extended to prove that steady-state EHL distributed damping and stiffness do not satisfy the transient conditions, and steady-state EHL lumped coefficients are not suitable for dynamic analysis.

Distribution law of EHL oil film damping and stiffness is attemptly proposed. Combining initial state of steady-state solution with transient EHL distributed stiffness and damping, dynamic behaviors of oil film are predicted.

Second, edge effect of roller/race contact is considered in bearing transmissions. First and second approximation methods are proposed to numerically interpret this effect. First approximation method concentrates on adopting influence coefficient method to replay edge effect as well as using normalization process to respect empirical results, while second approximation method focuses on a fast-analytical manner of describing Hertz pressure inside roller slice.

Third, practical bearing matrices are used to develop 3D bearing-rotor dynamics code, based on classical Hertz and EHL formulas. In time domain, four-order Adams method is improved to solve incremental nonlinear dynamics equations; In frequency domain, analytical method of HB-AFT is particularly employed to bridge 3D bearing matrices and 3D steady-state solutions, besides, arc-length continuation method increases calculation speed. Using both methods, some factors can be considered qualitatively and quantitatively, including initial states, damping, eccentricity, internal and external excitations.

Last, an alternative technique is proposed to reproduce contact behaviors inside bearings under heavy loading and high-frequency vibrations, when working parameters are beyond bench capacity.

This thesis gives new but simple insights into what happens to rolling and longitudinal contacts of bearing roller, how to model and solve nonlinear bearing-rotor system in both time and frequency domains, and where a way is to reproduce extreme contact conditions inside bearings using bench.

MOTS-CLÉS: Bearing, Transient EHL (elasto-hydrodynamic lubrication), Perturbation method, EHL stiffness and damping distributions, Edge effect of roller/race contact, Nonlinear bearing-rotor system, Enhanced four-order Adams method, HB-AFT, Bench reproduction technique

Laboratoire (s) de recherche : LaMCoS (CNRS UMR5259) et Key State Laboratory of Traction Power

Directeurs de thèse: **Daniel NELIAS et Weihua ZHANG**

Président de jury :

Composition du jury :

DUFRENOY, Philippe, Professeur, Université de Lille, Rapporteur

NELIAS, Daniel, Professeur, INSA Lyon, Directeur de thèse

ROUHAUD, Emmanuelle, Professeur, UT Troyes, Examinatrice

YIN, Honoré, Directeur de Recherche, ENPC, Rapporteur

ZHANG, Weihua, Professeur, Southwest Jiaotong University, Co-Directeur de thèse